



1987

# Diagenesis and porosity development of the Mission Canyon and Charles Formations (Mississippian), Treetop and Whiskey Joe Fields, North Dakota

Rebecca L. Durall  
*University of North Dakota*

Follow this and additional works at: <https://commons.und.edu/theses>

 Part of the [Geology Commons](#)

---

## Recommended Citation

Durall, Rebecca L., "Diagenesis and porosity development of the Mission Canyon and Charles Formations (Mississippian), Treetop and Whiskey Joe Fields, North Dakota" (1987). *Theses and Dissertations*. 77.  
<https://commons.und.edu/theses/77>

This Thesis is brought to you for free and open access by the Theses, Dissertations, and Senior Projects at UND Scholarly Commons. It has been accepted for inclusion in Theses and Dissertations by an authorized administrator of UND Scholarly Commons. For more information, please contact [zeinebyousif@library.und.edu](mailto:zeinebyousif@library.und.edu).

DIAGENESIS AND POROSITY DEVELOPMENT OF THE MISSION CANYON  
AND CHARLES FORMATIONS (MISSISSIPPIAN), TREETOP AND  
WHISKEY JOE FIELDS, NORTH DAKOTA

by

Rebecca L. Durall

Bachelor of Science, Eastern Washington University, 1982

A Thesis

Submitted to the Graduate Faculty

of the

University of North Dakota

in partial fulfillment of the requirements

for the degree of

Master of Science

Grand Forks, North Dakota

May  
1987

This thesis submitted by Rebecca L. Durall in partial fulfillment of the requirements for the Degree of Master of Science from the University of North Dakota has been read by the Faculty Advisory Committee under whom the work has been done, and is hereby approved.

Howard Fischer  
(Chairperson)

Don L. Halverson

Kenneth Olson

Robert Stevenson

This thesis meets the standards for appearance and conforms to the style and format requirements of the Graduate School of the University of North Dakota, and is hereby approved.

A. William Johnson 4-10-87  
Dean of the Graduate School

Permission

Title Diagenesis and Porosity Development of the  
Mission Canyon and Charles Formations  
(Mississippian), Treetop and Whiskey Joe  
Fields, North Dakota

Department Geology

Degree Master of Science

In presenting this thesis in partial fulfillment of the requirements for a graduate degree from the University of North Dakota, I agree that the Library of this University shall make it freely available for inspection. I further agree that permission for extensive copying for scholarly purposes may be granted by the professor who supervised my thesis work or, in his absence, by the Chairman of the Department or the Dean of the Graduate School. It is understood that any copying or publication or other use of this thesis or part thereof for financial gain shall not be allowed without my written permission. It is also understood that due recognition shall be given to me and the University of North Dakota in any scholarly use which may be made of any material in my thesis.

Signature Rebecca Dwall

Date April 6, 1987

## TABLE OF CONTENTS

### DIAGENESIS AND POROSITY DEVELOPMENT OF THE MISSION CANYON AND CHARLES FORMATIONS (MISSISSIPPIAN), TREETOP AND WHISKEY JOE FIELDS, NORTH DAKOTA

LIST OF ILLUSTRATIONS.....	vi
LIST OF TABLES.....	xii
ACKNOWLEDGMENTS.....	xiii
ABSTRACT.....	xiv
INTRODUCTION.....	1
Regional Geology and Study Area	
Nomenclature Review	
Previous Works	
Purpose	
Methodology	
LITHOTYPE DESCRIPTIONS.....	23
Introduction	
Echinoderm Wackestone Lithotype	
Dolomudstone Lithotype	
Neomorphic Wackestone Lithotype	
Intraclast Bioclast Wackestone Packstone Lithotype	
Laminated Mudstone Lithotype	
Anhydrite Lithotype	
DEPOSITIONAL SETTING.....	54
DIAGENESIS.....	57
Introduction	
Micritization	
Compaction	
Dolomitization	
Cementation	
Replacement	
Fracturing	
Neomorphism	
Pressure Solution	
POROSITY.....	108
Introduction	
Pore and Pore Throat Studies	
Interpore Minerals	
Porosity Distribution	
DIAGENETIC HISTORY.....	143
Introduction	
Eogenetic Diagenesis	
Mesogenetic Diagenesis	

CONCLUSIONS.....	161
APPENDICES.....	164
Appendix A. Legal Descriptions and Locations of Described Cores .....	165
Appendix B. Core and Thin Section Descriptions...	167
Appendix C. Procedure for Making Pore Casts.....	198
REFERENCES CITED.....	200

## LIST OF ILLUSTRATIONS

Figure #	Page
1. Generalized diagram of the Williston Basin showing the location of Billings County and major structural features.....	3
2. Structure map on top of the "Fryburg Pay" illustrating the location of the study area along the eastern edge of the Billings anticline.....	5
3. Index map showing the location of the study area.....	8
4. Example of the relation between typical log responses, nomenclature, and position of the cored interval within the upper MIssion Canyon and lower Charles Formations in the study area.....	12
5. Partial stratigraphic nomenclature chart of the Madison Group of the Williston Basin.....	15
6. Location of wells and described cores within the study area.....	19
7. Typical log responses and corresponding composite core illustrating the stratigraphic distribution of lithotypes within the study area.....	25
8. Core photograph of the echinoderm wackestone lithotype.....	31
9. Core photograph of the echinoderm wackestone lithotype showing compaction.....	31
10. Core photograph of the echinoderm wackestone lithotype with stylolite.....	31
11. Core photograph of the dolomudstone lithotype showing abundant porosity.....	34
12. Core photograph of the dolomudstone lithotype showing calcite and anhydrite-replaced burrows.....	34
13. Core photograph of the neomorphic wackestone lithotype with stylolite.....	38
14. Core photograph of the neomorphic wackestone lithotype with small burrows.....	38
15. Core photograph of the neomorphic wackestone lithotype with vertical, calcite-filled fractures...	41

16. Core photograph of the intraclast bioclast wackestone packstone lithotype.....	41
17. Core photograph of the intraclast bioclast wackestone packstone lithotype showing a siliceous zone.....	44
18. Core photograph of the laminated mudstone lithotype showing cryptalgal laminae and dessication cracks...	47
19. Core photograph of the laminated mudstone lithotype showing displacive anhydrite nodules.....	47
20. Core photograph of the laminated mudstone lithotype with microstylolites and lath-shaped, anhydrite replacement of matrix.....	47
21. Core photograph of the laminated mudstone lithotype showing anhydrite-filled fenestrae.....	50
22. Core photograph of the anhydrite lithotype showing nodular anhydrite displacement of matrix.....	50
23. Core photograph of the anhydrite lithotype showing bedded-massive anhydrite texture.....	53
24. Core photograph of the anhydrite lithotype showing elongated, distorted, nodular (swallowtail) anhydrite texture.....	53
25. Photomicrograph of intensely micritized allochems in the intraclast bioclast wackestone packstone lithotype.....	60
26. Photomicrograph of thin, micritic envelopes surrounding anhydrite-replaced allochems in the laminated mudstone lithotype.....	60
27. Photomicrograph of broken, horizontally aligned skeletal fragments in the echinoderm wackestone lithotype.....	64
28. Photomicrograph of microcrystalline dolomite in the laminated mudstone lithotype.....	67
29. Photomicrograph of sucrosic and saddle dolomite in the dolomudstone lithotype.....	67
30. Photomicrograph of isopachous calcite cement rimming peloids in the intraclast bioclast wackestone packstone lithotype.....	74



31. Photomicrograph of blocky calcite cement filling interparticle pores of the intraclast bioclast wackestone packstone lithotype.....	77
32. Photomicrograph of syntaxial overgrowth cement on an echinoderm grain in the intraclast bioclast wackestone packstone lithotype.....	77
33. Photomicrograph of poikilitic calcite cement in the dolomudstone lithotype.....	80
34. Photomicrograph of calcite and anhydrite nodule in the dolomudstone lithotype.....	80
35. Photomicrograph of anhydrite and silica cements in a grainstone of the intraclast bioclast wackestone packstone lithotype.....	80
36. Photomicrograph of a silica-lined, anhydrite-cemented vug in the intraclast bioclast wackestone packstone lithotype.....	80
37. Photomicrograph of a moldic pore cemented with saddle dolomite in the dolomudstone lithotype.....	84
38. Photomicrograph of a large vug cemented with saddle dolomite and blocky calcite in the intraclast bioclast wackestone packstone lithotype.....	84
39. Photomicrograph of an intraparticle pore (coral) cemented with pyrite and calcite in the dolomudstone lithotype.....	84
40. Photomicrograph of dedolomitization within the neomorphic wackestone lithotype.....	88
41. Photomicrograph of dedolomitization in the dolomudstone lithotype.....	88
42. Photomicrograph of anhydrite replacement of a sulfate nodule in the dolomudstone lithotype.....	88
43. Photomicrograph of lath-shaped anhydrite replacing matrix in the laminated mudstone lithotype.....	91
44. Photomicrograph of anhydrite replacement of an echinoderm grain in the echinoderm wackestone lithotype.....	91
45. Photomicrograph of saddle dolomite replacement of matrix and allochems in the intraclast bioclast wackestone packstone lithotype.....	91

46. Photomicrograph of chert-replaced, quartz-cemented, peloid grainstone in the intraclast bioclast wackestone packstone lithotype.....	94
47. Photomicrograph of fine-grained chert replacement of matrix in the intraclast bioclast wackestone packstone lithotype.....	94
48. Photomicrograph of authigenic quartz replacement of matrix surrounding anhydrite nodules in the laminated mudstone lithotype.....	94
49. Photomicrograph of celestite replacement of allochems and matrix in the laminated mudstone lithotype.....	94
50. Photomicrograph of large pyrite cubes replacing matrix in the dolomudstone lithotype.....	94
51. Photomicrograph of blocky calcite and saddle dolomite filling a fracture in the echinoderm wackestone lithotype.....	97
52. Photomicrograph of a calcite-filled fracture originating from a calcite and anhydrite nodule in the dolomudstone lithotype.....	97
53. SEM photograph of a silica-cemented fracture in the intraclast bioclast wackestone packstone lithotype..	97
54. Photomicrograph of an anhydrite-cemented fracture in the laminated mudstone lithotype.....	97
55. Photomicrograph of neomorphic spar and dolomite in the neomorphic wackestone lithotype.....	102
56. SEM photograph of neomorphic spar and dolomite in the neomorphic wackestone lithotype.....	102
57. Photomicrograph of allochems "floating" in neomorphic spar in the neomorphic wackestone lithotype.....	102
58. Photomicrograph of a low amplitude stylolite penetrating a skeletal fragment in the echinoderm wackestone lithotype.....	106
59. Photomicrograph of a grain contact suture between two echinoderm grains in the echinoderm wackestone lithotype.....	106
60. Core photograph of microstylolites around a rugose coral in the echinoderm wackestone lithotype.....	106

61. Core photograph of microstylolites in the dolomudstone lithotype.....	106
62. Illustration of time-porosity terms and their relation to major surface and burial zones.....	110
63. Example of the relation between the stratigraphic distribution of lithotypes, corresponding log responses, distribution of percent porosity, and distribution of pore types in the study area.....	112
64. Photomicrograph of interparticle pores in the intraclast bioclast wackestone packstone lithotype..	114
65. SEM photograph of calcite spar lining an interparticle pore in the intraclast bioclast wackestone packstone lithotype.....	114
66. Core photograph of intraparticle pores within rugose corals in the intraclast bioclast wackestone packstone lithotype.....	117
67. Photomicrograph of a moldic pore surrounded by saddle dolomite and quartz cements in the intraclast bioclast wackestone packstone lithotype.....	117
68. Photomicrograph of moldic pores in the dolomudstone lithotype.....	117
69. Photomicrograph of a large vug partially cemented with saddle dolomite in the dolomudstone lithotype..	120
70. SEM photograph of small vugs in the dolomudstone lithotype.....	120
71. Photomicrograph of intercrystalline pores in the dolomudstone lithotype.....	120
72. SEM photograph of intercrystalline pores and dolomite rhombohedrons within the dolomudstone lithotype.....	120
73. SEM photograph of a pore cast of intercrystalline pores in the dolomudstone lithotype.....	124
74. SEM photograph of a pore cast showing polyhedral-shaped, intercrystalline pores in the dolomudstone lithotype.....	124
75. SEM photograph of a pore cast of tetrahedral and interboundary-sheet-shaped, intercrystalline pores in the dolomudstone lithotype.....	124

76. Illustration of a cross section of a typical polyhedral-shaped pore.....	127
77. Illustration of the changes from polyhedral-shaped pores to interboundary-sheet-shaped pores and the resulting reduction in porosity as dolomite rhombohedra continue to grow.....	127
78. SEM photograph of a pore partially filled with calcite and surrounded by dolomite in the dolomudstone lithotype.....	130
79. Photomicrograph of an anhydrite-filled pore in the dolomudstone lithotype.....	130
80. SEM photograph of a dolomite-filled pore in the dolomudstone lithotype.....	130
81. SEM photograph of a silica-filled pore in the intraclast bioclast wackestone packstone lithotype..	130
82. Example of the relation between a typical log response and the stratigraphic distribution of the lower, middle, and upper porosity zones within the cored interval.....	132
83. Porosity isopach map of the lower porosity zone showing the aggregate footage of porous rock with greater than 8 percent critical porosity.....	135
84. Porosity isopach map of the middle porosity zone showing the aggregate footage of porous rock with greater than 8 percent critical porosity.....	137
85. Porosity isopach map of the upper porosity zone showing the aggregate footage of porous rock with greater than 8 percent critical porosity.....	139
86. Fence diagram illustrating the distribution of porous zones within the upper Mission Canyon Formation in the study area and their relation to the overlying anhydrite.....	141
87. Schematic diagram illustrating the relation between time and eogenetic fluids, processes, and products..	148
88. Schematic diagram illustrating the relation between time and mesogenetic fluids, processes, and products.....	157

LIST OF TABLES

Table #	Page
1. Petrographic summary of lithotypes.....	27
2. Relative timing of diagenetic events and their relation to the distribution of lithotypes.....	145

## ACKNOWLEDGEMENTS

I would like to thank my committee members, Drs. Howard J. Fischer, Kenneth L. Harris, Robert J. Stevenson, and Don Halvorson for their invaluable suggestions and critical review of the manuscript.

I would like to thank the North Dakota Geological Survey for allowing me access to materials and facilities used during this study. I would especially like to thank Julie LeFever for all the hours she spent drafting for me.

I am very grateful for the thesis funding generously provided by Shell and Meridian oil companies.

I would like to thank my fellow graduate students for their constant willingness to share their knowledge of carbonate geology. Special thanks go to Randall A. Stephens who always encouraged me and James M. Pappas who gave me the strength to overcome the difficult times.

I would like to thank my family for their love and understanding all these years. Finally, I would like to dedicate this manuscript to the memory of my mother for without her love and guidance I would never have come this far.

## ABSTRACT

Rocks of the upper Mission Canyon and lower Charles Formations (Mississippian) in central Billings County, North Dakota consist of interbedded limestones, dolostones, and anhydrites which were deposited in a shallow epeiric sea. This study was limited to the upper Mission Canyon and lower Charles Formations of Treetop and Whiskey Joe fields, located along the Billings anticline in central Billings County, North Dakota. Close examination of approximately 260 metres (850 feet) of upper Mission Canyon and lower Charles Formations core in the study area resulted in the separation of rocks into six lithotypes: 1) echinoderm wackestone, 2) dolomudstone, 3) neomorphic wackestone, 4) intraclast bioclast wackestone packstone, 5) laminated mudstone, and 6) anhydrite which represent sublittoral, littoral, and supralittoral depositional environments.

Numerous diagenetic processes were active in the upper Mission Canyon and lower Charles Formation rocks. Processes include micritization, compaction, dolomitization, cementation, replacement, fracturing, neomorphism, and pressure solution.

Pore types present within rocks of the upper Mission Canyon and lower Charles Formations include two primary pore types: interparticle and intraparticle, and four secondary pore types: intercrystalline, moldic, vuggy, and fracture.

Intercrystalline pores were examined in detail to determine the geometry of pores and pore throats. The three pore shapes found were polyhedral, tetrahedral, and interboundary-sheet. Polyhedral-shaped pores are the most common pore shape in the study area.

In the study area rocks of the upper Mission Canyon Formation were separated stratigraphically into lower, middle, and upper porosity zones. A comparison of porosity isopach maps of each porosity zone indicates that toward the north-northwest, porous zones tend to parallel the overlying anhydrite, and that the thickest accumulations of porous rock are developed progressively higher stratigraphically within each porosity zone. Progradation of littoral and supralittoral environments and early dolomitization may have been responsible for the distribution of porosity in the study area.

The diagenetic history of rocks of the upper Mission Canyon and lower Charles Formations represents a complex system of post-depositional processes. Pore fluids present during eogenetic diagenesis reflect near-surface water conditions and include hypersaline, marine and meteoric waters. Eogenetic diagenetic zones include hypersaline vadose and phreatic, sublittoral stagnant and agitated, meteoric, and meteoric and marine mixing diagenetic zones. Mesogenetic diagenesis resulted from a combination of local connate pore waters, fluids released during pressure solution, and an influx of fresher water.



## INTRODUCTION

### Regional Geology and Study Area

The Williston Basin is an intracratonic, sedimentary and structural basin underlying major parts of Montana, North Dakota, South Dakota, Saskatchewan, and Manitoba (Carlson and Anderson, 1965) (Fig. 1). Within North Dakota, the Williston Basin covers 133,700 square kilometres (51,600 square miles) (Carlson and Anderson, 1965). Representative sedimentary rocks from every geologic system of the Phanerozoic are found in the basin. Maximum thickness at the basin center is about 4,570 metres (15,000 feet) (Carlson and Anderson, 1965).

The Williston Basin contains both major and minor structures, including several anticlines, lineaments and structural highs (Gerhard and others, 1982). These structures, including the Nesson anticline, Cedar Creek anticline, Little Knife anticline, and the Billings anticline, trend north or northwest within the basin (Ballard, 1963; Gerhard and others, 1982) (Fig. 1).

The Billings anticline is a north-plunging anticlinal structure located in the central Williston Basin that encompasses parts of Slope, Golden Valley and Billings Counties of North Dakota. The Billings anticline, which extends from R. 100 W. to R. 103 W. and from T. 133 N. to T. 144 N., is approximately 97 kilometres (60 miles) long and 32 kilometres (20 miles) wide (Petroleum Information Corp., 1980) (Fig. 2). Six hydrocarbon-producing fields

Figure 1 Generalized diagram of the Williston Basin (shaded) showing the location of Billings County and major structural features (modified from Laird and Folsom, 1956 and Gerhard and others, 1982).

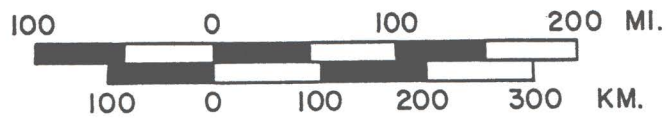
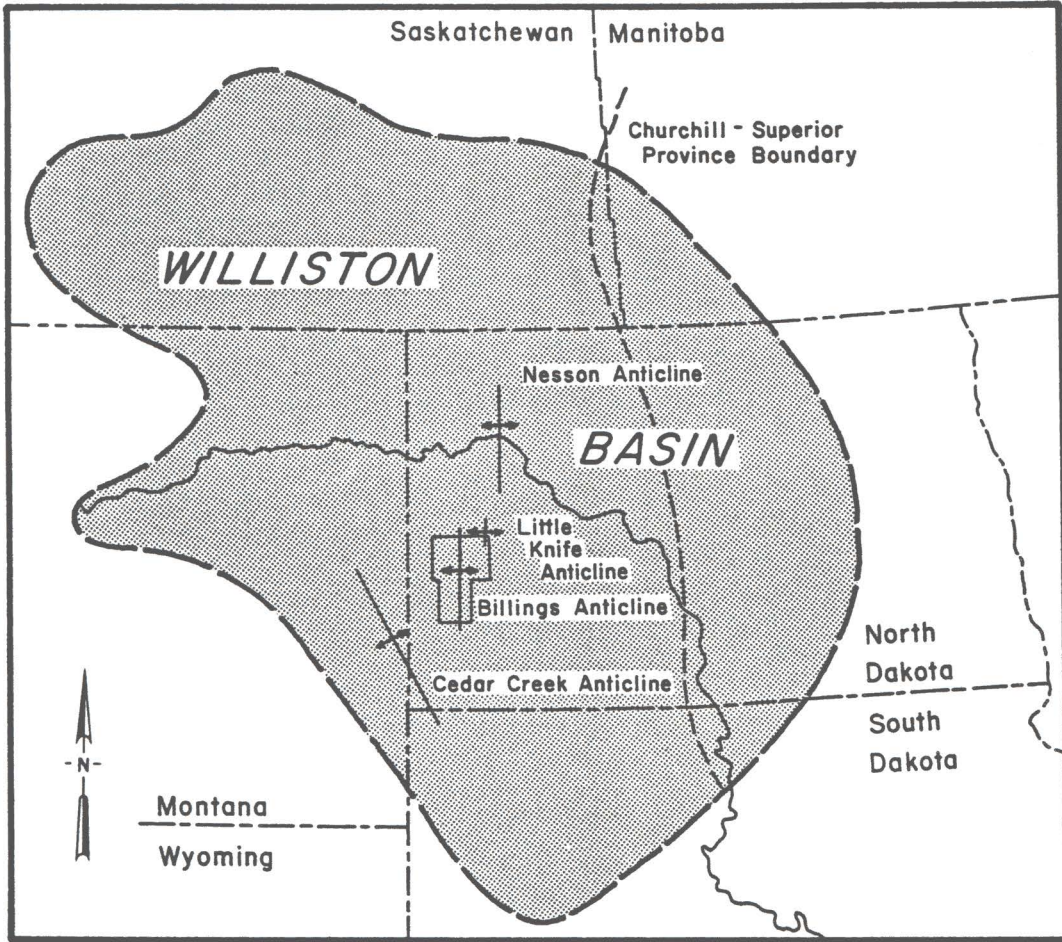
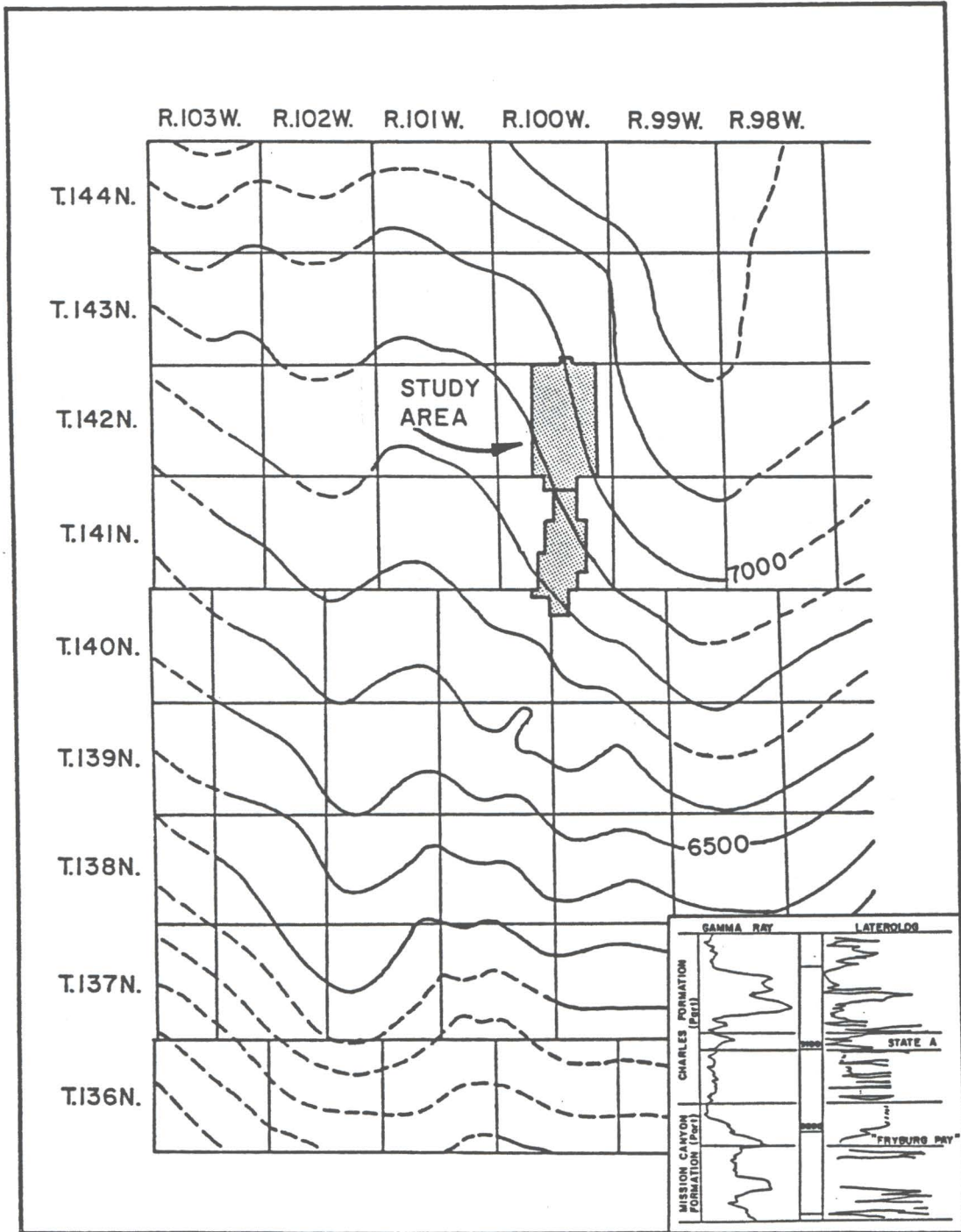


Figure 2 Structure map on top of the "Fryburg Pay" (Mission Canyon Formation) illustrating the location of the study area (shaded) along the eastern edge of the Billing anticline. The inset shows the stratigraphic position of the datum (modified from Anderson, 1966).



are located on the Billings anticline: Elkhorn Ranch, Four Eyes, Big Stick, T.R., Treetop and Whiskey Joe. The area under investigation in this study lies within two of these fields, Treetop and Whiskey Joe, located in central Billings County (Fig. 3).

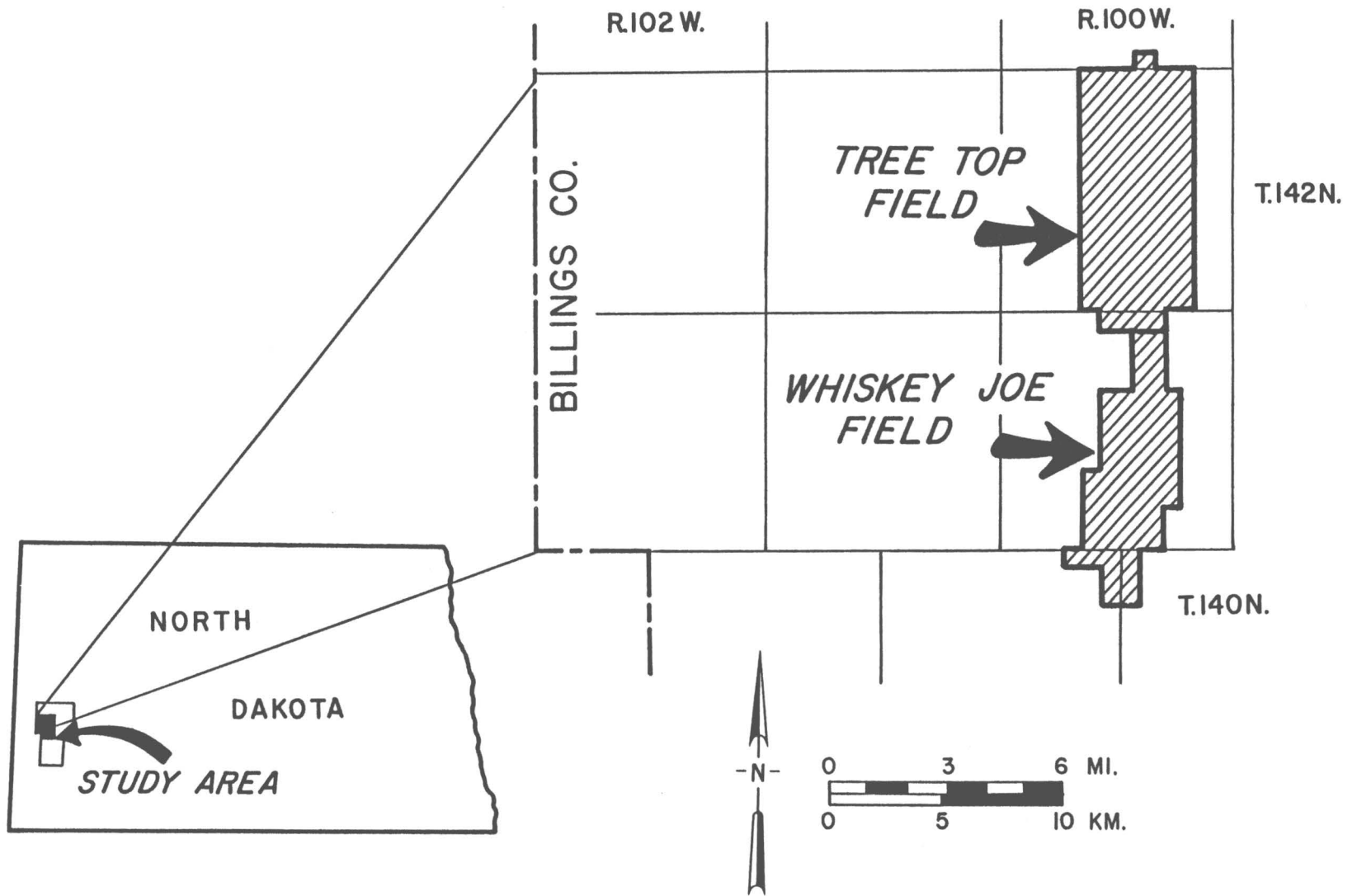
#### Nomenclature Review

Peale (1893) first named the Madison Formation from exposures in the Madison Range of the Three Forks area in Montana. Collier and Cathcart (1922) elevated the Madison Formation to group status and further divided it into the Mission Canyon and Lodgepole Limestones. Sloss and Hamblin (1942) agreed with Collier and Cathcart's proposed division of the Madison Group and extended the group to include exposures in both Montana and northern Wyoming.

Seager (1942) described a series of interbedded limestones, dolomites and anhydrites in southeastern Montana which he called the Charles Member. He ascribed this name to those rocks between the Big Snowy Group and the Madison Group. On the basis of porosity development near the top of the Madison Group, Seager placed the Charles Member in the Big Snowy Group. Sloss and Moritz (1951) recognized similarities between Seager's Charles Member and exposures in southwest Montana and suggested that the Charles Member be included in the Madison Group rather than the Big Snowy Group.

While working in the subsurface of the northeastern Williston Basin, Thomas (1954) divided the Madison Group

Figure 3 Index map showing the location of the study area.





into three formations which are, in ascending order, the Lodgepole Formation, the Mission Canyon Formation and the Charles Formation. Thomas further divided the Mission Canyon Formation into five informal units, MC-1 through MC-5, in ascending order. Thomas separated these units on the basis of subsurface, "persistent silt zones" discernible on electric and radioactive logs. Thomas concluded that these silt zones represented the final product of repeated limestone cycles in the Mission Canyon Formation.

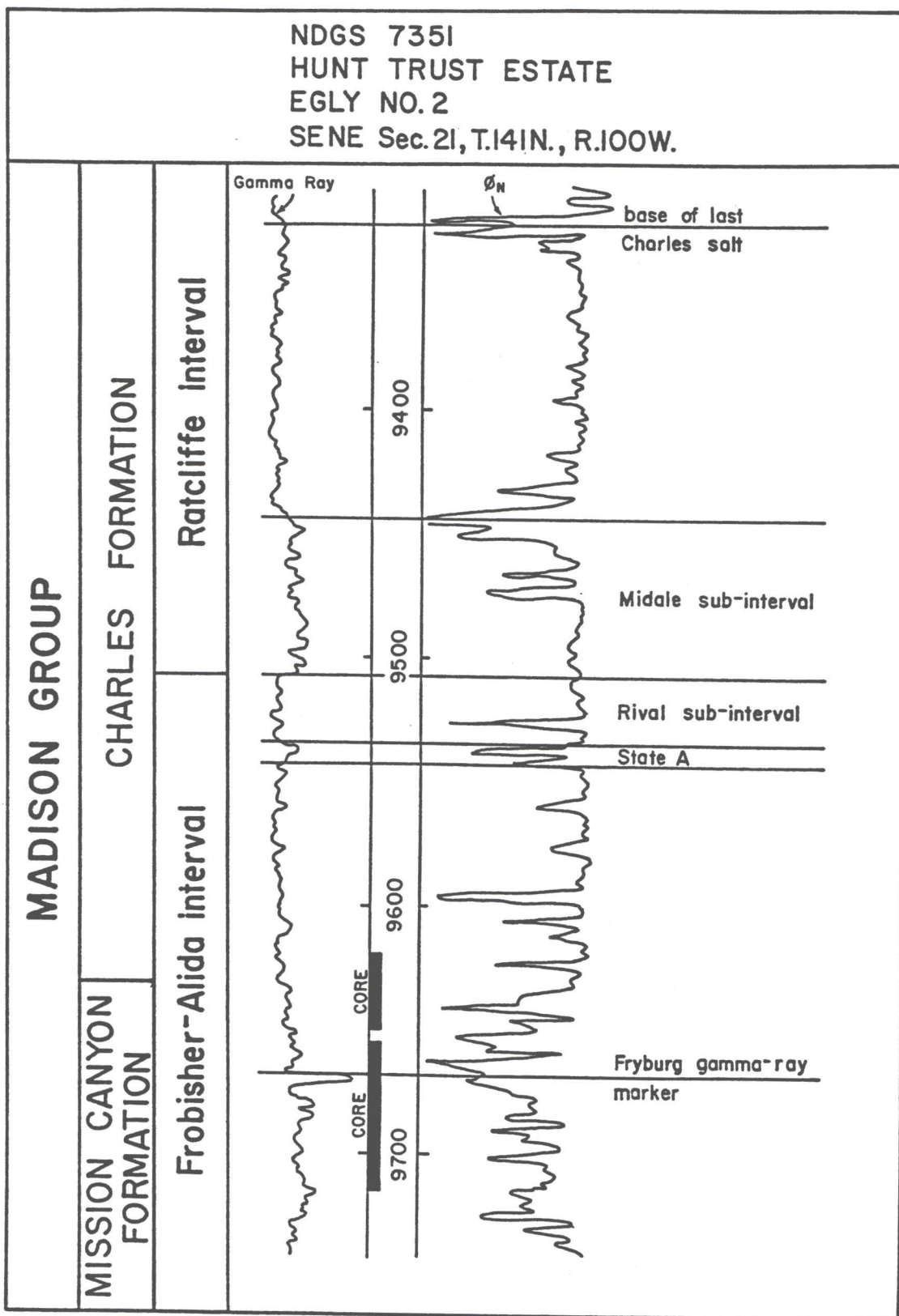
Porter (1955) discussed the facies relations within the Madison Group. Porter interpreted the thin, clastic seams within the limestone-evaporite sequences as time lines representing epierogenic fluctuations and represented "cyclic" deposition of the Mission Canyon Formation.

To standardize Mississippian subsurface terminology, a system of nomenclature for the Williston Basin was formally proposed (Saskatchewan Geological Society, 1956). The Madison Group was divided into six units called "beds". The name Souris Valley beds was given to the sequence of rocks equivalent to the Lodgepole Formation of Thomas (1954). The name Tilston beds was applied to rocks equivalent to Thomas' (1954) MC-1 and MC-2 units. Rocks corresponding to Thomas' (1954) MC-3, MC-4, and MC-5 units were designated Frobisher-Alida beds. The names given to rocks equivalent to the Charles Formation of Thomas (1954) are, in ascending order, the Midale, Ratcliffe and Poplar beds.

In the following years, as more wells were drilled in North Dakota, it became apparent that markers established by the Saskatchewan Geological Society (1956) were no longer adequate. Smith (1960), as chairman of a committee formed by the North Dakota Geological Society, proposed a nomenclature for the Madison Group in North Dakota. The committee redefined the Lodgepole, Mission Canyon and Charles Formations as facies and further subdivided these facies into five intervals and two subintervals. The term "interval", a marker-defined unit, replaced the term "bed", previously used by the Saskatchewan Geological Society (1956). The intervals are, in ascending order, Bottineau, Tilston, Frobisher-Alida (containing the Rival subinterval), Ratcliffe (containing the Midale subinterval) and the Poplar. The Tilston interval conformably overlies the Lodgepole Formation (Bottineau interval of Smith, 1960 and Bluemle and others, 1980) and is conformably overlain by the Frobisher-Alida interval. In 1965, Carlson and Anderson re-established the boundaries of these marker-defined units and returned the Madison to formation status within the Williston Basin of North Dakota.

The Mission Canyon Formation-Charles Formation boundary is defined as the base of the lowest Charles evaporite (Edie, 1958). Therefore, the stratigraphic section under investigation in this study covers the upper portion of the Mission Canyon Formation and lowermost Charles Formation. Figure 4 illustrates the relation

Figure 4 Example of the relation between typical log responses (gamma ray and compensated neutron log ( $\phi_N$ )), nomenclature, and position of cored interval within the upper Mission Canyon and lower Charles Formations in the study area.



between the Mission Canyon Formation-Charles Formation boundary and the informal markers present in the study area as seen on a typical log.

Bluemle and others (1980) returned the Madison to group status and the Lodgepole, Mission Canyon and Charles facies were again given formation status. The marker-defined intervals established by Smith (1960) were retained. This nomenclature is currently in use by the North Dakota Geological Survey and will be used in this report (Fig. 5).

#### Previous Works

Complicated vertical and lateral lithologic changes within the Madison Group are due to the complex facies relations within the Lodgepole, Mission Canyon, and Charles Formations (Fuller, 1956; Carlson and Anderson, 1966). At the basin center, the Mission Canyon Formation is 105 to 235 metres (350 to 775 feet) thick (Sandberg, 1962). Mission Canyon lithologies vary from dark, argillaceous, skeletal limestones near the basin center to light-colored, skeletal, oolitic to massive limestones near the perimeter of the basin (Carlson and Anderson, 1965). Near the top of the Mission Canyon, dolomites and anhydrites are common.

Edie (1958) described four Mission Canyon and upper Charles depositional environments in southeastern Saskatchewan. These environments are, in ascending order: 1) basin, 2) open marine shelf, 3) barrier, and 4) lagoon.

Figure 5 Partial stratigraphic nomenclature chart of the Madison Group (Mississippian) of the Williston Basin.

Peale, 1893	Collier & Cathcart, 1922	Thomas, 1954	Saskatchewan Geological Society, 1956	Smith, 1960	Bluemle & Others, 1980 (This study)	
		Charles Formation	Poplar Beds	Poplar Interval	Charles Formation	Poplar Interval
			Ratcliffe Beds	Ratcliffe Interval ----- Midale Subinterval		Ratcliffe Interval ----- Midale Subinterval
			Midale Beds	Rival Subinterval -----		Rival Subinterval -----
MADISON FORMATION	MADISON GROUP	MADISON GROUP	Mission Canyon Formation	MC-5	Frobisher - Alida Beds	Frobisher - Alida Interval
				MC-4		
				MC-3		
				MC-2	Tilston Beds	Tilston Interval
				MC-1		
Lodgepole Limestone	Lodgepole Formation	Souris Valley Beds	Bottineau Interval	Lodgepole Formation	Bottineau Interval	

In recent work in northcentral North Dakota (Haas field), Elliott (1982) interpreted the Mission Canyon Formation as a cyclic series of shallowing upwards sequences. Lindsay and Roth (1982) described the Mission Canyon Formation of the Little Knife field in western North Dakota as a regressive-upward carbonate to anhydrite sequence deposited in a shoaling epiherc sea and advancing sabkha. Using the scanning electron microscope for studies of core samples and relief pore casts, Lindsay and Roth (1982) determined four major pore types, one moldic and three dolomite inter-crystalline types similar to those found in this study. Altschuld and Kerr (1982) and Kupecz (1984) dealt with both depositional environments and diagenesis of the Mission Canyon Formation in the Billings Anticline area. Stephens and Durall (1985) interpreted the diagenesis, Stephens (1986) studied deposition and diagenesis, and Fischer and others (1986) interpreted the depositional environments of rocks in the Billings Anticline area.

#### Purpose

The purpose of this study of the upper Mission Canyon Formation and lowermost Charles Formation (Treetop and Whiskey Joe fields, Billing County, North Dakota) is: 1) to characterize the diagenetic features present and determine their distribution, 2) to determine the paragenetic sequence of diagenetic events in the study area through a detailed study of the diagenetic features present, 3) to



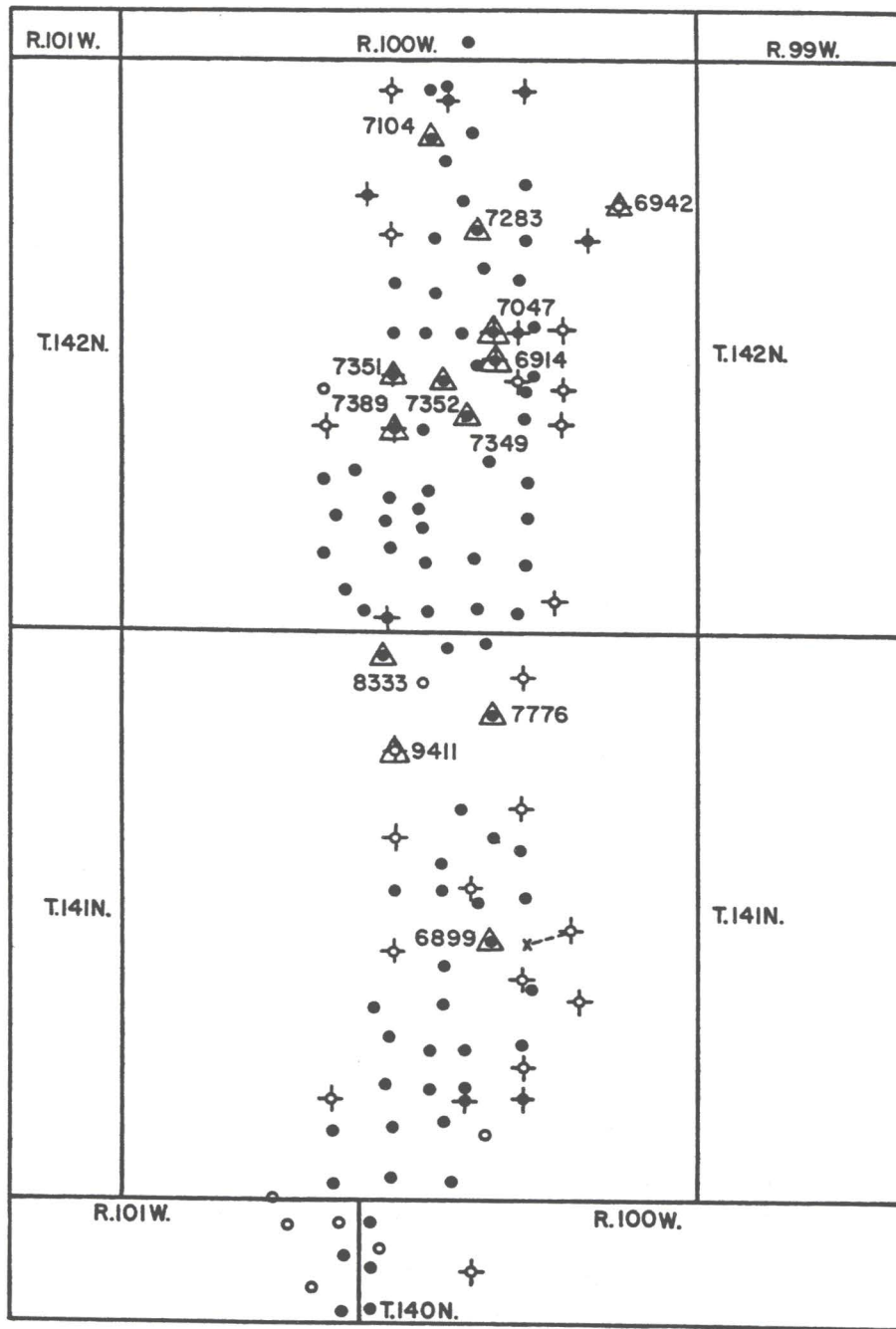
determine the distribution of pore types, and the geometry of the pores and pore throats using chips and pore casts with a high resolution scanning electron microscope, 4) evaluate the relation between paragenesis within the rocks and porosity development, and 5) interpret the diagenetic history of rocks in the study area using a combination of diagenetic features, paragenesis and porosity data.

#### Methodology

Cores used in this study are housed in the North Dakota Geological Survey's Wilson M. Laird Core and Sample Library located on the University of North Dakota Campus, Grand Forks. Approximately 260 metres (850 feet) of core from 13 wells taken from Treetop and Whiskey Joe fields were studied (Fig. 6; Appendix A). Cores ranged in length from 12 metres (42 feet) to 34 metres (112 feet), with an average of approximately 20 metres (65 feet). All cores occur stratigraphically within the lowermost Charles Formation and upper Mission Canyon Formation.

Approximately 150 wire-line logs within the study area and in the surrounding area were used to determine tops of relevant intervals and log-defined markers. The log-derived information was then incorporated into various isopach maps, structure maps, cross sections, and fence diagrams for correlation purposes. Gamma-ray, compensated neutron ( $\phi_N$ ), and formation density ( $\phi_D$ ) logs were used in conjunction with core and thin section data for correlation

Figure 6 Location of wells and described cores within the study area. Cores described in this study are indicated by a triangle and the corresponding North Dakota Geological Survey (NDGS) well number is given.



- Producer
- ✦ Dry Hole
- ✦--x Directional Hole
- ✦ Abandoned Producer
- Location
- △ Core Location

of lithologies, distribution of diagenetic features, and porosity mapping. Porosity isopach maps were constructed using compensated formation density logs and a critical porosity of 8 percent was chosen.

Selected cores were first slabbed, cleaned, and polished using 400 grit followed by 600 grit emery paper to obtain the best possible clarity and detail of the constituents. A reflected light microscope and a hand lens were used for macroscopic analysis of core. Cores are described as follows: core depth (log footage), textural name using Dunham's (1962) classification, mineralogy (in decreasing order of importance), color, allochems present (in decreasing order of abundance), depositional features, diagenetic features and, lastly, type and percent of estimated visual porosity present (Appendix B).

Approximately 270 core samples were taken from selected core intervals to be made into thin sections and to be used as core chips for scanning electron microscope (SEM) studies. All thin sections were impregnated with purple dyed epoxy to aid in distinguishing pore type, size and abundance as well as their relation to lithology and mineralogy. To distinguish calcite from dolomite, thin sections were stained in a solution of alizarin red S as described by Friedman (1959). Thin sections were described using a polarizing light microscope for detailed petrographic analysis, and a scanning electron microscope for difficult mineral identification and pore studies. A

microfiche reader was used to determine grain size and textural relations. Thin sections were described as follows: thin section (core footage), mineralogical modifiers (based on percent dolomite; dolomitic (10 to 39 percent), dolomitized (40 to 69 percent), and dolo- (70 to 100 percent), and other minerals present), allochems present, textural name, percent and type of minerals present (description of minerals in decreasing order of abundance), depositional features, diagenetic features, and percentage and type of pores present (Appendix B).

Diagenetic features are described according to Folk (1965), Longman (1980) and Wanless (1979). The terminology applied to porosity is that of Choquette and Pray (1970) and Wardlaw (1976). Carbonate textural terminology used is that of Dunham (1962) with modifiers described by Folk (1959); anhydrites are described using Maiklem and others (1969).

One hundred and thirty-five sample chips were prepared for pore cast and morphological mineral studies under the scanning electron microscope. Sample chips were taken from the same stratigraphic interval as corresponding thin sections for comparison studies of pores and diagenetic features. Samples were first broken into pieces approximately 1 centimetre (0.5 inches) in diameter. One piece from each sample was used to study mineral morphology and one was prepared for pore cast studies. To achieve the best possible adhesion of coating for scanning electron

microscopy and to prepare rock chips for impregnation, hydrocarbons were removed from the rock chips. Hydrocarbon removal was achieved using methylene chloride in a Soxhlet extractor.

The process for impregnating rock chips was developed with assistance from Dr. Robert J. Stevenson (Director, Natural Materials Analytical Laboratory) in order to produce the best pore casts for electron microscope studies. A detailed description of the procedure used for making pore casts is given in Appendix C.

Although microprobe studies were not a major concern of this project, it was necessary to set up carbonate standards in order to determine the chemistry of unknown minerals. Many minerals could not be identified using a standard light microscope and had to be probed for an accurate determination of their mineralogy.

## LITHOTYPE DESCRIPTIONS

### Introduction

As part of this study, rocks of the upper Mission Canyon Formation and lowermost Charles Formation within the study area have been separated into six lithotypes. These lithotypes (in ascending order) are: 1) the Echinoderm Wackestone Lithotype, 2) the Dolomudstone Lithotype, 3) the Neomorphic Wackestone Lithotype, 4) the Intraclast Bioclast Wackestone Packstone Lithotype, 5) the Laminated Mudstone Lithotype and 6) the Anhydrite Lithotype. Each lithotype was defined on the basis of an abundance of a group of features common to a set of rocks and which together, differentiate these rocks from other rocks. The dominant allochems or dominant features were then used as descriptive modifiers when giving each lithotype a name. Table 1 illustrates the features common to each lithotype. Figure 7 illustrates the stratigraphic distribution of lithotypes.

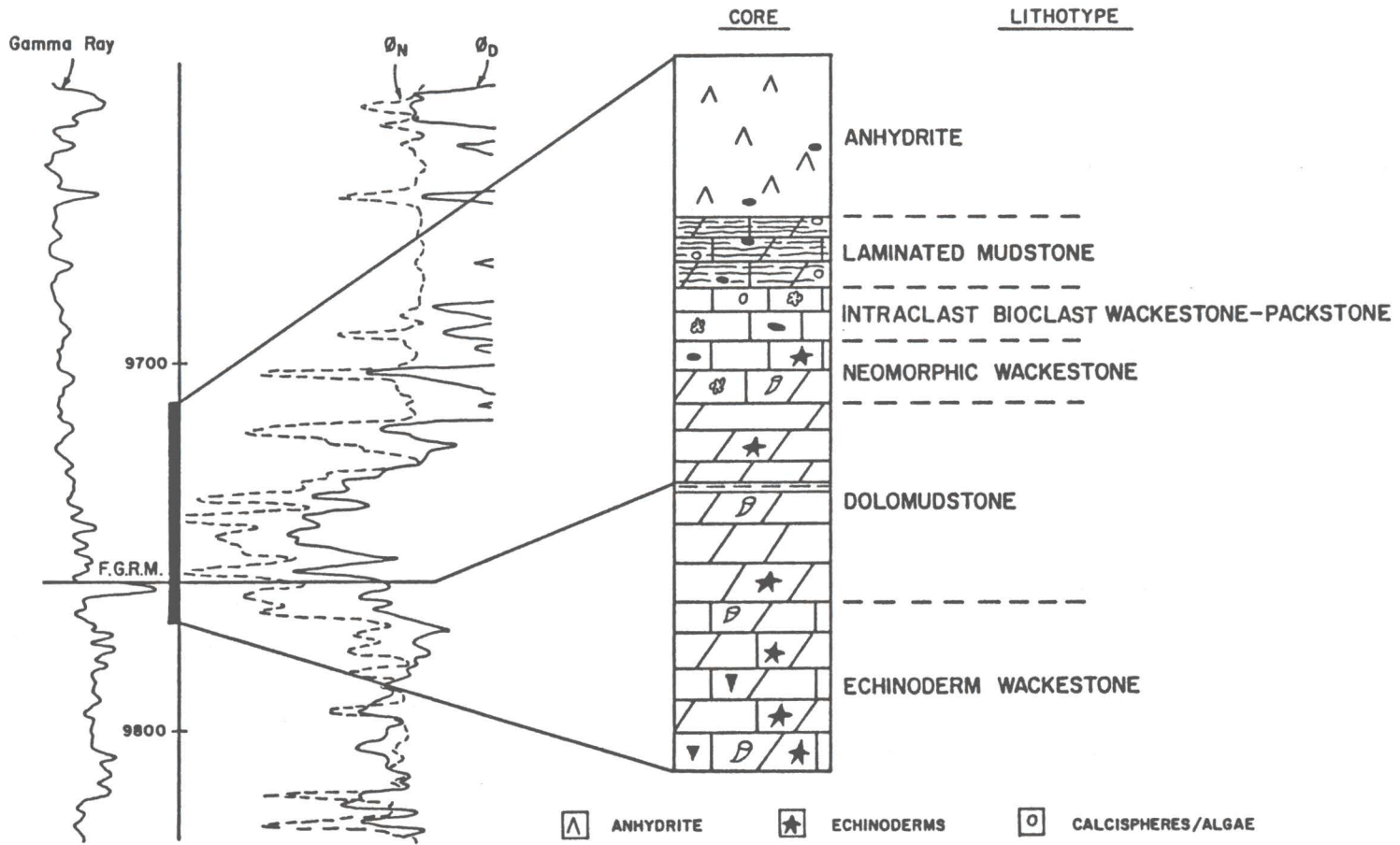
### Echinoderm Wackestone Lithotype

Rocks of the echinoderm wackestone lithotype are present in 5 cores and range in thickness from 1 to 11 metres (4 to 37 feet), averaging 5 metres (17 feet) thick. Rocks of this lithotype are commonly dark gray to black limestone and dolomitic limestone. Textures present in this lithotype include wackestones, mudstones and

Figure 7 Typical log responses (gamma ray, compensated neutron log ( $\phi_N$ ), and compensated formation density log ( $\phi_D$ )) and corresponding composite core illustrating the stratigraphic distribution of lithotypes. The Fryburg gamma-ray marker is represented by F. G. R. M. on this figure.



NDGS 7104  
 RODAKOWSKI #1  
 SE SW, SEC. 3, T142N, R100W



- |   |                     |   |             |   |                     |
|---|---------------------|---|-------------|---|---------------------|
| △ | ANHYDRITE           | ★ | ECHINODERMS | ○ | CALCISPHERES/ALGAE  |
| □ | LIMESTONE           | ∂ | CORALS      | ● | PELOIDS/INTRACLASTS |
| ▧ | DOLOSTONE           | ▽ | BRACHIOPODS | ▨ | LAMINATIONS         |
| ▩ | DOLOMITIC LIMESTONE | ⊕ | FORAMS      |   |                     |

Table 1 Petrographic summary of lithotypes. Abbreviations used in Table 1 are as follows: anhy=anhydrite, art=articulated, cal=calcite, colms=columns, crin plts=crinoid plates, deform=deformation, diam=diameter, disart=disarticulated, fen fab=fenestral fabric, frags=fragments, lg=long, micr=micritization, repl=replacement, sad dolo=saddle dolomite, sed=sediment, surfs=surfaces, syntax over=syntaxial overgrowths, and vert=vertical

TABLE 1 PETROGRAPHIC SUMMARY  
OF LITHOTYPES

ALLOCHEMS	ECHINODERM WACKESTONE	DOLOMUDSTONE	NEOMORPHIC WACKESTONE
Echinoderms	Abundant; crin plts, colms; up to 3mm lg	Rare; crin plts; up to 2mm lg	Common; crin plts, colms; up to 3mm lg
Corals	Common; rugose, tabulate frags; up to 10cm lg	Rare; rugose, tabulate frags; up to 6cm lg	Common; rugose frags; up to 2cm lg
Brachiopods	Common; disart frags; up to 10mm lg	-	Rare; disart frags; up to 7mm lg
Bryozoans	Rare; fenestrae frags; up to 5cm lg	-	Rare; fenestrae frags; up to 5cm lg
Molluscs	Rare; frags; up to 2mm lg	-	-
Forams	Rare; benthic; up to 1mm in diam	-	Rare; benthic; up to 1mm in diam
Ostracodes	Rare; disart; 0.5 to 1mm lg	Rare; art, disart; up to 1mm lg; anhy, sad dolo repl	Rare; disart; 0.5 to 1mm lg
Calcispheres	-	-	Rare; up to 0.3mm in diam
Algae	-	-	-
Intraclasts	-	-	-
Peloids	-	-	Rare; subrounded; up to 0.5mm in diam
Pellets	-	-	-
DEPOSITIONAL FEATURES			
Laminations	Common; organic wisps	-	Common; organic wisps
Bioturbation/ Burrows	Rare; random orientated burrows; minor chert repl	Abundant; lg vert burrows to homogenized	Common; small burrows to homogenized
Dessication Cracks	-	-	-
Other Features	-	-	-

TABLE 1 (continued)

ALLOCHEMS	INTRACLAST BIOCLAST WACKESTONE PACKSTONE	LAMINATED MUDSTONE	ANHYDRITE
Echinoderms	Rare; crin plts, colms; up to 3mm lg; syntax over	-	-
Corals	Rare; rugose, tabulate frags; up to 1.5cm lg	-	-
Brachiopods	Rare; frags, spines; up to 3mm lg	-	-
Bryozoans	Rare; fenestrae frags; up to 1cm lg	-	-
Molluscs	Rare; gastropods, frags; up to 5mm lg	-	-
Forams	Common; benthic; 0.5 to 1mm lg	-	-
Ostracodes	Common; disart; up to 1mm in diam	Common; art, disart; up to 1mm in diam	Rare; disart; up to 1mm in diam
Calcispheres	Common; 0.1 to 0.3mm in diam; anhy, cal repl; micr	Common; 0.1 to 0.3mm in diam; anhy, cal repl	Rare; up to 0.3mm in diam
Algae	Common; green, frags; up to 3mm lg	Common; blue-green; occurs as laminae	Rare; blue-green frags; up to 1mm lg
Intraclasts	Common; up to 3mm lg	-	Rare; up to 2mm lg
Peloids	Abundant; rounded; up to 2mm in diam	Common; rounded; up to 1.5mm in diam	Rare; rounded; up to 1mm in diam
Pellets	-	Rare; up to 0.1mm in diam	-
DEPOSITIONAL FEATURES			
Laminations	Rare; graded bedding (?); up to 1.5mm thick	Abundant; flat to cryptalgal wavy; 1 to 20cm thick	Common; massive to nodular-bedded; distorted
Bioturbation/ Burrows	-	-	-
Dessication Cracks	-	Common; associated with cryptalgal laminae	-
Other Features	-	Rare; fen fab; up to 2mm lg scour surfs; soft sed deform	-

packstones (Fig. 8). Common allochems within the echinoderm wackestone lithotype include both whole and broken skeletal material. The most abundant skeletal grains are disarticulated echinoderms (mainly crinoid plates and columnals) (Fig. 8). Other allochems include (in decreasing order of abundance): brachiopod fragments, whole coral and coral fragments (tabulate (Syringopora) and rugosan), unidentifiable bioclasts and rare bryozoan fragments (Fig. 9; Table 1).

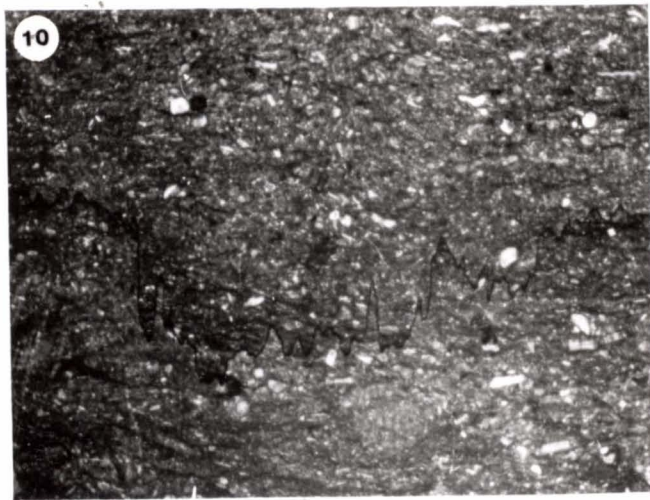
Calcite is present in amounts ranging from 30 to 60 percent, occurs as micrite, allochems and, rarely, cement. Microspar and pseudospar are present but not common. Dolomite comprises less than 40 percent of the rock and is present as scattered subhedral to euhedral rhombohedrons 20 to 50 micrometres in size. Some dolomite is associated with stylolites. Anhydrite, in amounts of less than 10 percent, is present as allochem replacements or as cement. Chert, in amounts less than 10 percent, is present as discrete nodules with intercalated dolomite and calcite.

Bioturbation is commonly associated with dolomitic rocks. Compaction is prevalent throughout this lithotype. Compaction features include horizontally aligned skeletal fragments, draped appearance around allochem, and broken allochems (Fig. 9). Small stylolites less than 4 millimetres (0.16 inches) in amplitude are present and are commonly associated with compaction features (Fig. 10). Grain contact sutures are common between echinoderm grains.

Figure 8 Core photograph of the echinoderm wackestone lithotype. NDGS Well Number 7351 at 2950 metres (9679 feet). Bar scale is 1 centimetre (0.4 inches).

Figure 9 Core photograph of the echinoderm wackestone lithotype showing compaction (draped appearance around rugose corals). NDGS Well Number 7351 at 2953 metres (9687 feet). Bar scale is 1 centimetre (0.4 inches).

Figure 10 Core photograph of the echinoderm wackestone lithotype with stylolite. NDGS Well Number 7351 at 2957 metres (9701 feet). Bar scale is 1 centimetre (0.4 inches).



Microstylolites are most abundant in calcareous rocks. Filled fractures are present rarely.

Pore types include intercrystalline, interparticle, intraparticle, and rare vuggy. Porosity is highest in the dolomitic mudstones and wackestones.

#### Dolomudstone Lithotype

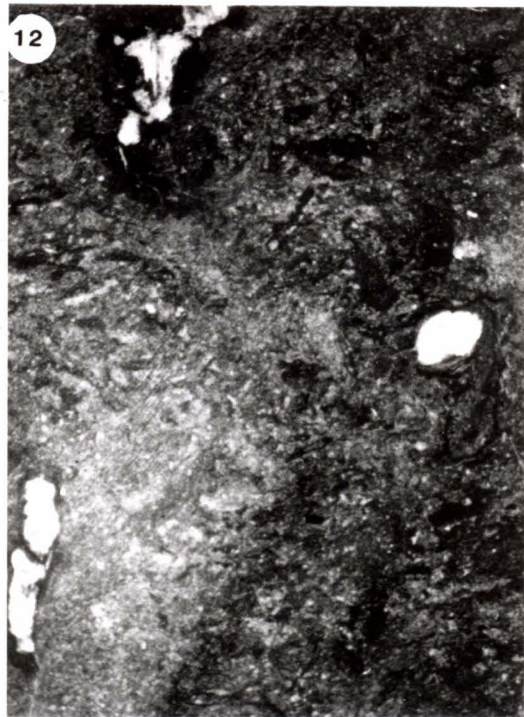
Rocks of the dolomudstone lithotype are present in all 13 studied cores. The thickness of this lithotype varies from 2 to 11 metres (7 to 37 feet) and averages 6 metres (21 feet). The dolomudstone lithotype is dominated by medium to dark brown dolostone and calcareous dolostone. Textures present in this lithotype include mudstones and occasional wackestones (Figs. 11, 12). Allochems found in this lithotype include (in decreasing abundance) echinoderms (disarticulated crinoid plates and columnals), unidentifiable bioclasts and rugosan corals (up to three centimetres) (Table 1). Allochems are most common in the less dolomitic wackestones.

Euhedral to subhedral dolomite rhombohedrons 10 to 100 micrometres in size make up between 50 to 99 percent of the rock. Dolomite commonly occurs as a pervasive matrix replacement. Replacement of allochems by saddle dolomite and saddle dolomite cement are observed occasionally. Calcite occurs sporadically in amounts up to 30 percent, usually less than 10 percent. Poikilitic calcite cement occludes intercrystalline pores and replaces allochems and matrix (dedolomitization). Anhydrite, generally less than



Figure 11 Core photograph of the dolomudstone lithotype showing abundant porosity. NDGS Well Number 8333 at 2875 metres (9431 feet). Bar scale is 1 centimetre (0.4 inches).

Figure 12 Core photograph of the dolomudstone lithotype showing calcite and anhydrite-replaced burrows. NDGS Well Number 8333 at 2869 metres (9413 feet). Bar scale is 1 centimetre (0.4 inches).



10 percent, is present as an allochem replacement and a vug-filling cement. Calcite, anhydrite and saddle dolomite-filled vugs, 1 millimetre to 2 centimetres (0.04 to 0.8 inches) in width may be surrounded by authigenic pyrite.

Bioturbation is very common and has resulted in a relatively homogeneous appearing rock with occasional, scattered, vertical to subvertical burrows (Fig. 12). Small calcite and anhydrite-filled vertical fractures are occasionally present. Black, wispy stringers and microstylolites are abundant. Large stylolites, up to 6 centimetres (2.4 inches) in amplitude, are present but not common. Angular to subangular quartz silt is generally present in trace amounts except where it has been concentrated in thin, horizontal zones. The Fryburg gamma ray marker, stratigraphically located within this lithotype, represents one such zone of concentration.

The Fryburg gamma-ray marker is commonly 2 to 8 centimetres (1 to 3 inches) in height. Angular quartz silt (20 to 25 percent), clay (50 to 55 percent, generally concentrated along stylolites), dolomite (15 to 20 percent) and trace amounts of rutile, apatite, and potassium feldspar comprise the marker.

The percentage of porosity is higher in the dolomudstone lithotype than other lithotypes. Porosity ranges from 5 to 30 percent and averages from 10 to 15 percent. Intercrystalline, vuggy and moldic pores are the

most common pore types. The greatest porosity occurs where poikilitic calcite cementation of intercrystalline pores is sparse or absent. Rocks of the dolomudstone lithotype are commonly oil stained.

#### Neomorphic Wackestone Lithotype

Rocks of the neomorphic wackestone lithotype are present in 11 cores. Thickness of this lithotype varies from 0.6 to 7 metres (2 to 23 feet) and averages 4 metres (12 feet) thick. The neomorphic wackestone lithotype is composed of dark brown to dark gray limestones and dolomitic limestones. Common textures include wackestones, packstones and mudstones (Fig. 13). Whole and broken allochems present include (in decreasing order of abundance): echinoderms (disarticulated crinoid columnals and plates), subrounded, micritic peloids (up to 0.5 millimetres), brachiopod fragments, coral debris, forams, calcispheres, unidentifiable bioclasts, and rare fenestrate bryozoan fragments (Table 1).

Calcite, ranging from 30 to 80 percent, comprises a majority of the matrix and allochems present. Euhedral dolomite rhombohedrons (20 to 60 micrometres in size) are scattered throughout the matrix, usually in amounts less than 40 percent. Minor amounts of blocky anhydrite cement are present locally.

Bioturbation is present in mudstones and some wackestones with small burrows commonly preserved (Fig. 14). Compaction is not common. Microspar and pseudospar

Figure 13 Core photograph of the neomorphic wackestone lithotype with stylolite. NDGS Well Number 7283 at 2947 metres (9669 feet). Bar scale is 1 centimetre (0.4 inches).

Figure 14 Core photograph of the neomorphic wackestone lithotype with small burrows (arrows). NDGS Well Number 8333 at 2861 metres (9387.5 feet). Bar scale is 1 centimetre (0.4 inches).



commonly replace matrix, allochems, and dolomite rhombohedrons. Dedolomitization occurs throughout this lithotype and appears closely associated with neomorphism. Small, calcite- or anhydrite-filled vugs are present in some cores. Calcite-filled fractures are common (Fig. 15). Microstylolites, rare stylolites, and black wispy stringers and laminations are present.

Pore types found in the neomorphic wackestone lithotype include intercrystalline, vuggy, and rare interparticle and intraparticle. Porosity generally does not exceed 5 percent of the rock.

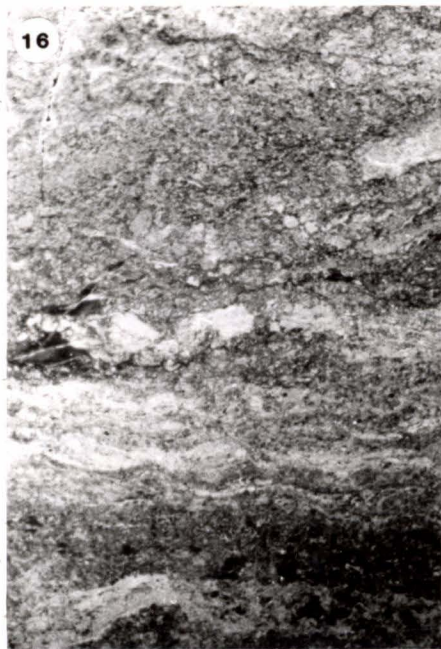
#### Intraclast Bioclast Wackestone Packstone Lithotype

Rocks of the intraclast bioclast wackestone packstone lithotype are present in 12 cores and range in thickness from 1 to 6 metres (3 to 20 feet) and average 3 metres (10 feet). Of all the lithotypes present in the study area, this lithotype exhibits the most textural variability. The intraclast bioclast wackestone packstone lithotype is commonly interbedded and gradational with the underlying neomorphic wackestone lithotype and the overlying laminated mudstone lithotype. Rocks of the intraclast bioclast wackestone packstone lithotype contain medium to dark brown limestones and dolomitic limestones. Textures present in this lithotype include wackestones, packstones and rare mudstones and grainstones (Fig. 16). Abundant allochems are present and include (in decreasing abundance):

Figure 15 Core photograph of the neomorphic wackestone lithotype with vertical, calcite-filled fractures. NDGS Well Number 7283 at 2948 metres (9671 feet). Bar scale is 1 centimetre (0.4 inches).

Figure 16 Core photograph of the intraclast bioclast wackestone packstone lithotype. NDGS Well Number 7283 at 2946 metres (9666 feet). Bar scale is 1 centimetre (0.4 inches).





unidentifiable bioclasts, intraclasts, peloids, foraminifers, ostracodes, calcispheres, and algae (Table 1).

Calcite ranges from 40 to 90 percent and is present as allochems, matrix, and isopachous, blocky, and syntaxial overgrowth cement. Dolomite rhombohedrons (less than 40 micrometres in size) comprise less than 30 percent of this lithotype and are found replacing allochems, matrix, and calcite cement locally. Anhydrite, usually in amounts less than 10 percent, replaces allochems, matrix, and calcite cement. Silica, in the form of chert and authigenic quartz, is present in amounts up to 40 percent and occurs in thin, distinct zones or as patchy, nodular replacements (Fig. 17). Chert commonly replaces matrix and allochems while authigenic quartz forms cement in grainstones and packstones.

Neomorphic spar is present locally. Stylolites and microstylolites are present but not common. Many allochems show varying degrees of micritization. Compaction features are rarely present. Fractures are calcite, anhydrite, or silica-filled.

Pore types include (in decreasing order of abundance): vuggy, moldic, intercrystalline, interparticle, and intraparticle. Porosity is generally less than 5 percent, with up to 15 percent porosity present locally.

Figure 17 Core photograph of the intraclast bioclast wackestone packstone lithotype showing a siliceous zone (S). NDGS Well Number 7283 at 2948 metres (9673 feet). Bar scale is 1 centimetre (0.4 inches)



### Laminated Mudstone Lithotype

Rocks of the laminated mudstone lithotype are present in 12 cores. The thickness of this lithotype varies from 0.6 to 10 metres (2 to 34 feet) and averages 4 metres (12 feet). Rocks of this lithotype are closely associated with overlying anhydrites and commonly grade into them. The laminated mudstone lithotype is composed of rocks which are light to medium brown dolostone, anhydritic dolostone, and calcareous dolostone. Textures in this lithotype include laminated mudstones, wackestones, and occasional packstones (Figs. 18, 19). Allochems present include (in decreasing order of abundance): peloids, ostracodes, calcispheres, intraclasts, algae, and unidentifiable bioclasts (Table 1).

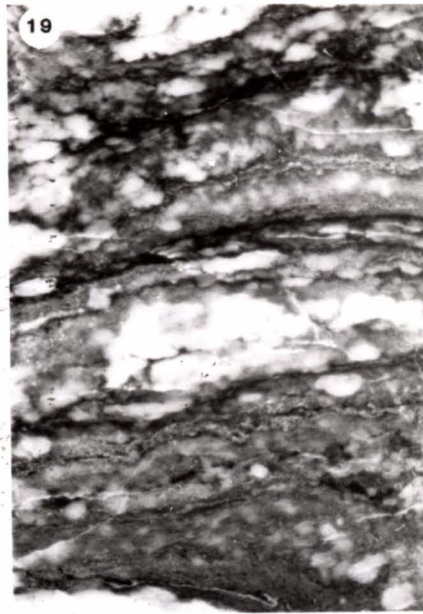
Subhedral to euhedral dolomite rhombohedrons (10 to 30 micrometres) occur as matrix and allochem replacement in amounts ranging from 20 to 90 percent (average 50 to 60 percent). Anhydrite, ranging from 10 to 50 percent, occurs as blocky and lath-shaped replacements of allochems and matrix (Fig. 20), and in displacive nodules within the dolomite matrix. Calcite, present in allochems and matrix, is found in amounts less than 30 percent (generally 10 to 15 percent). Silica, generally less than 10 percent, occurs as chert and authigenic quartz cement. Rare celestite occurs as cement and anhydrite replacement.

Rocks of the laminated mudstone lithotype are typically thinly bedded to laminated to cryptalgally laminated (Figs. 18, 19). Dessication cracks and rare

Figure 18 Core photograph of the laminated mudstone lithotype showing cryptalgal laminae and dessication cracks (arrows). NDGS Well Number 6942 at 2961 metres (9714.5 feet). Bar scale is 1 centimetre (0.4 inches).

Figure 19 Core photograph of the laminated mudstone lithotype showing displacive anhydrite nodules. NDGS Well Number 7283 at 2945 metres (9661 feet). Bar scale is 1 centimetre (0.4 inches).

Figure 20 Core photograph of the laminated mudstone lithotype with microstylolites (M) and lath-shaped anhydrite (arrows) replacement of matrix. NDGS Well Number 7283 at 2943 metres (9657 feet). Bar scale is 1 centimetre (0.4 inches).



fenestrae, associated with cryptalgal laminations, are filled with calcite or anhydrite (Figs. 18, 21). Soft sediment deformation occurs rarely.

Microstylolites and wispy, black stringers and laminations are common (Fig. 20). Stylolites occur rarely. Many allochems are partially to completely micritized. Fractures are filled with anhydrite, calcite, and rarely, celestite. Pores in this lithotype are limited to minor occurrences of moldic, vuggy, intercrystalline, intraparticle, and interparticle.

#### Anhydrite Lithotype

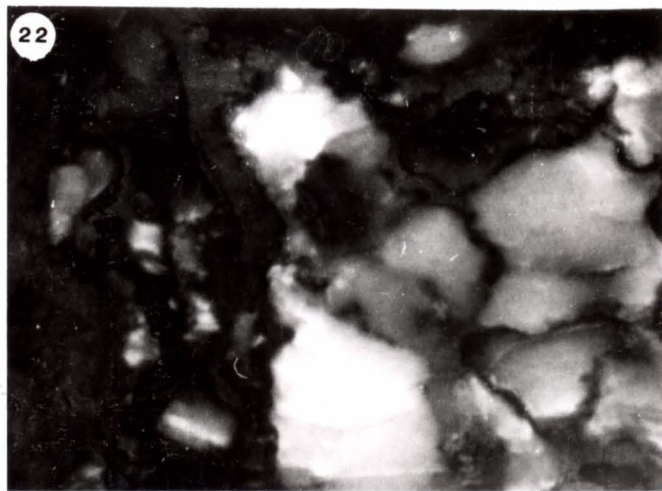
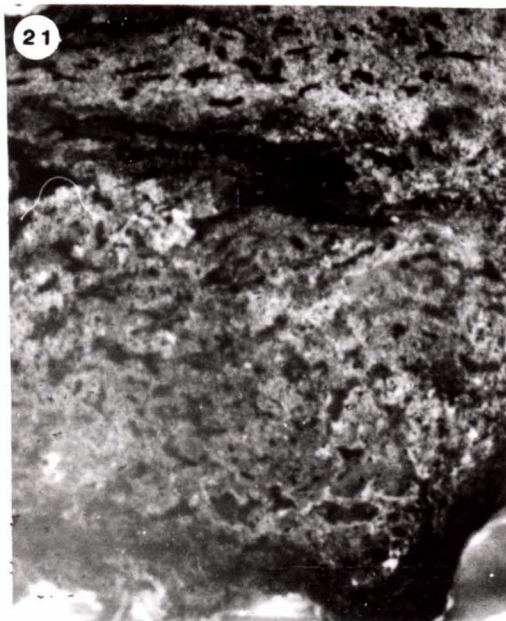
Rocks of the anhydrite lithotype consist of light gray, light olive gray, and tan anhydrite and anhydritic dolostone. Textures of this lithotype are predominantly mudstones (Fig. 22). Allochems are rare and locally include (in decreasing order of abundance): peloids, intraclasts, ostracodes, algae, and calcispheres (Table 1). Detrital gypsum crystals (now anhydrite) are abundant locally. Detrital quartz silt is present rarely. Rocks of this lithotype are present in 10 cores and range in thickness from 0.6 to 12 metres (2 to 38 feet), averaging 2 metres (7 feet).

Anhydrite ranges from 10 to 100 percent. Microscopically, the anhydrite has a fine-grained, felted texture. Nodular, bedded-nodular, massive, bedded-massive, mosaic, bedded-mosaic, and elongated, distorted nodular



Figure 21 Core photograph of the laminated mudstone lithotype showing anhydrite-filled fenestrae. NDGS Well Number 6942 at 2958 metres (9705 feet). Bar scale is 1 centimetre (0.4 inches).

Figure 22 Core photograph of the anhydrite lithotype showing nodular anhydrite displacement of matrix. NDGS Well Number 6942 at 2953 metres (9689 feet). Bar scale is 1 centimetre (0.4 inches).

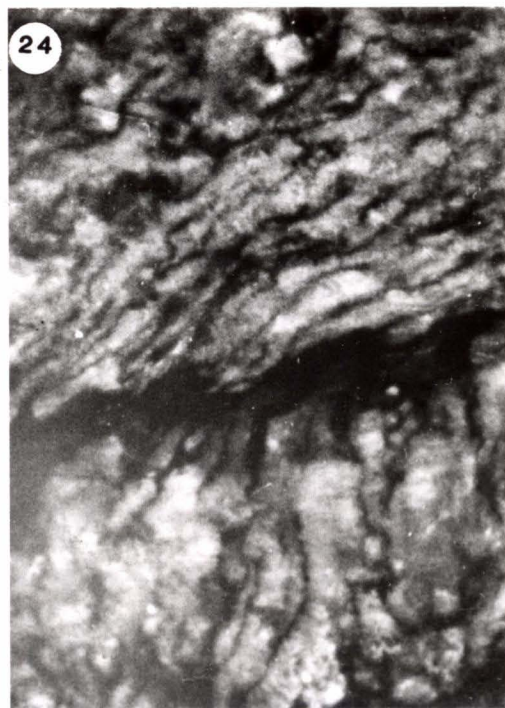
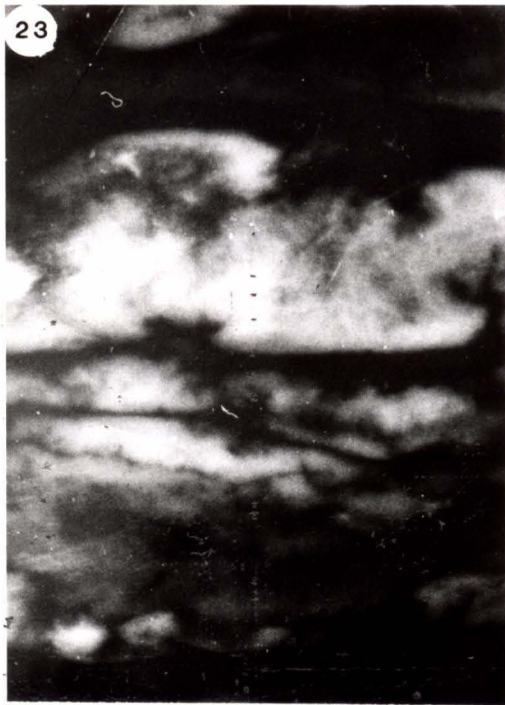


(swallowtail) megascopic textures are present (Figs. 22, 23, 24). Dolomite rhombohedra (less than 20 micrometres in size) range from 10 to 70 percent and occur as matrix and allochem replacements, and as contorted, wispy stringers within anhydrite. Silica, in the form of chert and authigenic quartz, is found in amounts less than 10 percent. Silica replaces dolomite matrix and allochems and, rarely, partially replaces anhydrite nodules. Celestite replacement of anhydrite is rare. Rocks of the anhydrite lithotype are not porous.

Figure 23 Core photograph of the anhydrite lithotype showing bedded-massive anhydrite texture. NDGS Well Number 6942 at 2968 metres (9738 feet). Bar scale is 1 centimetre (0.4 inches).

Figure 24 Core photograph of the anhydrite lithotype showing elongated, distorted, nodular (swallowtail) anhydrite texture. NDGS Well Number 6942 at 2962 metres (9717 feet). Bar scale is 1 centimetre (0.4 inches).

S  
Bar



## DEPOSITIONAL SETTING

Although deposition will not be discussed in detail in this report, an understanding of the depositional setting is necessary to accurately depict the diagenetic history and porosity development. Deposition controls the distribution of textures, original mineralogy, and the lateral and vertical relations of the rocks, factors which affect any subsequent changes in the rock.

A general setting for rocks within the study area is that of a broad, shallow epeiric sea. Although there are no true modern epeiric seas, evidence suggests they existed in the past. Epeiric seas lie within a continental landmass and are thought to have had bottom slopes of around 0.02 to 0.06 metres per kilometre (0.1 to 0.3 feet per mile). Generally, depths averaged less than 27 metres (90 feet) (Shaw, 1964; Irwin, 1965).

When discussing depositional environments in this section of the report, the terms sublittoral, littoral, and supralittoral, established by Hedgepeth (1957), will be used. Sublittoral refers to the area which is below low water and is continually submerged. Littoral refers to the area lying between high and low water where sediments are periodically submerged and exposed. The term supralittoral refers to the area above high water in which sediments are submerged only during periods of storm activity. Rocks within the study area were deposited mainly as a thick succession of sediments which represent a long period of

quiescent, sublittoral deposition. Progradation of littoral, supralittoral, and sabkha environments resulted in the deposition of a thin succession of sediments formed in those environments over previously deposited sublittoral sediments.

Shallow sublittoral sediments in the study area are commonly mud-rich and contain a variety of biota including echinoderms, brachiopods, rugose and tabulate corals, and bryozoans. These stenohaline biota are indicative of a well-oxygenated environment of normal salinity and circulation (Wilson and Jordan, 1983).

A decrease in circulation during deposition of sublittoral sediments resulted in a more restricted shallow sublittoral environment. These quiet waters contained fewer epifaunal organisms (echinoderms, ostracodes, and rugose corals), and the sediments containing the organisms were extensively bioturbated. Individual burrows are generally vertical to subvertical and are approximately 5 millimetres to 1 centimetre (0.2 to 0.4 inches) in width. The length of these burrows varies from 2 to 7 centimetres (0.8 to 2.8 inches).

Later in the depositional history of the area, echinoderm, brachiopod, coral, foraminifer, calcisphere and rare bryozoan biota existed in the shallow, sublittoral environment. Burrowing organisms were still present although burrows are smaller (less than 3 millimetres (0.1 inches) in width), fewer, and more nearly horizontal in

orientation than those discussed previously.

Small, intraclastic, bioclastic shoals were also developed on localized topographic highs within the shallow, sublittoral environment. Similar shoals have been reported to the east of the study area in Little Knife Field (Lindsay and Roth, 1982). Intershoal areas, containing mud-rich sediments, supported restricted biota. The presence of more euryhaline biota such as calcispheres, ostracodes, foraminifers, and algae as well as peloids and intraclasts, indicates a more restricted environment (Heckel, 1972).

Shallow sublittoral environments grade upward into a littoral flat environment. Numerous sedimentary structures including cryptalgal laminations, dessication cracks and rare fenestrae are present in this environment. Euryhaline biota including calcispheres and ostracodes, and peloids are present. The structures, along with the sparsity of biota, are indicative of littoral flat environments (Laporte, 1967; Laporte, 1969).

Within the studied section, the uppermost rocks are characterized by evaporative minerals, a lack of biota, peloids, and rare intraclasts, all of which indicate deposition in supralittoral and sabkha environments. The abundant anhydrite textures common in these rocks represent both subaerial and subaqueous evaporite deposition possibly in a supralittoral-sabkha environment indunated with evaporitic ponds.



## DIAGENESIS

### Introduction

All processes acting on carbonate sediments and rocks following final deposition but prior to entering the realm of metamorphism are considered to be diagenetic processes (Blatt and others, 1980). Rocks of the upper Mission Canyon and lower Charles Formations have undergone numerous diagenetic processes, and the results of these processes are evident in the diagenetic features present in the rocks. Diagenetic features in the upper Mission Canyon and lower Charles rocks of Treetop and Whiskey Joe Fields include micritization, compaction, dolomitization, cementation, replacement, fracturing, neomorphism, and pressure solution. The development of porosity by diagenetic processes will be considered in a separate chapter.

### Micritization

Micritization, as described originally by Bathurst (1966), is a three stage process of centripetal replacement of a carbonate grain by a stable micrite envelope. The first stage consists of penetration of the outer surface of a grain by boring organisms. Endolithic (boring) algae, mainly filamentous cyanophytes and chlorophytes, are the most common type of boring organism (Alexandersson, 1972; Kobluk and Risk, 1977; May and Perkins, 1979).

During the second stage, bores are vacated, usually following the death of the organisms. The final stage of

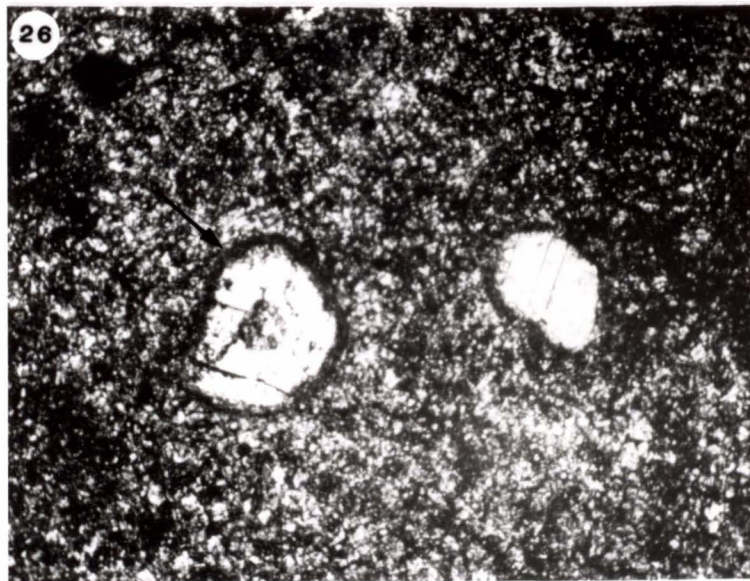
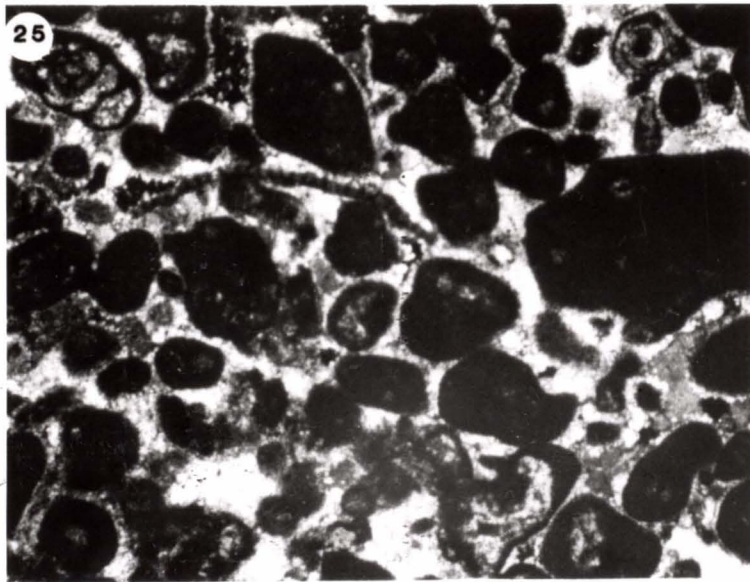
micritization results in the infilling of vacated bores by micrite. This process may continue until an envelope of micrite surrounds the carbonate grain. If the process is allowed to continue until completion, the entire carbonate grain will become micritized. Micritization is common at and below the sediment-water interface (May and Perkins, 1979). Carbonate grains which have undergone boring are weakened and are susceptible to mechanical abrasion, and carbonate grains which have been intensely bored generally exhibit a rounded appearance (Bathurst, 1975).

Allochems within the study area have undergone varying degrees of micritization. The neomorphic wackestone, intraclast bioclast wackestone packstone, laminated mudstone and anhydrite lithotypes all contain micritized allochems. Micritization in these lithotypes ranges from thin micritic envelopes around allochems to allochems which show nearly complete micritization (Figs. 25, 26).

Grainstones of the intraclast bioclast wackestone-packstone lithotype contain abundant micritized allochems. These allochems are generally subrounded to rounded due to the intense micritization (Fig. 25). Many of the peloids within this lithotype may represent carbonate grains that have undergone complete micritization which obliterated any of the original structures. Micrite envelopes surrounding bioclasts are common in the neomorphic wackestone lithotype, and complete micritization is occasionally present in these rocks. Micritic envelopes and completely

Figure 25 Photomicrograph (plane polarized) of intensely micritized allochems in the intraclast bioclast wackestone packstone lithotype. NDGS Well Number 6899 at 2886 metres (9469 feet). Bar scale is 1 millimetre (0.04 inches).

Figure 26 Photomicrograph (crossed nichols) of thin, micritic envelopes (arrow) surrounding anhydrite-replaced allochems in the laminated mudstone lithotype. NDGS Well Number 7351 at 2933 metres (9623.5 feet). Bar scale is 0.5 millimetres (0.02 inches).



micritized allochems occur mainly between cryptalgal laminations of the laminated mudstone lithotype. Within the anhydrite lithotype, micritization is limited to thin micritic envelopes surrounding anhydrite-replaced allochems (Fig. 26).

#### Compaction

Mechanical compaction is the physical compression of rocks and is generally a result of overburden pressures. Beach and Schumacher (1982) stated evidence for mechanical compaction which includes: 1) horizontal aspects of mottling (burrows), 2) horizontal orientation of fossil fragments, 3) the presence of drag, drape and penetration features, 4) broken and crushed fossils, and 5) the presence of microstylolitic "horsetail" swarms. Laboratory experiments by Shinn and Robbin (1983) on artificial compaction of cores of mud sediments resulted in the reduction of sediment thickness, the loss of porosity, the creation of textures very similar to those found in ancient mudstones and wackestones, the creation of organic, wispy "stylolite-like" layers, grain penetration or early chemical compaction, and flattened burrows.

Mechanical compaction features in the present study are found within rocks of the echinoderm wackestone and dolomudstone lithotypes and occasionally in the neomorphic wackestone and laminated mudstone lithotypes. Evidence for mechanical compaction in the echinoderm wackestone lithotype includes the draping of features around grains or

burrows, fossil fragments broken in place, and possibly the horizontal orientation of some fossil grains (mainly ostracodes and brachiopods) (Fig. 27). Black wispy laminations and stringers within the dolomudstone lithotype and, occasionally, the laminated mudstone and the neomorphic wackestone lithotypes also present possible evidence for compaction in the studied section (Figs. 12, 14). These black, wispy stringers and laminations resemble microstylolites and are commonly associated with them.

Initial porosity in the lower three lithotypes was greatly reduced by compaction. No evidence of porosity reduction due to compaction was found in the upper three lithotypes.

#### Dolomitization

According to Folk and Land (1975), the mineralogy, crystal size, and crystal habit of dolomite are influenced by the concentration and ionic composition of the natural solutions from which they precipitated. The shape and size of dolomite crystals are also influenced by the density of nucleation sites and the mechanism of crystal growth (Gregg and Sibley, 1984). Sibley (1982) concluded that micrite is the most favorable substrate for dolomitization because the high surface area provides abundant nucleation sites for the dolomitization process to begin. Early dolomitization is generally confined to fine-grained sediments but will eventually replace coarser-grained material (Harris and others, 1985).

Figure 27 Photomicrograph (crossed nichols) of broken, horizontally aligned skeletal fragments in the echinoderm wackestone lithotype. NDGS Well Number 6914 at 2936 metres (9634 feet). Bar scale is 0.5 millimetres (0.02 inches).



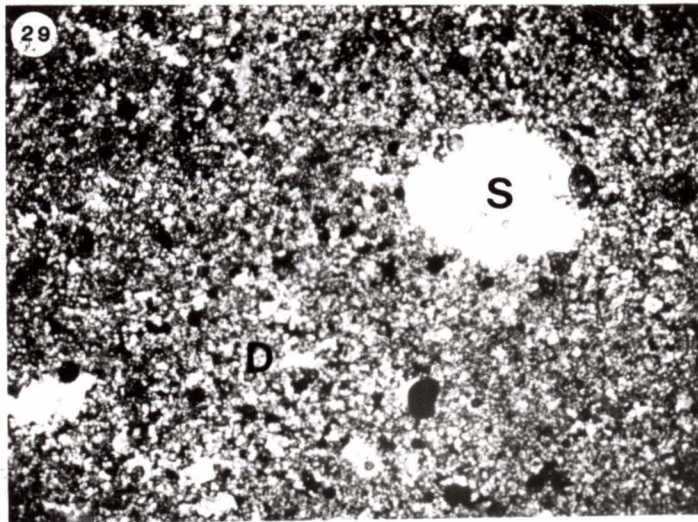
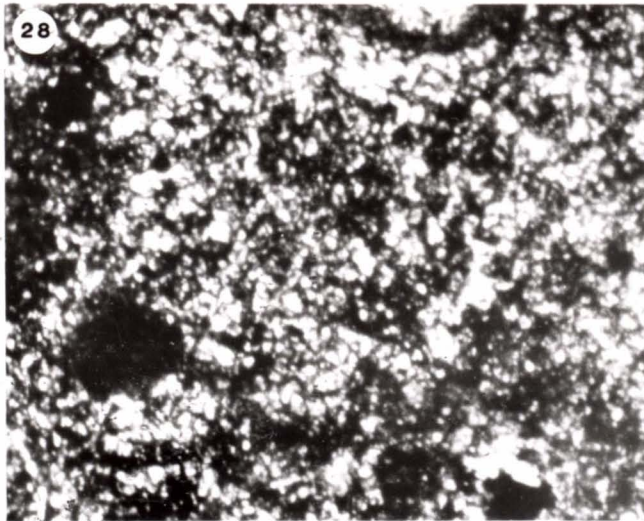


Dolomitization is the most important diagenetic process to affect Mission Canyon rocks of Treetop and Whiskey Joe fields. Rocks of all the lithotypes have undergone dolomitization to some degree, although the originally uncemented, mud-rich sediments were most easily dolomitized by the magnesium-rich fluids. Three types of dolomite, based on crystal size and shape, are present in the studied section. They are: 1) microcrystalline dolomite (euhedral to subhedral, less than 15 micrometres in size) (Fig. 28), 2) sucrosic dolomite (euhedral to anhedral, 15 to 100 micrometres in size) (Fig. 29), and 3) saddle dolomite (anhedral, variable in size depending on size of pore or allochem being filled or replaced) (Fig. 29).

Microcrystalline dolomite is common as thin stringers within the anhydrite lithotype, as replacement of laminae and cryptalgal laminae within the laminated mudstone lithotype, and as replacement of matrix in the dolomudstone lithotype. Sucrosic dolomite is common in all lithotypes except the anhydrite lithotype. It occurs as scattered, euhedral to anhedral crystals replacing matrix and/or allochems within the echinoderm wackestone, the neomorphic wackestone, the intraclast bioclast wackestone packstone, and the laminated mudstone lithotypes. Euhedral, sucrosic dolomite replaces matrix in the dolomudstone lithotype. Saddle dolomite is commonly found in the dolomudstone lithotype and less commonly in the neomorphic wackestone

Figure 28 Photomicrograph (crossed nichols) of microcrystalline dolomite in the laminated mudstone lithotype. NDGS Well Number 7351 at 2933 metres (9623.5 feet). Bar scale is 0.5 millimetres (0.02 inches).

Figure 29 Photomicrograph (crossed nichols) of sucrosic (D) and saddle dolomite (S) in the dolomudstone lithotype. NDGS Well Number 7776 at 2893 metres (9490 feet). Bar scale is 0.5 millimetres (0.02 inches).



(D)  
ces  
02

and intraclast bioclast wackestone packstone lithotypes as an allochem replacement and as pore-filling cement (see sections on saddle dolomite cementation and replacement for further discussion).

Numerous models explaining the processes of dolomitization are present in the literature. Dolomitization models include primary precipitation, seepage reflux, fresh water-marine water mixing, solution cannibalism, evaporative and algal processes (including evaporative pumping), and deep burial processes. Of these models, evaporative and algal processes, seepage reflux, mixing, and deep burial processes appear to have operated within the study area and formed the dolomite present.

Penecontemporaneous replacement of Recent sediments by dolomite occurs by evaporative processes (Illing and others, 1965; Shinn and others, 1965; McKenzie and others, 1980) in arid, hypersaline supralittoral environments. As evaporation of marine waters increases landward, salinities rise, evaporite minerals begin to form, and the Mg/Ca ratio of the fluids increases. When the Mg/Ca ratio exceeds 10:1, dolomite replacement of the sediment can occur (Folk and Land, 1975). Modern dolomites which form in this manner are generally cryptocrystalline to microcrystalline in size (less than 5 micrometres) and are present from depths of a few inches to a few feet (less than 1 metre) below the surface (Illing and others, 1965). Experimental studies by Hsu and Siegenthaler (1969) suggest evaporite

crusts may form by a process termed "evaporative pumping" where fluids trapped between grains in tidal flat areas will evaporate causing a concentration of ions and eventually the precipitation of gypsum and dolomite. Within the anhydrite lithotype, the close association of microcrystalline dolomite and evaporative minerals suggests these dolomites probably formed by penecontemporaneous replacement and evaporative processes in a hypersaline, supralittoral environment.

Most of the dolomite found in the upper Mission Canyon Formation in Treetop and Whiskey Joe fields was formed by a seepage reflux process similar to that described by Adams and Rhodes (1960), Deffeyes and others (1965), and Sears and Lucia (1980). Adams and Rhodes (1960) attributed the distribution of Permian dolomites in West Texas to seepage reflux. Adams and Rhodes, in order to explain their dolomite distribution, suggested a model in which high evaporation in coastal lagoons concentrated sea water, increased the density of the water, and allowed gypsum precipitation to occur. Gypsum precipitation removed calcium ions from the water and thus increased the Mg/Ca ratio of the brine. The combination of an increased density difference and the development of a hydraulic head created conditions which allowed the heavy brines to seep downward into the underlying carbonate sediment, displace the less dense pore waters, and dolomitize large quantities of carbonate sediment. A continuous supply of magnesium

ions was provided to the evaporitic water bodies by waters flowing in from the open ocean. A similar dolomitization process was suggested for dolomites in Big Stick and T. R. fields, Billings County (Stephens, 1986) adjacent to Treetop and Whiskey Joe fields.

Microcrystalline and sucrosic dolomites of the sublittoral, echinoderm wackestone, dolomudstone, and neomorphic wackestone lithotypes were formed mainly by seepage reflux of dense, surface-derived brines originating in water bodies located in the supralittoral sediments (anhydrite lithotype) and percolating downward. Magnesium ions were continually replenished from waters flowing in from the open sea. Early cementation of the allochem-rich, sublittoral and littoral sediments (mainly packstones and grainstones of the intraclast bioclast wackestone packstone lithotype and laminated mudstone lithotypes) may have inhibited the influx of dolomitizing fluids through these sediments and thus prevented dolomitization from affecting them.

The original composition and texture of the reflux dolomites, no longer present, suggests that the original dolomites underwent stabilization and enlargement later in their diagenetic history. Continued dolomite growth, especially in the dolomudstone lithotype, led to the development of a complex system of pore geometries (see section on pore geometry for further discussion).

Fresh water-marine water mixing in the shallow

subsurface is responsible for a small percentage of the sucrosic dolomite in the intraclast bioclast wackestone packstone and neomorphic wackestone lithotypes. The zone of mixing creates conditions of great variability in fluid composition and position (Harris and others, 1985).

Seawater sulfate concentration may significantly inhibit dolomite precipitation under experimental conditions (Baker and Kastner, 1981). In mixing zones, sulfate concentration may be reduced by dilution, allowing dolomite to form (Ward and Halley, 1985). Limpid, euhedral dolomite is evidence of precipitation of dolomite in mixed water with relatively low Mg/Ca ratio (Folk and Siedlecka, 1974; Folk and Land, 1975; Weaver, 1975; Ward and Halley, 1985).

Deep burial processes may have produced a minor amount of sucrosic and saddle dolomite in the study area. These sucrosic dolomites are concentrated along stylolites and microstylolites. Wanless (1979) stated that dolomite may form in association with stylolites if a significant amount of magnesium ions are released during pressure solution. Beales and Hardy (1980) and Ward and Halley (1985) suggest that saddle dolomite may form following the dissolution and removal of sulfate by migrating, basin-derived, sulfate-depleted solutions. Saddle dolomite in the study area was largely controlled by an influx of fresher water late in the diagenetic history. Fresher waters migrating updip through the basin into the porous dolomudstone lithotype

could have effectively removed sulfate and created mixing conditions between the fresher waters and the more saline pore waters. The removal of the inhibiting sulfate, coupled with a source of magnesium ions, would have allowed the subsequent precipitation of saddle dolomite to occur.

### Cementation

Cement is defined as the chemically precipitated material filling pores between or within grains (Longman, 1981). Cement is found in all lithotypes except the anhydrite lithotype. Cements consist of calcite, anhydrite, silica, dolomite, and, rarely, pyrite. Calcite cements include isopachous coatings on allochems, blocky pore-filling, rare syntaxial overgrowths, and poikilitic pore-filling varieties.

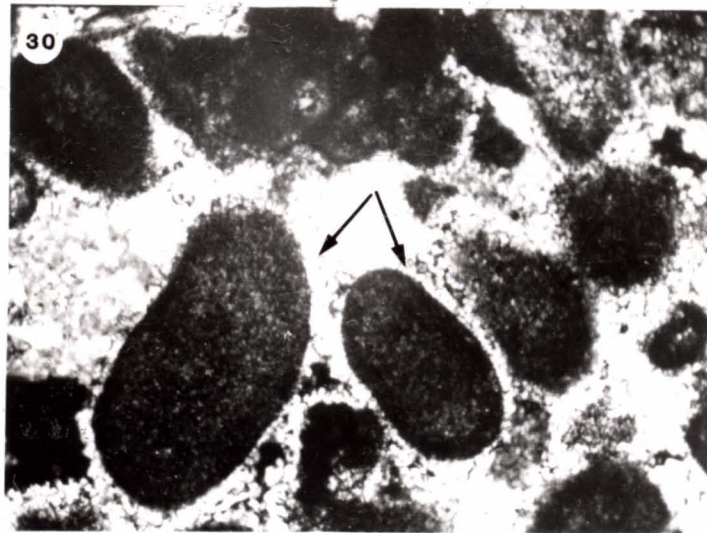
Isopachous calcite cement is rare in the study area and is restricted to grainstones of the intraclast bioclast wackestone packstone lithotype (Fig. 30). Similar cements found forming in modern shallow marine environments are composed of fibrous aragonite or bladed magnesium calcite (Harris and others, 1985; Bathurst, 1975).

Blocky calcite commonly forms in phreatic meteoric, mixing, and marine zones (Folk, 1974; Given and Wilkinson, 1985; Harris and others, 1985). Folk (1974) suggests that under mixing conditions, the seawater filling pores is displaced by fresher waters, magnesium is selectively lost, the Mg/Ca ratio is reduced, and coarse, sparry calcite cement is precipitated. Given and Wilkinson (1985),



Figure 30 Photomicrograph (plane polarized) of isopachous calcite cement (arrows) rimming peloids in the intraclast bioclast wackestone packstone lithotype. NDGS Well Number 6899 at 2886 metres (9469 feet). Bar scale is 0.5 millimetres (0.02 inches).

ous  
ne  
res  
02



however, state that it is the availability of carbonate ions and not magnesium which controls the morphology of calcite crystals. Generally, the less the agitation and the lower the flow velocities through the pores, along with a lesser degree of carbonate saturation, the more equant the calcite crystals will become (Given and Wilkinson, 1985; Harris and others, 1985).

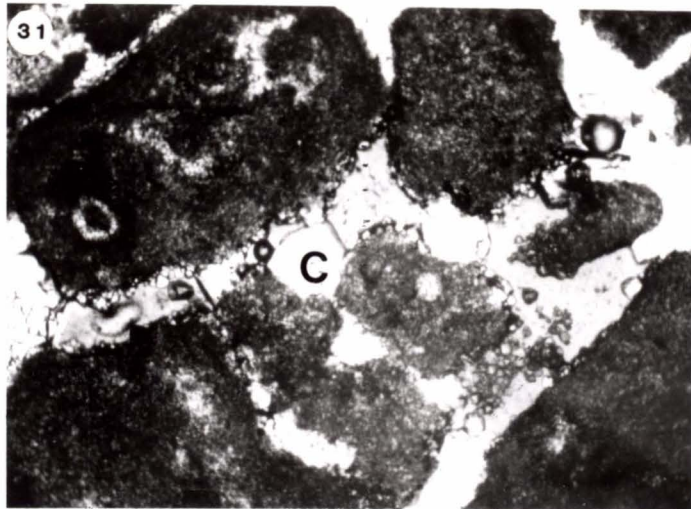
Blocky calcite cement occludes interparticle pores within grainstones of the intraclast bioclast wackestone packstone lithotype where the blocky calcite crystals commonly extend from pore edges and lie against the earlier-formed isopachous marine cements (Fig. 31). Fractures of the echinoderm wackestone and neomorphic wackestone lithotypes and intraparticle pores of the neomorphic wackestone, intraclast bioclast wackestone packstone, and laminated mudstone lithotypes may also contain blocky calcite cement. Blocky calcite cement in the study area may have formed as a result of precipitation from calcite-saturated, meteoric waters infiltrating the sediment during periodic rainstorms. Blocky calcite may also have precipitated from marine waters. Isopachous grain coatings around some grains may have reduced the amount of fluid movement through the grainstones and allowed the precipitation of blocky calcite to occur.

Syntaxial overgrowths are rare in the study area and are limited to unmicritized echinoderm grains of the intraclast bioclast wackestone packstone lithotype (Fig. 32).

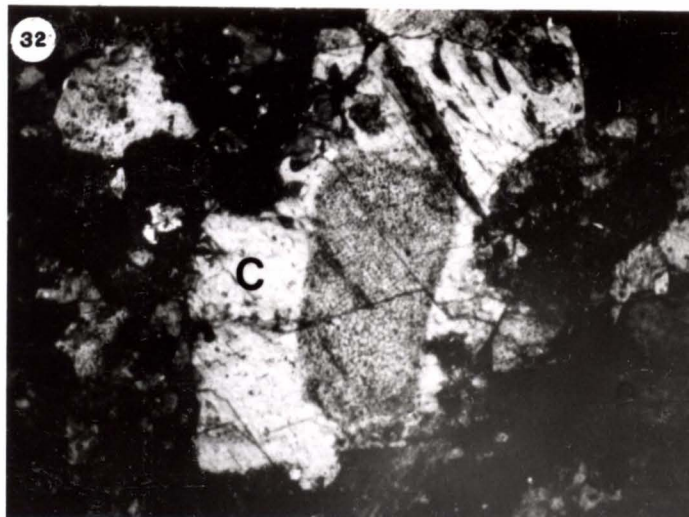
Figure 31 Photomicrograph (plane polarized) of blocky calcite cement (C) filling interparticle pores of the intraclast bioclast wackestone packstone lithotype. NDGS Well Number 9411 at 2881 metres (9452 feet). Bar scale is 0.5 millimetres (0.02 inches).

Figure 32 Photomicrograph (crossed nichols) of syntaxial overgrowth cement (C) on an echinoderm grain in the intraclast bioclast wackestone packstone lithotype. NDGS Well Number 8333 at 2860 metres (9384 feet). Bar scale is 0.5 millimetres (0.02 inches).

s of  
res  
.02



n  
es  
02



Syntaxial overgrowth cement is common around echinoderm grains without micritic rims or micrite-filled skeletal pores (Bathurst, 1975).

Calcite cement associated with deep subsurface fluids is commonly equant and coarse-grained with poikilitopic textures (Harris and others, 1985; Moore and Druckman, 1981). Poikilitic calcite cement in the study area is a late stage cement which fills intercrystalline pores of the dolomudstone lithotype (Fig. 33), and less commonly, moldic pores and vugs in the intraclast bioclast wackestone packstone and laminated mudstone lithotypes. Poikilitic calcite cement is also found in calcite and/or anhydrite nodules of the dolomudstone lithotype where it fills secondary pores created by earlier partial dissolution of anhydrite (Fig. 34). Many of these poikilitic calcite-cemented nodules contain remnant inclusions of anhydrite.

Anhydrite cement is present in the study area as a poikilitic to coarsely crystalline cement. Anhydrite cement fills interparticle pores in grainstones of the intraclast bioclast wackestone packstone lithotype (Fig. 35) and moldic pores and vugs in the dolomudstone and laminated mudstone lithotypes (Fig. 36). Fractures in the laminated mudstone lithotype are also cemented with anhydrite.

The proximity of the anhydrite-cemented intraclast bioclast wackestone packstone and laminated mudstone lithotypes to the overlying anhydrite lithotype, the post-

Figure 33 Photomicrograph (plane polarized) of poikilitic calcite cement (arrow) in the dolomudstone lithotype. NDGS Well Number 7104 at 2971 metres (9749 feet). Bar scale is 0.5 millimetres (0.02 inches).

Figure 34 Photomicrograph (crossed nichols) of anhydrite (A) and calcite (C) nodule in the dolomudstone lithotype. Partial dissolution of anhydrite was followed by cementation by poikilitic calcite cement. NDGS Well Number 6914 at 2942 metres (9642 feet). Bar scale is 0.5 millimetres (0.02 inches).

Figure 35 Photomicrograph (crossed nichols) of anhydrite (A) and silica (S) cements in a grainstone of the intraclast bioclast wackestone packstone lithotype. NDGS Well Number 7283 at 2947 metres (9667 feet). Bar scale is 0.5 millimetres (0.02 inches).

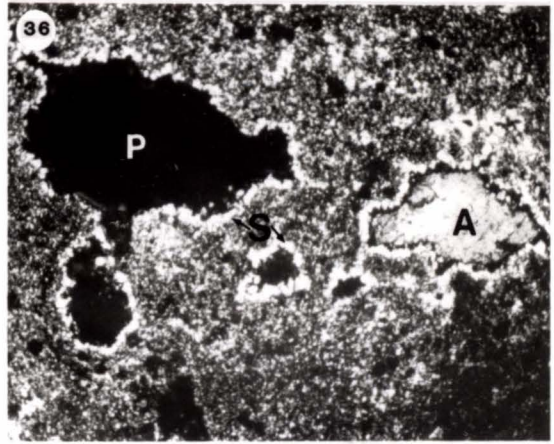
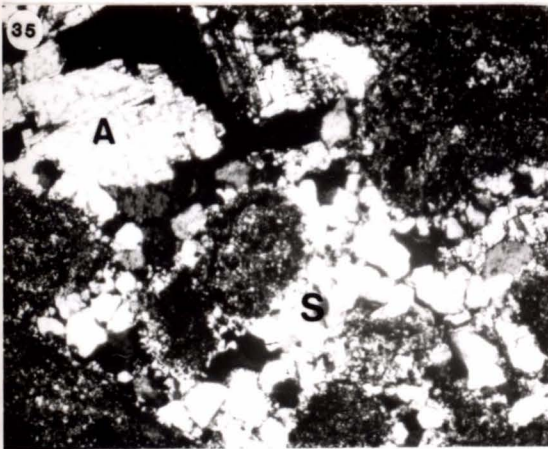
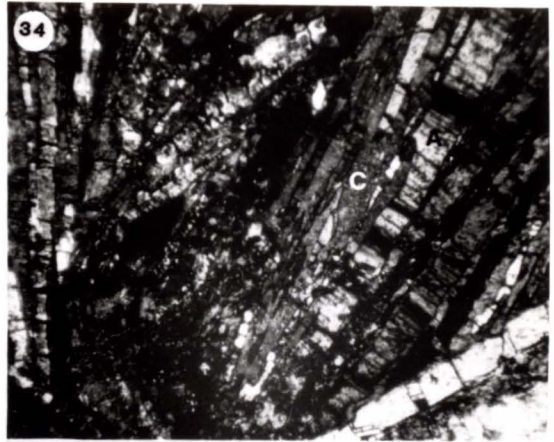
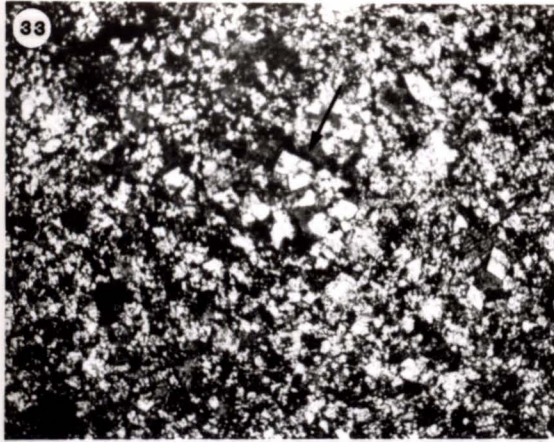
Figure 36 Photomicrograph (crossed nichols) of a silica-lined (S), anhydrite-cemented (A) vug and a silica-lined vug (P) in the intraclast bioclast wackestone packstone lithotype. NDGS Well Number 7283 at 2947 metres (9667 feet). Bar scale is 1 millimetre (0.04 inches).

itic  
etres  
(0.02

te  
ne  
was  
e  
s  
0.02

te  
the  
res  
02

t  
ber  
l





dolomitization timing of the anhydrite cementation, the presence of small fractures (commonly anhydrite-filled), and the presence of intercrystalline porosity created by dolomitization, suggest that the anhydrite cement may have originated from a remobilization of the overlying sulfates (anhydrite lithotype) following dolomitization.

Silica cement is found locally as thin lenses in the intraclast bioclast wackestone packstone lithotype. In some wells in the study area, as many as three horizons of silica cementation or replacement are present. Authigenic quartz and chert occur as a pore-filling and pore-lining cement in interparticle pores of some grainstones (Fig. 35). Chert is also found lining vugs in mudstones, wackestones and packstones of the intraclast bioclast wackestone packstone lithotype (Fig. 36).

There is no direct evidence for the source of the silica; however, detrital quartz silt is present in minor amounts throughout the studied section and within all the lithotypes. Although detrital quartz silt is never a major constituent except in the Fryburg gamma ray marker, there may have been enough present along some horizons to have been a minor, local source of some of the silica. Another possible source of silica may have been siliceous organisms. Knauth (1979) stated that there were abundant siliceous organisms present during the Paleozoic. Thayer (1983) stated that siliceous organisms may have been responsible for silica in the Madison Limestone of Montana

and Wyoming.

Saddle dolomite, also called baroque dolomite, white sparry dolomite, and late ferroan dolomite (Radke and Mathis, 1980), is found in minor amounts as a coarsely crystalline, pore-filling cement. Saddle dolomite is present in the dolomudstone, neomorphic wackestone, and intraclast bioclast wackestone packstone lithotypes where it fills intercrystalline, vuggy, and moldic pores (Fig. 37). Saddle dolomite cement is also found associated with large, blocky calcite cement in vugs (Fig. 38). A similar association of contemporaneously grown calcite and saddle dolomite was noted by Beales (1971). In the dolomudstone lithotype, saddle dolomite cement is associated with calcite and anhydrite nodules. As previously stated in the dolomitization section, sulfate may be an effective deterrent to saddle dolomite precipitation (Ward and Halley, 1985). Removal of the sulfate is evidenced by the existence of rectangular re-entrants and sharp projections along remnant anhydrite crystal edges (Schenk and Richardson, 1985). Once the partial dissolution of anhydrite occurred, and a source of magnesium became available, saddle dolomite was precipitated as cement.

Pyrite cement is rare in the studied section and is only found in the dolomudstone lithotype where it generally lines intraparticle pores in corals and occurs in a dendritic pattern or as large euhedral cubes associated with calcite and anhydrite nodules (Fig. 39). The type of

Figure 37 Photomicrograph (crossed nichols) of a moldic pore cemented with saddle dolomite (S) in the dolomudstone lithotype. NDGS Well Number 7283 at 2955 metres (9695 feet). Bar scale is 0.5 millimetres (0.02 inches).

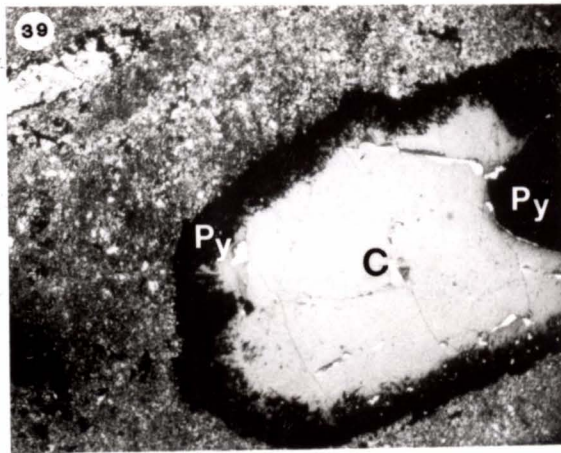
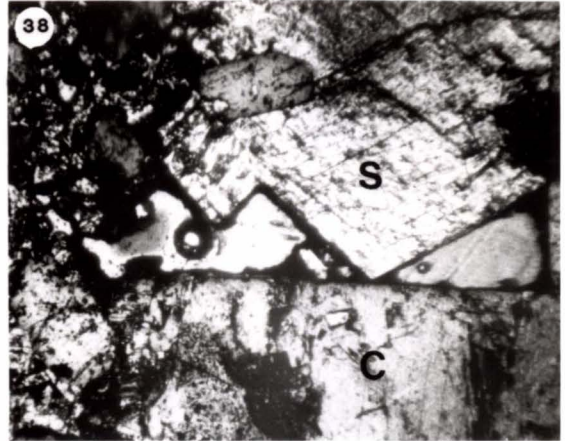
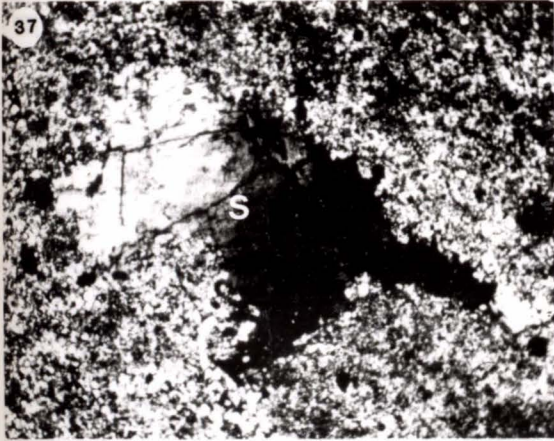
Figure 38 Photomicrograph (plane polarized) of a large vug cemented with saddle dolomite (S) and blocky calcite (C) in the intraclast bioclast wackestone packstone lithotype. NDGS Well Number 8333 at 2860 metres (9384 feet). Bar scale is 0.5 millimetres (0.02 inches).

Figure 39 Photomicrograph (plane polarized) of an intraparticle pore (coral) cemented with pyrite (Py) and calcite (C) in the dolomudstone lithotype. NDGS Well Number 8333 at 2871 metres (9420 feet). Bar scale is 1 millimetre (0.04 inches).

ic  
he  
283 at

vug  
stone  
at

ite  
res



sediment and the chemistry of the pore waters is important to pyrite cementation (Raiswell, 1982). Pyrite precipitates as a cement under conditions of low pH where pore waters are supersaturated with respect to pyrite (Raiswell, 1982).

#### Replacement

Replacement of one mineral by another is common in rocks of the upper Mission Canyon and lower Charles Formations in Treetop and Whiskey Joe fields. Replacement minerals in the study area consist of calcite (dedolomite), anhydrite, saddle dolomite, silica, and rarely, celestite and pyrite. All of the lithotypes described contain replacement minerals, commonly anhydrite, calcite or saddle dolomite.

Replacement of dolomite by calcite, called dedolomitization or calcitization (Bathurst, 1975), is the process whereby dolomite is converted to calcite, usually in a calcium-rich solution (Lippman, 1973). Dedolomitization can occur under near surface and deep burial conditions (Budai and others, 1984). Petrographic evidence used to determine dedolomitization includes 1) corroded dolomite rhombohedra edges, 2) partial rhombohedrons floating in a calcite matrix, and 3) calcite patches within dolomite rhombohedra (Budai and others, 1984).

Dedolomitization is found in the dolomudstone and neomorphic wackestone lithotypes. Evidence for two stages

of dedolomitization was found in rocks of the study area: 1) an early stage associated with neomorphism in the neomorphic wackestone lithotype, and 2) a late stage of dedolomitization associated with late stage poikilitic calcite cementation in the dolomudstone lithotype. Within the neomorphic wackestone lithotype, dedolomitization is associated with neomorphism and is evidenced by the corrosion of edges of dolomite rhombohedra and the partial replacement of dolomite by calcite (Fig. 40).

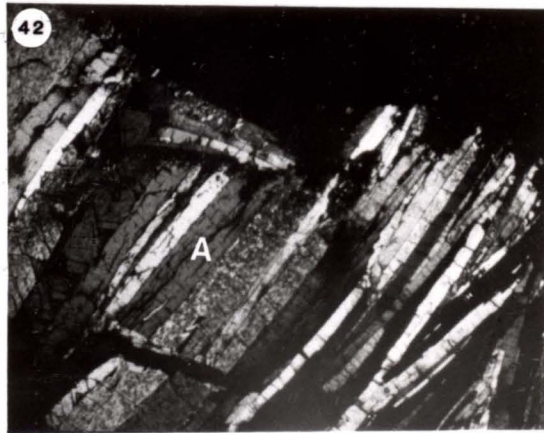
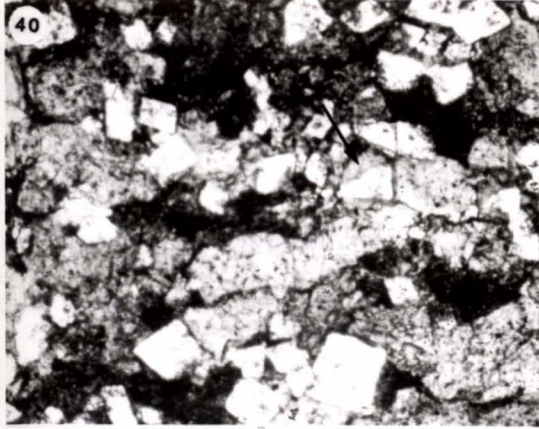
Dedolomitization in the neomorphic wackestone lithotype may have occurred during neomorphism when the migrating, calcite-enriched solution films penetrated the edges of scattered dolomite rhombohedra. The patchy areas of dedolomitization in the dolomudstone lithotype are closely associated with the late-stage poikilitic calcite cementation (Fig. 41). Although the timing of the two dedolomitization events is different, dedolomitization in the dolomudstone lithotype occurred under conditions similar to those which formed dedolomite in the neomorphic wackestone lithotype.

Replacement anhydrite is found in the echinoderm wackestone, dolomudstone, intraclast bioclast wackestone packstone, laminated mudstone, and anhydrite lithotypes. The earliest anhydrite replacement observed was in the anhydrite and laminated mudstone lithotypes. In those cases, previously formed displacive gypsum nodules were replaced by anhydrite (Fig. 42). Evidence of a later

Figure 40 Photomicrograph (plane polarized) of dedolomitization (arrow) within the neomorphic wackestone lithotype. NDGS Well Number 7352 at 2935 metres (9629.5 feet). Bar scale is 0.25 millimetres (0.01 inches).

Figure 41 Photomicrograph (plane polarized) of dedolomitization (arrow) in the dolomudstone lithotype. NDGS Well Number 9411 at 2890 metres (9480 feet). Bar scale is 0.5 millimetres (0.02 inches).

Figure 42 Photomicrograph (crossed nichols) of anhydrite replacement (A) of a sulfate nodule in the dolomudstone lithotype. NDGS Well Number 7352 at 2931 metres (9617.5 feet). Bar scale is 1 millimetre (0.04 inches).





episode of anhydrite replacement was observed in the laminated mudstone lithotype where scattered, blocky and lath-like anhydrite crystals replaced cryptalgal laminations (Fig. 43). In the echinoderm wackestone and dolomudstone lithotypes, bioclasts have been replaced by anhydrite (Fig. 44). Bioclasts and cement in the intraclast bioclast wackestone packstone lithotype have been selectively anhydrite-replaced.

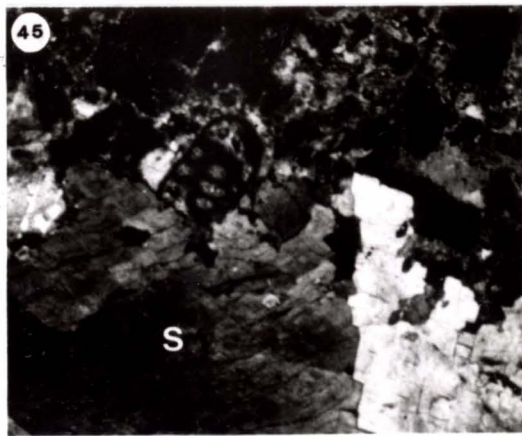
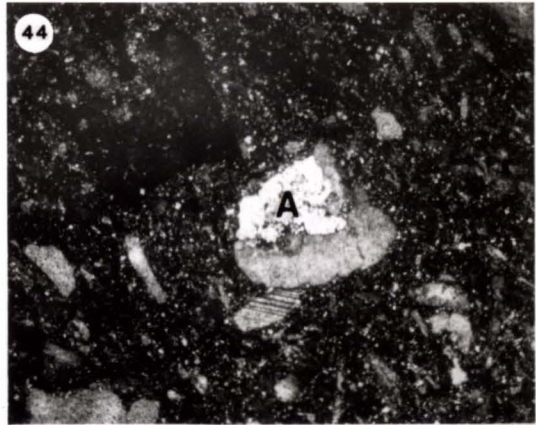
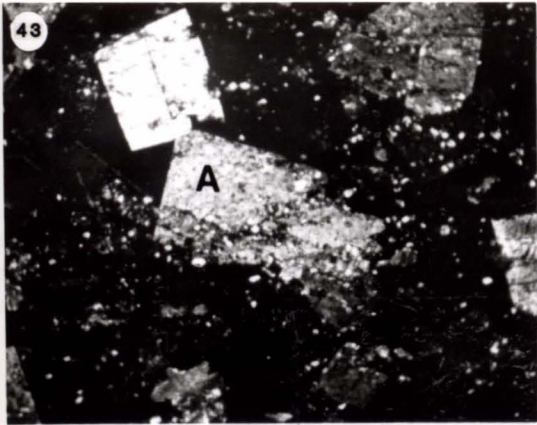
Saddle dolomite replaces allochems and matrix in the dolomudstone and intraclast bioclast wackestone packstone lithotypes. Replaced skeletal grains in the dolomudstone lithotype have retained much of their original exterior morphology (ostracodes) (Fig. 29). In the intraclast bioclast wackestone packstone lithotype, saddle dolomite replacement of allochems and matrix destroyed any original textures (Fig. 45).

The process of silicification is favored by relatively low pH and temperature, and pore fluids saturated with silica (Blatt and others, 1980). Silica, in the form of chert and authigenic quartz, replaces matrix and allochems in the dolomudstone, intraclast bioclast wackestone packstone, and laminated mudstone lithotypes. Within the dolomudstone lithotype, occasional chert nodules are present. Authigenic quartz replacement is occasionally associated with the calcite and anhydrite nodules in the dolomudstone lithotype.

Figure 43 Photomicrograph (crossed nichols) of lath-shaped anhydrite (A) replacing matrix in the laminated mudstone lithotype. NDGS Well Number 8333 at 2851 metres (9355 feet). Bar scale is 0.5 millimetres (0.02 inches).

Figure 44 Photomicrograph (crossed nichols) of anhydrite replacement (A) of an echinoderm grain in the echinoderm wackestone lithotype. NDGS Well Number 7351 at 2951 (9680.5 feet). Bar scale is 1 millimetre (0.04 inches).

Figure 45 Photomicrograph (crossed nichols) of saddle dolomite (S) replacement of matrix and allochems in the intraclast bioclast wackestone packstone lithotype. NDGS Well Number 7776 at 2947 metres (9670 feet). Bar scale is 1 millimetre (0.04 inches).



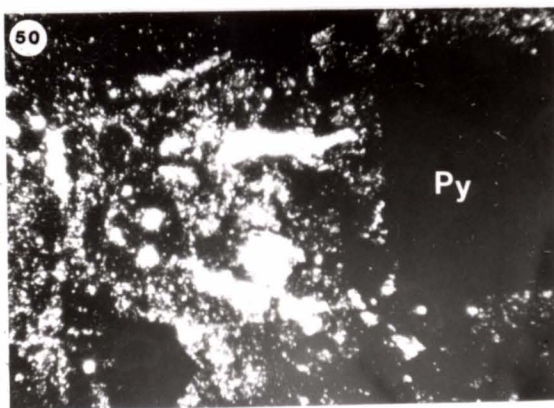
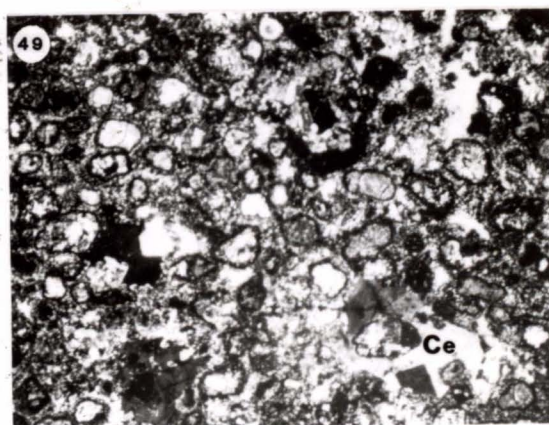
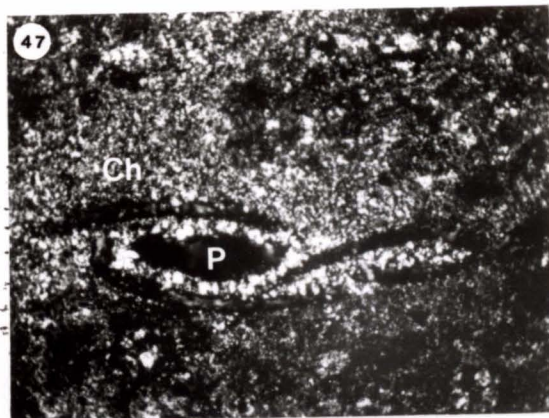
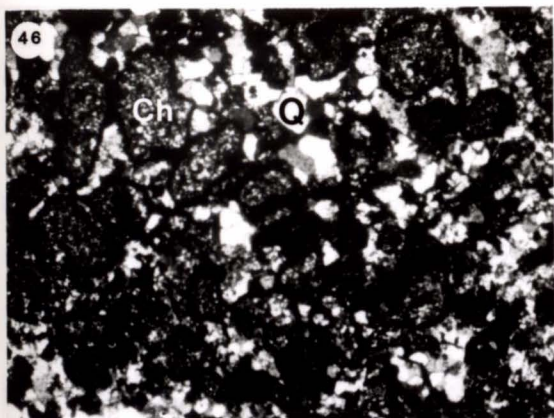
Silica replacement in the intraclast bioclast wackestone packstone lithotype is associated with silica cementation and is found selectively replacing peloid interiors and leaving the earlier-formed dolomitized micritic envelope unsilicified (Fig. 46). In wackestones of the intraclast bioclast wackestone packstone lithotype, fine-grained chert replaces matrix (Fig. 47). In many cases, these silicified wackestones contain moldic pores which are well-preserved in the chert. In the laminated mudstone lithotype, authigenic quartz replaces the dolomitized matrix surrounding anhydrite nodules (Fig. 48).

Celestite replacement may occur at any time up to deep burial (Carlson, 1986). Liberation of strontium ions needed for the formation of celestite commonly occurs by the conversion of aragonite to calcite or during the dolomitization of limestones (Carlson, 1986).

Celestite replacement occurs only in the laminated mudstone lithotype where it replaces calcispheres between cryptalgal laminations (Fig. 49). Celestite replacement is associated with anhydrite cementation and the early anhydrite replacement in the laminated mudstone lithotype.

Pyrite replacement was observed in the echinoderm wackestone and dolomudstone lithotypes. Generally forming large cubes up to two millimetres (0.08 inches) in width, pyrite replaces calcite and dolomite and is associated with black, possibly organic, material (Fig. 50).

- Figure 46 Photomicrograph (crossed nichols) of chert-replaced (Ch), quartz-cemented (Q), peloid grainstone in the intraclast bioclast wackestone packstone lithotype. NDGS Well Number 7283 at 2947 metres (9667 feet). Bar scale is 0.5 millimetres (0.02 inches).
- Figure 47 Photomicrograph (crossed nichols) of fine-grained chert (Ch) replacement of matrix in the intraclast bioclast wackestone packstone lithotype. A moldic pore (P) is evident within the chert. NDGS Well Number 7283 at 2947 metres (9667 feet). Bar scale is 0.5 millimetres (0.02 inches).
- Figure 48 Photomicrograph (crossed nichols) of authigenic quartz (Q) replacement of matrix surrounding anhydrite nodules (A) in the laminated mudstone lithotype. NDGS Well Number 6942 at 2964 metres (9725 feet). Bar scale is 1 millimetre (0.04 inches).
- Figure 49 Photomicrograph (crossed nichols) of celestite (Ce) replacement of allochems and matrix in the laminated mudstone lithotype. NDGS Well Number 7352 at 2928 metres (9606 feet). Bar scale is 0.5 millimetres (0.02 inches).
- Figure 50 Photomicrograph (crossed nichols) of large pyrite cubes (Py) replacing matrix in the dolomudstone lithotype. NDGS Well Number 8333 at 2868 metres (9408.5 feet). Bar scale is 0.5 millimetres (0.02 inches).



### Fracturing

Fracturing of rocks of the upper Mission Canyon Formation in Treetop and Whiskey Joe fields, while not common, is important. Fractures are found in all but the anhydrite lithotype.

Within the echinoderm wackestone lithotype, fractures are rare and are generally cemented with calcite and saddle dolomite (Fig. 51). Fractures in the dolomudstone lithotype are generally cemented with calcite and tend to branch outward from calcite and/or anhydrite nodules (Fig. 52). Fractures are fairly common in the neomorphic wackestone lithotype and are generally cemented by calcite and dolomite. Fractures in the intraclast bioclast wackestone packstone lithotype are cemented with calcite and occasionally, silica (Fig. 53). These fractures are rare and occur mainly in the packstones and grainstones. Fractures in the laminated mudstone lithotype are cemented with anhydrite and rarely, celestite (Fig. 54). They are generally small and truncate against bedding planes.

Fracturing took place at least two different times during the diagenetic history of the study area, in early, eogenetic time and in mesogenetic time. Fractures in the neomorphic wackestone, intraclast bioclast wackestone packstone and laminated mudstone lithotypes probably resulted from early compactional forces and may have created the pathways which allowed fluids to migrate downward into the underlying sediments.

Figure 51 Photomicrograph (crossed nichols) of blocky calcite (C) and saddle dolomite (S) filling a fracture in the echinoderm wackestone lithotype. NDGS Well Number 7351 at 2951 metres (9680.5 feet). Bar scale is 1 millimetre (0.04 inches).

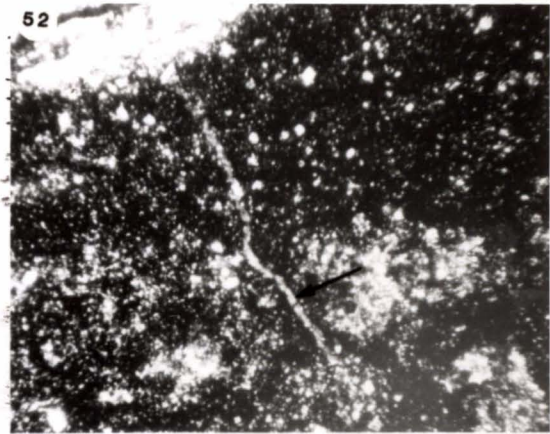
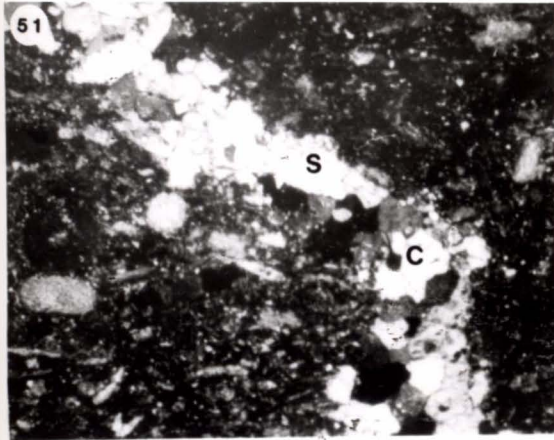
Figure 52 Photomicrograph (crossed nichols) of a calcite-filled fracture (arrow) originating from a calcite and anhydrite nodule in the dolomudstone lithotype. NDGS Well Number 6914 at 2942 metres (9652 feet). Bar scale is 0.5 millimetres (0.02 inches).

Figure 53 SEM (secondary electron image) photograph of a silica-cemented (S) fracture in the intraclast bioclast wackestone packstone lithotype. NDGS Well Number 7283 at 2947 metres (9667 feet). Bar scale is 100 micrometres.

Figure 54 Photomicrograph (crossed nichols) of an anhydrite-cemented (A) fracture in the laminated mudstone lithotype. NDGS Well Number 7097 at 2947 metres (9668.3 feet). Bar scale is 1 millimetre (0.04 inches).

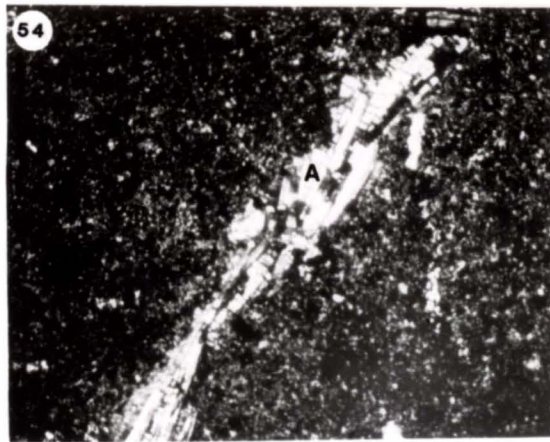


pe.  
s).  
e-  
one  
res  
.02



Bar

d



Fractures in the echinoderm wackestone and the dolomudstone lithotypes formed late in the diagenetic sequence. Within the dolomudstone lithotype, some of the fractures formed perpendicular to stylolites, suggesting they may have been a result of stylolitization. Fractures such as these, called "tension gashes", are produced during stylolitization and form parallel to the maximum stress direction (Nelson, 1981).

### Neomorphism

The term "neomorphism" was first proposed by Folk in 1965 as a comprehensive term for any change between a mineral and itself or a polymorph. Neomorphism includes both inversion and recrystallization, regardless of whether the newly formed crystals are larger, smaller, or differ in shape (Folk, 1965).

Inversion of aragonite to calcite occurs as a wet, in situ process (Bathurst, 1975). The process of inverting aragonite to calcite may result in partial calcite cementation of the existing porosity (Harris and others, 1985). Recrystallization generally refers to wet recrystallization in which the mineralogy remains the same. During recrystallization, changes in the crystal volume, crystal shape, and crystal lattice orientation may occur (Bathurst, 1975).

Aggrading neomorphism, a product of wet recrystallization, is the process whereby finer crystals are replaced by coarser crystals of the same mineralogy

(Bathurst, 1975). Folk (1974) suggested that magnesium ions surround carbonate particles and retard the process of neomorphism. Removal of the surrounding "magnesium cage" will allow the growth of microspar and pseudospar to begin. The solution film stage of aggrading neomorphism occurs when the rock is composed of pure calcite spar and has little remaining permeability and only 1 to 2 percent remaining porosity. The remaining porosity is within solution films between intercrystalline boundaries. Wet boundary migration along the solution film allows selected calcite crystals to coarsen at the expense of their neighbors. Most neomorphism occurs during this stage (Bathurst, 1975).

Neomorphic spar is separated into two types based on crystal size. Microspar is considered to be between 4 and 30 micrometres in width while pseudospar is greater than 30 micrometres (Folk, 1965). Microspar can be distinguished on the basis of its uniformity in size, equant and gently curved crystal boundaries, cloudy appearance due to clays trapped during neomorphism, patchy appearance, poorly packed appearance, and crosscutting relation to allochems and matrix. Although pseudospar may resemble calcite cement, its characteristic irregular shape with wiggly crystal boundaries helps to identify it (Folk, 1965).

Rocks of the upper Mission Canyon Formation in Treetop and Whiskey Joe fields have undergone aggrading neomorphism. Neomorphism is present mainly in the

neomorphic wackestone and intraclast bioclast wackestone packstone lithotypes. Within the neomorphic wackestone lithotype, neomorphism is especially evident. Small patchy areas of micrite lie within the coarser microspar (Fig. 55). Much of the microspar present appears cloudy, and scanning electron microscopy readily reveals calcite crystals larger than 5 micrometres in width with many up to 20 micrometres (Fig. 56). Neomorphic spar is rare in the intraclast bioclast wackestone packstone lithotype and is generally associated with undolomitized, mud-rich rocks. Where neomorphic calcite does occur, loosely packed allochems appear to "float" in neomorphic calcite (Fig. 57).

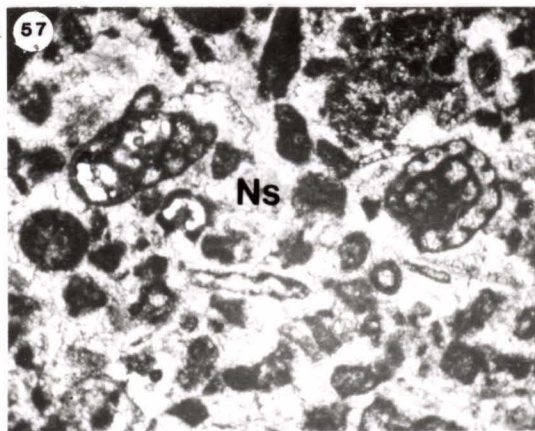
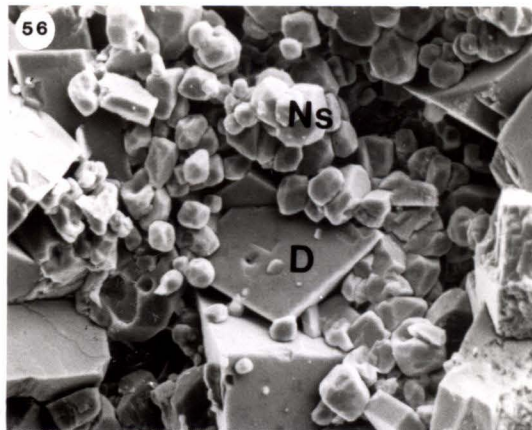
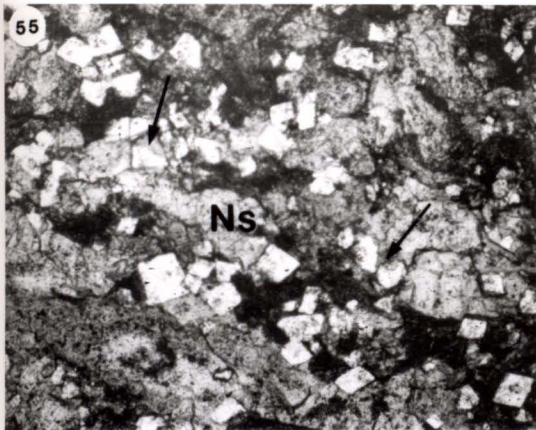
Neomorphism of rocks in the study area may have proceeded in the following manner: 1) inversion of originally aragonitic mud to calcite, 2) infiltration and migration of meteoric-derived fluids downward through the sediment, 3) mixing of meteoric-derived fluids with marine pore waters, 4) patchy dolomitization of the sediment and depletion of the magnesium ion supply, 5) calcite cementation within the intercrystalline pores and associated reduction of porosity and permeability, until remaining porosity exists only within thin calcite-enriched solution films between intercrystalline pores, 6) local aggrading neomorphism of mud-rich rocks to microspar and pseudospar along the edges of the calcite-enriched solution films and, finally, 7) migration of the calcite-

Figure 55 Photomicrograph (plane polarized) of neomorphic spar (Ns) and dolomite (D) in the neomorphic wackestone lithotype. Dedolomitization (arrow) of dolomite rhombohedra is evident. NDGS Well Number 7352 at 2935 metres (9629.5 feet). Bar scale is 0.5 millimetres (0.02 inches).

Figure 56 SEM (secondary electron image) photograph of neomorphic spar (Ns) and dolomite (D) in the neomorphic wackestone lithotype. NDGS Well Number 7389 at 2916 metres (9567 feet). Bar scale is 20 micrometres.

Figure 57 Photomicrograph (plane polarized) of allochems "floating" in neomorphic spar (Ns) in the neomorphic wackestone lithotype. NDGS Well Number 7776 at 2947 metres (9670 feet). Bar scale is 1 millimetre (0.04 inches).

nic  
ow)  
l  
r



enriched solution film boundaries which encounter scattered dolomite rhombohedra and allow dedolomitization to occur (see section on replacement for further discussion on dedolomitization).

#### Pressure Solution

Wanless (1979) described pressure solution as a limestone response to overburden or tectonic stress. Overburden stress in the upper Mission Canyon Formation of Treetop and Whiskey Joe fields is suggested because of the relative lack of tectonic deformation in the Williston Basin (Gerhard and others, 1982), the horizontal orientation of pressure solution features, and an average burial depth of 2865 to 2987 metres (9400 to 9800 feet) in the study area. Three major factors which affect limestone responses to stress are the presence of fine, platy minerals such as clay, the presence of magnesium ions, and the structural resistivity of the rock (Wanless, 1979).

The terms stylolite, grain contact suture, microstylolite and microstylolite swarm, used in this study, are from the classification of Wanless (1979). Stylolites and grain contact sutures are believed to form in structurally resistant rocks containing little or no insoluble material. Microstylolites and microstylolite swarms can form in both structurally resistant and nonresistant rocks. Other responses to stress include compaction, deformation, neomorphism and local dolomitization.

Pressure solution features, in the form of stylolites,

grain suture contacts, microstylolites, and microstylolite swarms, are present in all but the anhydrite lithotype. Within the echinoderm wackestone lithotype, stylolites are commonly of low amplitude with thin seams of insoluble material present along them (Fig. 58). Dolomite rhombohedrons are occasionally found associated with these stylolites. Grain contact sutures are common in the echinoderm wackestone lithotype and generally lie between echinoderm grains (Fig. 59). Stylolites in the dolomudstone lithotype, while not common, may have high amplitudes, up to 15 centimetres (5.9 inches), and contain thick seams of associated insoluble material. Stylolites of the neomorphic wackestone lithotype are generally similar in appearance to the echinoderm wackestone lithotype. The laminated mudstone and intraclast bioclast wackestone packstone lithotypes contain low amplitude stylolites with minor amounts of associated insoluble material.

Microstylolites are present in the echinoderm wackestone, the dolomudstone, the neomorphic wackestone, rarely in the intraclast bioclast wackestone packstone, and in the laminated mudstone lithotypes (Figs. 60, 61). Within the echinoderm wackestone lithotype, microstylolites are generally associated with the more calcareous rocks. Microstylolites and thick microstylolite swarms are abundant in the dolomudstone lithotype. Both contain abundant clays, detrital quartz silt, authigenic pyrite,

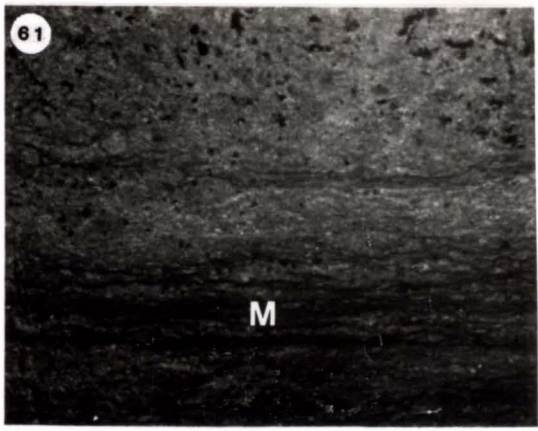
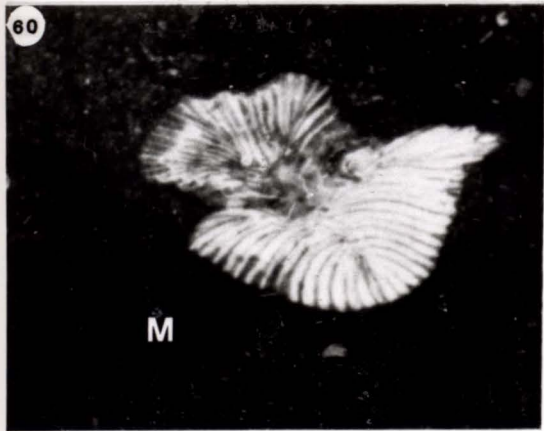
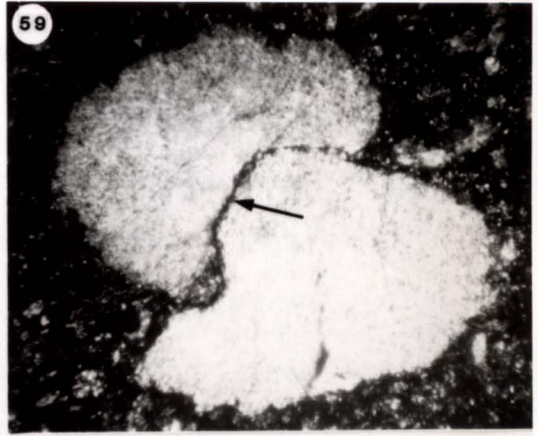
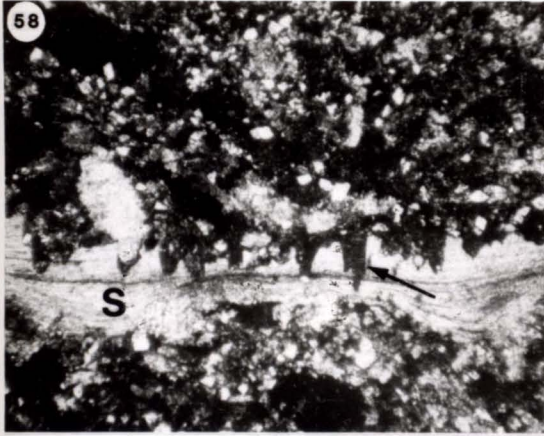


Figure 58 Photomicrograph (crossed nichols) of a low amplitude stylolite (arrow) penetrating a skeletal fragment (S) in the echinoderm wackestone lithotype. NDGS Well Number 6899 at 2890 metres (9481 feet). Bar scale is 0.5 millimetres (0.02 inches).

Figure 59 Photomicrograph (crossed nichols) of a grain contact suture (arrow) between two echinoderm grains in the echinoderm wackestone lithotype. NDGS Well Number 9411 at 2894 metres (9494 feet). Bar scale is 0.5 millimetres (0.02 inches).

Figure 60 Core photograph of microstylolites (M) around a rugose coral in the echinoderm wackestone lithotype. NDGS Well Number 7351 at 2953 metres (9687 feet). Bar scale is 1 centimetre (0.4 inches).

Figure 61 Core photograph of microstylolites (M) in the dolomudstone lithotype. NDGS Well Number 7283 at 2956 metres (9697 feet). Bar scale is 1 centimetre (0.4 inches).



and other insoluble material. Scattered dolomite rhombohedra are associated with microstylolites of the neomorphic wackestone, intraclast bioclast wackestone packstone, and laminated mudstone lithotypes.

The presence of pressure solution features may indicate a vertical thinning of the rocks, result in the development of permeability barriers, and liberate carbonate for subsequent cementation (Bathurst, 1975; Dunnington, 1967). Within the studied section, the presence of thick seams of insoluble material along stylolites, microstylolites, and microstylolite swarms, and the high amplitude of some of the stylolites, suggest significant rock removal may have occurred. Stylolite formation may also have created permeability barriers, especially in rocks of the dolomudstone lithotype where less porous zones commonly contain abundant stylolites and microstylolites. Magnesium and calcium ions liberated during stylolitization may have been a source of ions needed for the formation of scattered dolomite rhombohedra and fracture-fill calcite cement occasionally associated with stylolites. Calcium ions may also have contributed to the formation of poikilitic calcite and saddle dolomite cement.

## POROSITY

### Introduction

Pore types within the upper Mission Canyon rocks of Treetop and Whiskey Joe fields are both primary and secondary. According to the time-porosity concepts developed by Choquette and Pray (1970), primary porosity forms during the predepositional and depositional stages of porosity evolution, while secondary porosity forms during the postdepositional stage (Fig. 62).

The classification of porosity and porosity evolution developed by Choquette and Pray (1970) was utilized in this study. Each pore type described in this classification is defined by its pore size, pore shape, genesis, and relation to either a particular constituent or the overall rock fabric (Choquette and Pray, 1970). Two primary pore types are present in the studied section, interparticle and intraparticle. The four secondary pore types include intercrystalline, moldic, vuggy, and rarely, fracture. An example of the distribution of primary and secondary pore types and their relation to the lithotypes is illustrated in Figure 63.

Interparticle pores are primary pores lying between grains (Choquette and Pray, 1970). Within the studied section, interparticle pores are found almost exclusively in grainstones of the intraclast bioclast wackestone packstone lithotype (Figs. 64, 65). Interparticle pores range in size from 100 to 200 micrometres.

Figure 62 Illustration of time-porosity terms (top diagram) and their relation to major surface and burial zones (bottom schematic diagram) (Choquette and Pray, 1970).

TIME-POROSITY TERMS					
STAGE	PRE-DEPOSITION	DEPOSITION	POST-DEPOSITION		
POROSITY TERM	PRIMARY POROSITY		SECONDARY POROSITY		
	PRE-DEPOSITIONAL POROSITY	DEPOSITIONAL POROSITY	POST-DEPOSITIONAL POROSITY		
			EOGENETIC POROSITY	MESOGENETIC POROSITY	TELOGENETIC POROSITY
"TYPICAL" RELATIVE TIME SPAN					

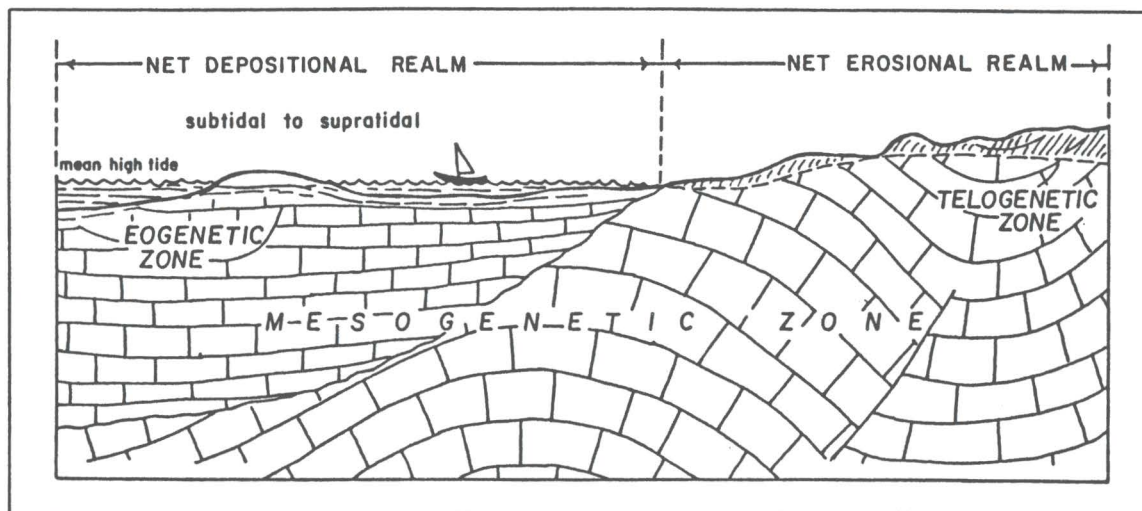


Figure 63 Example of the relation between the stratigraphic distribution of lithotypes, corresponding log responses (compensated neutron log ( $\phi_N$ ) and compensated formation density log ( $\phi_D$ )), distribution of percent porosity, and distribution of pore types in the study area.

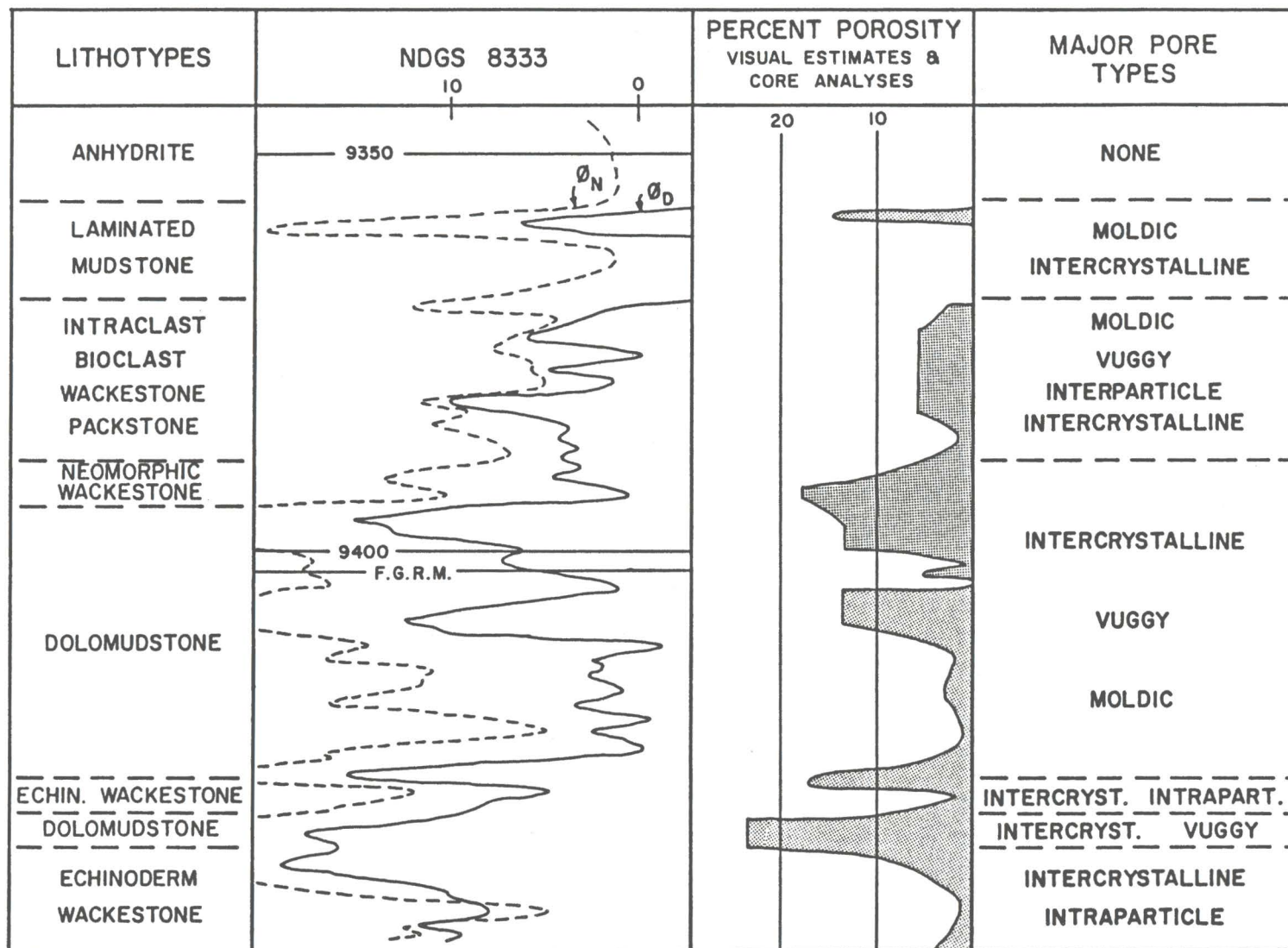
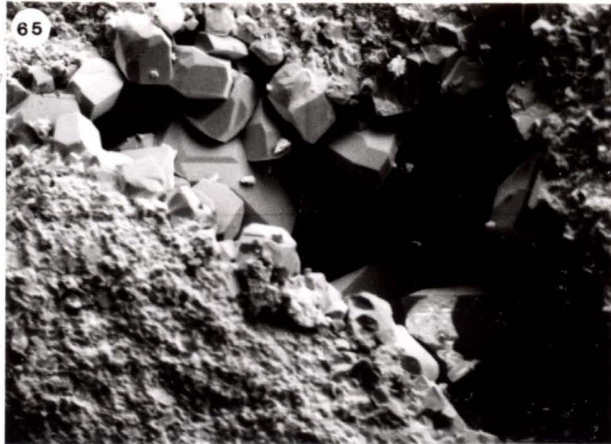
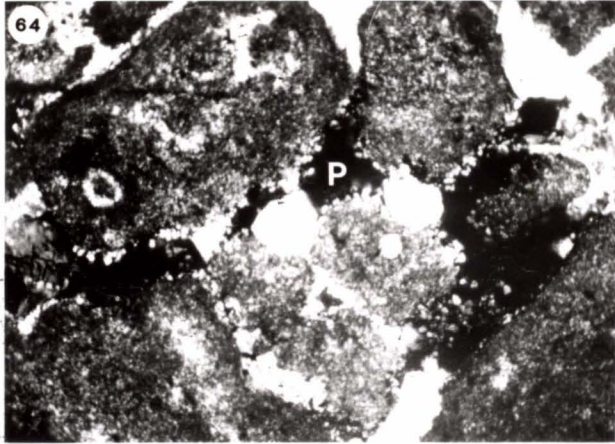




Figure 64 Photomicrograph (crossed nichols) of interparticle pores (P) in the intraclast bioclast wackestone packstone lithotype. NDGS Well Number 9411 at 2881 metres (9452 feet). Bar scale is 0.5 millimetres (0.02 inches).

Figure 65 SEM (secondary electron image) photograph of calcite spar lining an interparticle pore in the intraclast bioclast wackestone packstone lithotype. NDGS Well Number 9411 at 2881 metres (9452 feet). Bar scale is 50 micrometres.

DGS  
Bar



the  
res

Intraparticle pores are primary pores located within individual allochems (Choquette and Pray, 1970). Intraparticle pores are rare in the studied section and occur mainly within rocks of the echinoderm wackestone, dolomudstone, neomorphic wackestone, and intraclast bioclast wackestone packstone lithotypes. The most common occurrence of intraparticle pores in these lithotypes is within corals, ostracodes and, rarely, foraminifers (Fig. 66). Intraparticle pores are variable in size, ranging from 100 micrometres to 1 millimetre (up to 0.4 inches) depending on the allochem involved.

Moldic pores are secondary pores formed by the selective dissolution of a former individual allochem and are distinguished on the basis of size, shape, wall ornamentation and relict features (Choquette and Pray, 1970). Dissolution of allochems within the dolomudstone, neomorphic wackestone, intraclast bioclast wackestone packstone, and laminated mudstone lithotypes led to the formation of moldic pores (Figs. 67, 68). Moldic pores vary in size depending on the size of the original allochem. Common allochems which have been removed to create moldic pores in the studied section include ostracodes, peloids, echinoderms, foraminifers, and unknown skeletal fragments.

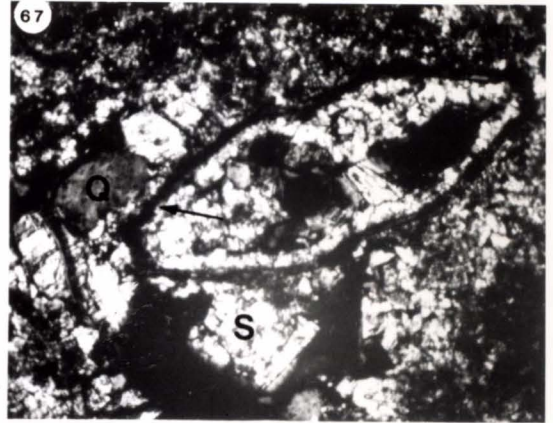
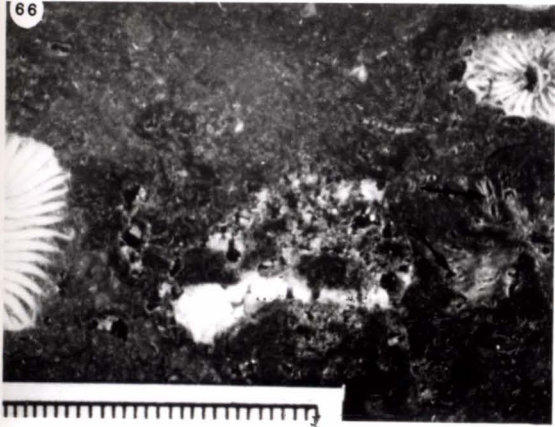
Vuggy pores are secondary pores that are generally equant in shape, greater than 62.5 micrometres in size and are usually a result of solution enlargement of moldic

Figure 66 Core photograph of intraparticle pores (arrows) within rugose corals in the intraclast bioclast wackestone packstone lithotype. NDGS Well Number 8333 at 2862 metres (9389 feet). Bar scale is 1 centimetre (0.4 inches).

Figure 67 Photomicrograph (crossed nichols) of a moldic pore (arrow) surrounded by saddle dolomite (S) and quartz cements (Q) in the intraclast bioclast wackestone packstone lithotype. NDGS Well Number 7283 at 2947 metres (9667 feet). Bar scale is 0.5 millimetres (0.02 inches).

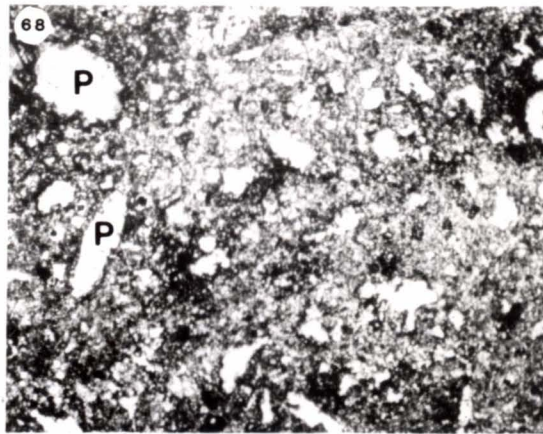
Figure 68 Photomicrograph (plane polarized) of moldic pores (P) in the dolomudstone lithotype. NDGS Well Number 8333 at 2875 metres (9432 feet). Bar scale is 0.5 millimetres (0.02 inches).

ows)  
last  
umber  
is 1



c  
S)  
clast  
umber  
is

pores  
l



pores (Choquette and Pray, 1970). Vuggy pores are found within the dolomudstone, neomorphic wackestone, and intraclast bioclast wackestone packstone lithotypes (Figs. 69, 70). Vuggy pores range from 0.1 to 1.5 millimetres (0.004 to 0.06 inches) in size.

Some of the moldic and vuggy pores within the dolomudstone lithotype were created by the partial dissolution of anhydrite-replaced skeletal grains. Evidence for the dissolution of anhydrite was given by Schenk and Richardson (1985) and includes rectangular re-entrants and sharp projections along remnant crystal edges and irregular birefringence zonation along remnant crystal edges due to local variations in crystal thicknesses.

Fracture porosity, a type of secondary porosity, is rare in the study area. Open fractures are generally discontinuous and are found in the dolomudstone and neomorphic wackestone lithotypes.

Intercrystalline pores are secondary pores which form between individual crystals of relatively equant and equal size (Choquette and Pray, 1970). In this study, intercrystalline pores refer to those pores lying between dolomite rhombohedra. Intercrystalline pores are the dominant pore type in the study area and are found in all but the anhydrite lithotype. Intercrystalline pores are most common in the dolomudstone lithotype where they range from 1 to 70 micrometres in size with an average of 20 to 30 micrometres (Figs. 71, 72). Intercrystalline pores of

Figure 69 Photomicrograph (crossed nichols) of a large vug (P) partially cemented with saddle dolomite (S) in the dolomudstone lithotype. NDGS Well Number 7389 at 2916 metres (9567 feet). Bar scale is 0.5 millimetres (0.02 inches).

Figure 70 SEM (secondary electron image) photograph of small vugs (P) in the dolomudstone lithotype. NDGS Well Number 8333 at 2895 metres (9633 feet). Bar scale is 100 micrometres.

Figure 71 Photomicrograph (crossed nichols) of intercrystalline pores in the dolomudstone lithotype. Dark areas represent pores. NDGS Well Number 7351 at 2936 metres (9633 feet). Bar scale is 0.5 millimetres (0.02 inches).

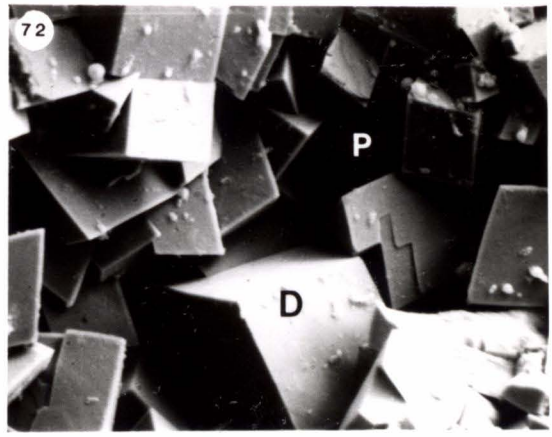
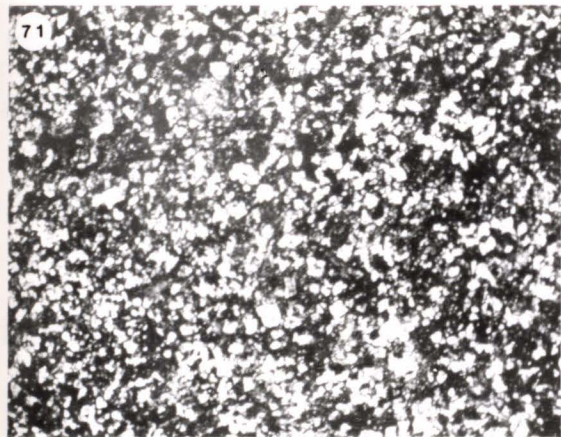
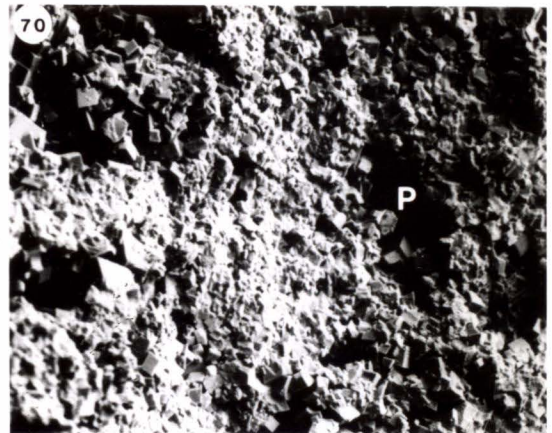
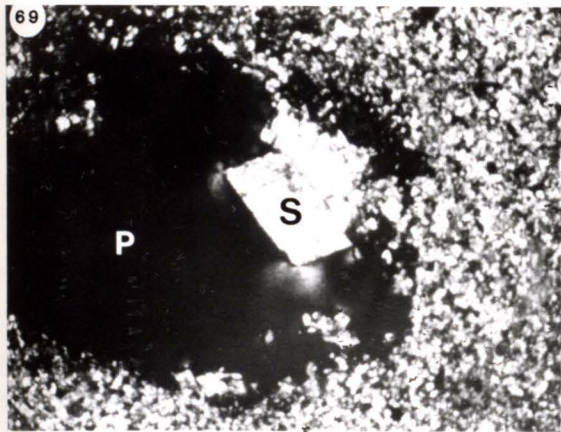
Figure 72 SEM (secondary electron image) photograph of intercrystalline pores (P) and dolomite rhombohedrons (D) within the dolomudstone lithotype. NDGS Well Number 7389 at 2913 metres (9557 feet). Bar scale is 20 micrometres.

e vug  
(S)  
umber  
is

et).

S  
Bar

res





the echinoderm wackestone and laminated mudstone lithotypes are rare and are generally less than 10 micrometres in size. Within the neomorphic wackestone and intraclast bioclast wackestone packstone lithotypes, intercrystalline pores range from 1 to 30 micrometres in size with an average of 5 to 15 micrometres.

Intercrystalline pores appear to have formed during early dolomitization of the rocks. Mudstones and wackestones in the studied section contain the majority of intercrystalline pores. Early replacement dolomite rhombohedra generally prefer mud-rich sediments containing isolated allochems (Murray, 1960) similar to the wackestones and mudstones of the dolomudstone lithotype. Continued dolomitization, the enlargement of existing dolomite rhombohedra, compaction, and cementation have led to a reduction in pore size and abundance in some rocks in the study area.

#### Pore and Pore Throat Studies

Pore casts and rock samples from rocks of all but the anhydrite lithotype were used to study pore and pore throat geometries. Samples were taken and pore casts made of all pore types. Rock samples and their corresponding pore casts were chosen based on petrographic observations of the thin sections. This phase of the study concentrated mainly on intercrystalline pores. The majority of intercrystalline pores are found in the dolomudstone lithotype, therefore, most of the pore casts

and rock samples used are from this lithotype.

To describe the intercrystalline pores, the classification of pore and pore throat geometry proposed by Wardlaw (1976) was used. According to Wardlaw, most intercrystalline pores can be classified into three shapes depending on the stage of growth of dolomite rhombohedrons: 1) polyhedral, 2) tetrahedral, and 3) interboundary-sheet (Fig. 73).

Polyhedral-shaped pores usually form first and are a result of randomly-orientated, planar crystal faces (Wardlaw, 1976). The majority of pores in the study area are polyhedral pores and average 30 to 40 micrometres across their longest dimension (Fig. 74). Polyhedral pores formed early in the diagenetic history of the study area. They are mainly a result of the reflux dolomitization.

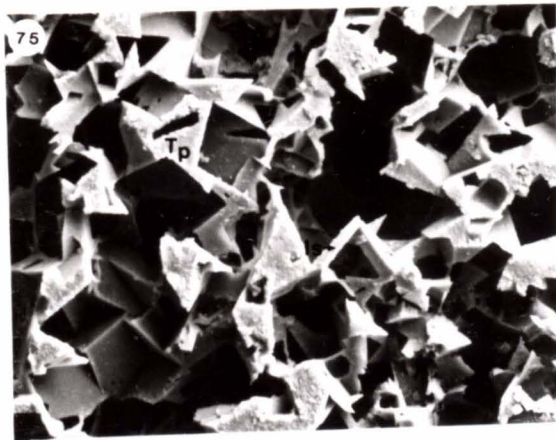
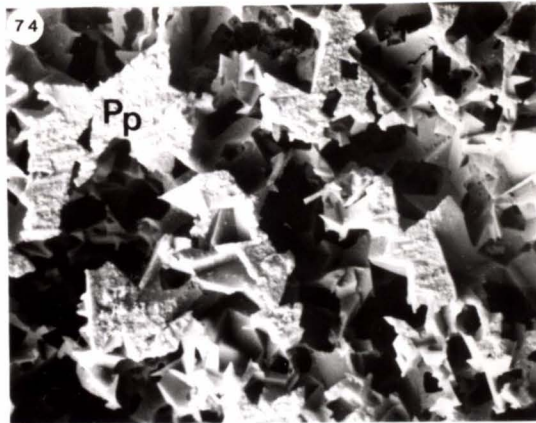
Tetrahedral-shaped pores form as a result of continued dolomite crystal growth. As dolomite rhombohedrons grow, planar compromise boundaries develop, geometric complexity is reduced, and polyhedral pores reduce to tetrahedral pores (Wardlaw, 1976). Within the study area, tetrahedral pores average 15 to 25 micrometres across their longest dimension (Fig. 75). The continued growth of dolomite rhombohedrons in Mission Canyon rocks in the study area led to the formation of tetrahedral pores.

Continued growth of dolomite rhombohedrons produces thin, sheet-like pore shapes which form at crystal boundaries (Wardlaw, 1976). These pores are called

Figure 73 SEM (secondary electron image) photograph of a pore cast of intercrystalline pores (P) in the dolomudstone lithotype. Polyhedral, tetrahedral, and interboundary-sheet-shaped pores stand out in relief. NDGS Well Number 7776 at 2893 metres (9490 feet). Bar scale is 100 micrometres.

Figure 74 SEM (secondary electron image) photograph of a pore cast showing polyhedral-shaped, intercrystalline pores (Pp) in the dolomudstone lithotype. NDGS Well Number 6942 at 2967 metres (9733 feet). Bar scale is 100 micrometres.

Figure 75 SEM (secondary electron image) photograph of a pore cast of tetrahedral (Tp) and interboundary-sheet (Is)-shaped, intercrystalline pores in the dolomudstone lithotype. NDGS Well Number 7283 at 2953 metres (9688 feet). Bar scale is 100 micrometres.



interboundary-sheet pores. Interboundary-sheet pores in the study area average 0.1 to 5 micrometres in width (Fig. 75) and are a result of the progressive dolomite growth into tetrahedral pores. Most pore throats in the study area are either tetrahedral or interboundary-sheet pores.

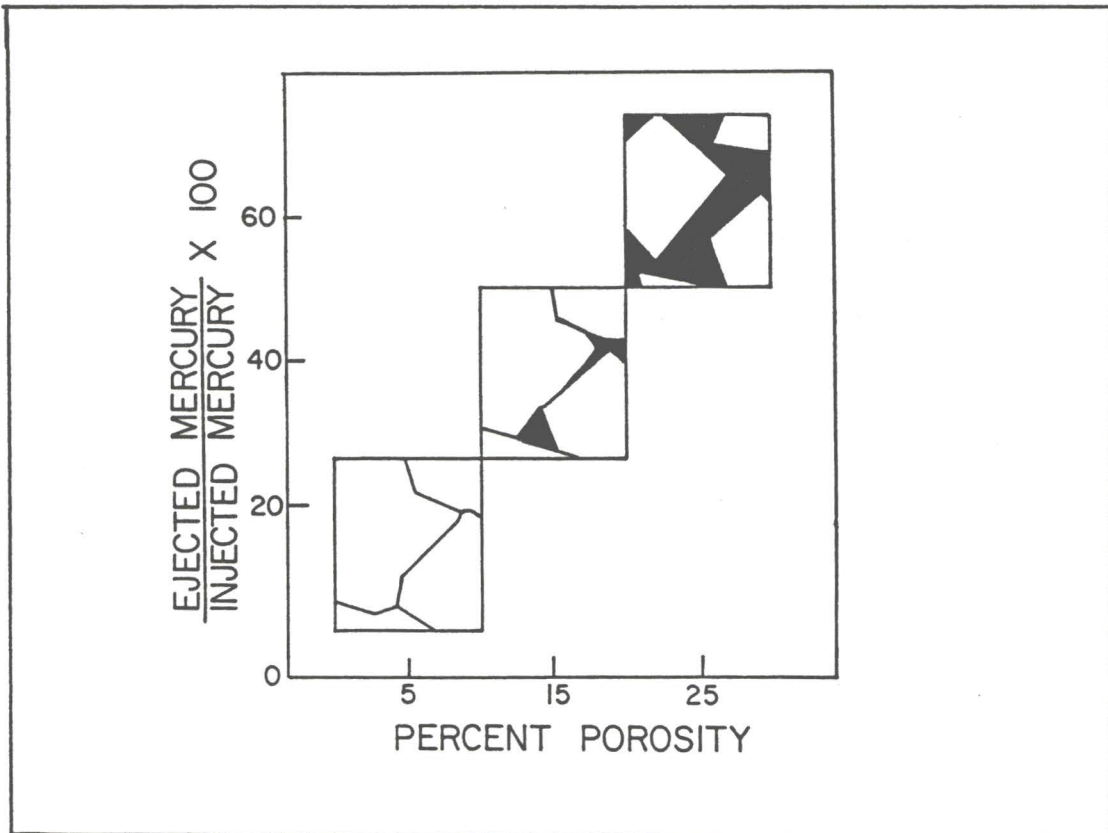
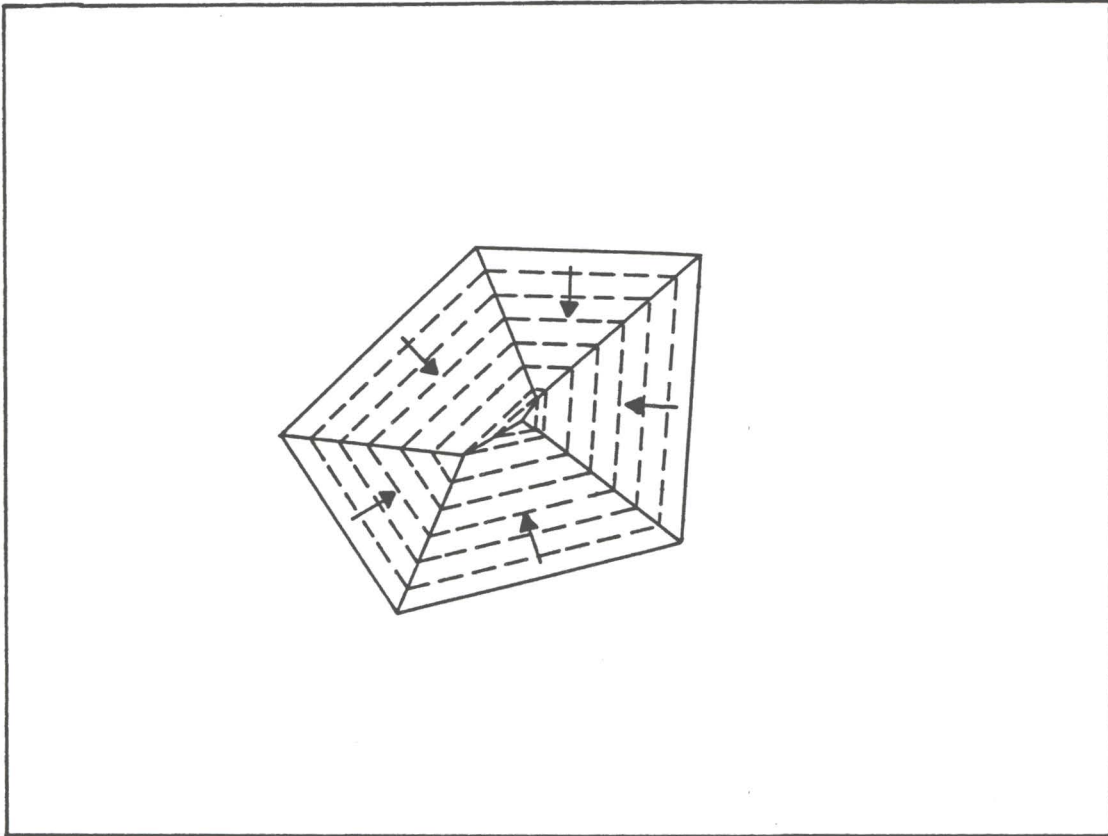
The inhibition of crystal growth is of fundamental importance to dolomite growth and the formation of intercrystalline porosity (Wardlaw, 1976). There are three stages when dolomite crystal growth is temporarily stopped: 1) when rhombohedrons have grown sufficiently large enough to touch in three dimensions, 2) when compromise boundaries have become extensive enough to leave tetrahedral pores at triple junctions, and 3) when interboundary-sheet pores are the only remaining pore type (Wardlaw, 1976) (Fig. 76). There appears to be a threshold, once dolomite rhombohedrons are touching, at which dolomite growth is limited. When conditions change so that this threshold is breached, compromise boundaries form and polyhedral pores reduce to tetrahedral pores (Wardlaw, 1976) (Fig. 77). Polyhedral and tetrahedral pores at this stage may be connected by interboundary-sheet pores. There is a second threshold when the triple junctions that form tetrahedral pores are eliminated by continued crystal growth and only interboundary-sheet pores remain (Wardlaw, 1976).

#### Interpore Minerals

Six pore-filling minerals were identified petrographically and with the aid of the scanning electron

Figure 76 Illustration of a cross section of a typical polyhedral-shaped pore. Continued overgrowth of dolomite rhombohedra into pore reduces the number of containing faces from five to three adjacent crystal faces (Wardlaw, 1976).

Figure 77 Illustration of the changes from polyhedral-shaped pores to interboundary-sheet-shaped pores and the resulting reduction in porosity as dolomite rhombohedra continue to grow (Wardlaw, 1976).



microscope and microprobe: calcite, anhydrite, dolomite, silica, pyrite, and celestite (Figs. 78, 79, 80, and 81). Of the six inter pore minerals, pyrite and celestite are the least abundant and rarely completely occlude pores. Calcite, anhydrite, dolomite, and silica vary in abundance and importance depending on their stratigraphic location within each lithotype.

The echinoderm wackestone lithotype contains mainly calcite pore-filling minerals. Calcite, dolomite (including saddle dolomite), and anhydrite occlude pores of the dolomudstone lithotype. Calcite and occasionally dolomite (including saddle dolomite) are the main pore-filling minerals of the neomorphic wackestone lithotype. Calcite, anhydrite, and silica are important in the intraclast bioclast wackestone packstone lithotype. Pores of the laminated mudstone lithotype contain calcite and anhydrite.

#### Porosity Distribution

The distribution of porosity in the study area can be discussed by separating the studied section into three porosity zones, the lower, middle, and upper (Fig. 82). The three porosity zones were defined using correlatable wire-line log characteristics. Within each porosity zone, isopach maps were constructed to depict the aggregate footages of porous rock displaying porosity greater than a critical porosity value. A critical porosity of 8 percent as measured on the compensated formation density log was



Figure 78 SEM (secondary electron image) photograph of a pore partially filled with calcite (C) and surrounded by dolomite (D) in the dolomudstone lithotype. NDGS Well Number 7776 at 2893 metres (9490 feet). Bar scale is 20 micrometres.

Figure 79 Photomicrograph (crossed nichols) of an anhydrite-filled pore (A) in the dolomudstone lithotype. NDGS Well Number 8333 at 2871 metres (9420 feet). Bar scale is 0.5 millimetres (0.02 inches).

Figure 80 SEM (secondary electron image) photograph of a dolomite-filled pore (D) in the dolomudstone lithotype. NDGS Well Number 7389 at 2907 metres (9538 feet). Bar scale is 20 micrometres.

Figure 81 SEM (secondary electron image) photograph of a silica-filled pore (S) in the intraclast bioclast wackestone packstone lithotype. NDGS Well Number 7283 at 2947 metres (9667 feet). Bar scale is 100 micrometres.

F a  
one  
etres

e  
tres  
0.02

a  
res

a  
last  
mber  
s

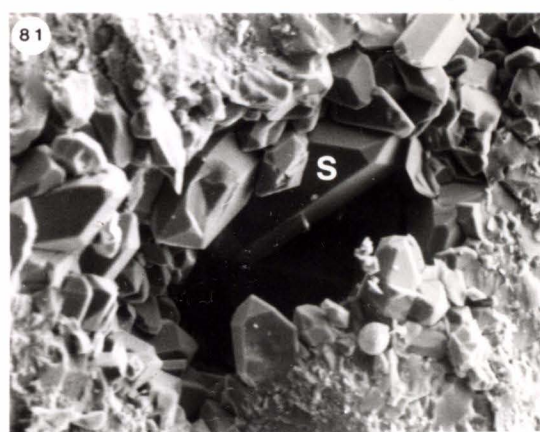
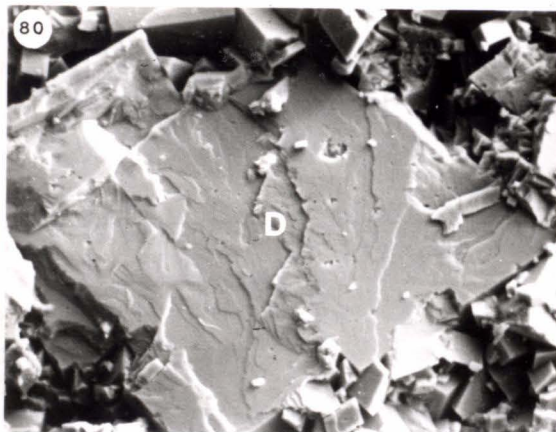
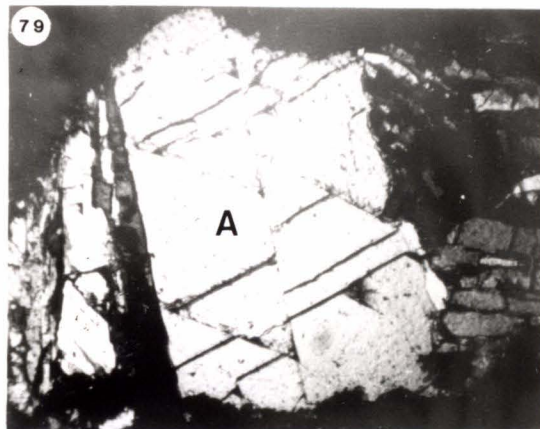
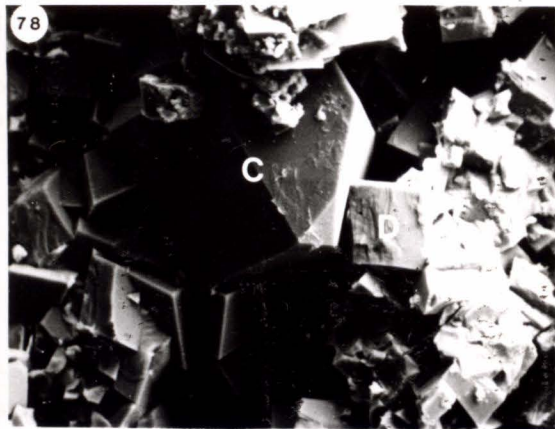
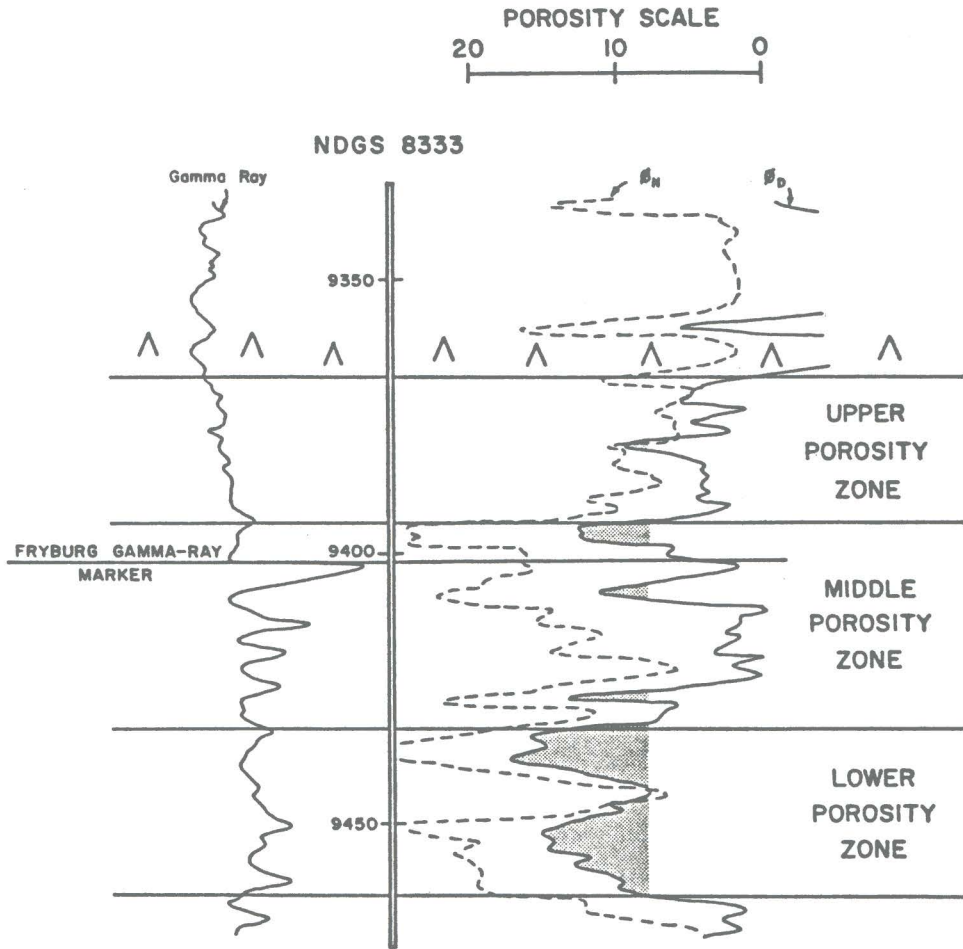


Figure 82 Example of the relation between a typical log response (gamma ray, compensated neutron log ( $\phi_N$ ) and compensated formation density log ( $\phi_D$ )) and the stratigraphic distribution of the lower, middle and upper porosity zones within the study area. Shaded portions indicate areas with more than 8 percent compensated formation density porosity (critical porosity). The upper porosity zone is capped by anhydrite.



chosen to aid in determining the distribution of porosity.

The lower porosity zone includes rocks of the echinoderm wackestone and lower portion of the dolomudstone lithotypes. The isopach map of the lower porosity zone shows that a thicker section of porous rock exists in the southern and central portions of the study area (Fig. 83).

The middle porosity zone corresponds to rocks of the dolomudstone and occasionally the neomorphic wackestone lithotypes. The isopach map of the middle porosity zone displays a greater thickness of porous rock in the central and northern portions of the study area (Fig. 84).

The upper porosity zone contains rocks of the neomorphic wackestone, intraclast bioclast wackestone packstone, and laminated mudstone lithotypes. Porous rocks in the upper porosity zone are limited mainly to the northern portion of the study area (Fig. 85).

When isopach maps of the three porosity zones are compared, two trends in the distribution of porous zones become apparent: 1) north-northwestward across the study area, porous zones within the rocks tend to parallel the overlying anhydrite, and 2) toward the north-northwest, the thickest aggregate footages of porous rock are developed progressively higher stratigraphically within each porosity zone (Fig. 86). Progradation of littoral and supralittoral environments north-northwestward over sublittoral environments may have been a controlling factor in the aerial distribution of porosity in the study area. As

Figure 83 Porosity isopach map of the lower porosity zone showing the aggregate footage of porous rock with greater than 8 percent critical porosity. Shaded portions indicate areas with 10 feet or more of porous rock. Contour interval is 4 feet.

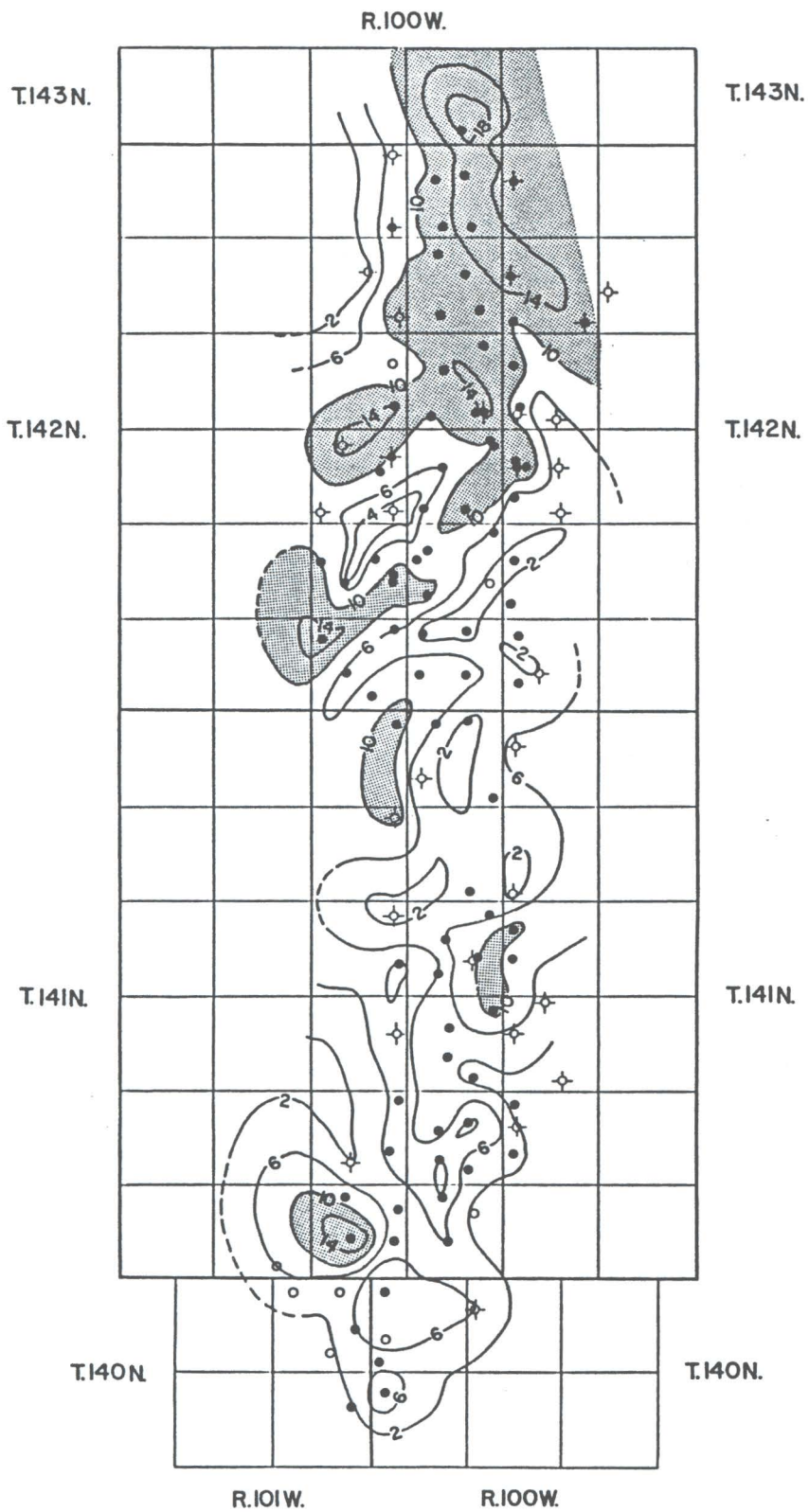


Figure 84 Porosity isopach map of the middle porosity zone showing the aggregate footage of porous rock with greater than 8 percent critical porosity. Shaded portions indicate areas with 10 feet or more of porous rock. Contour interval is 4 feet.



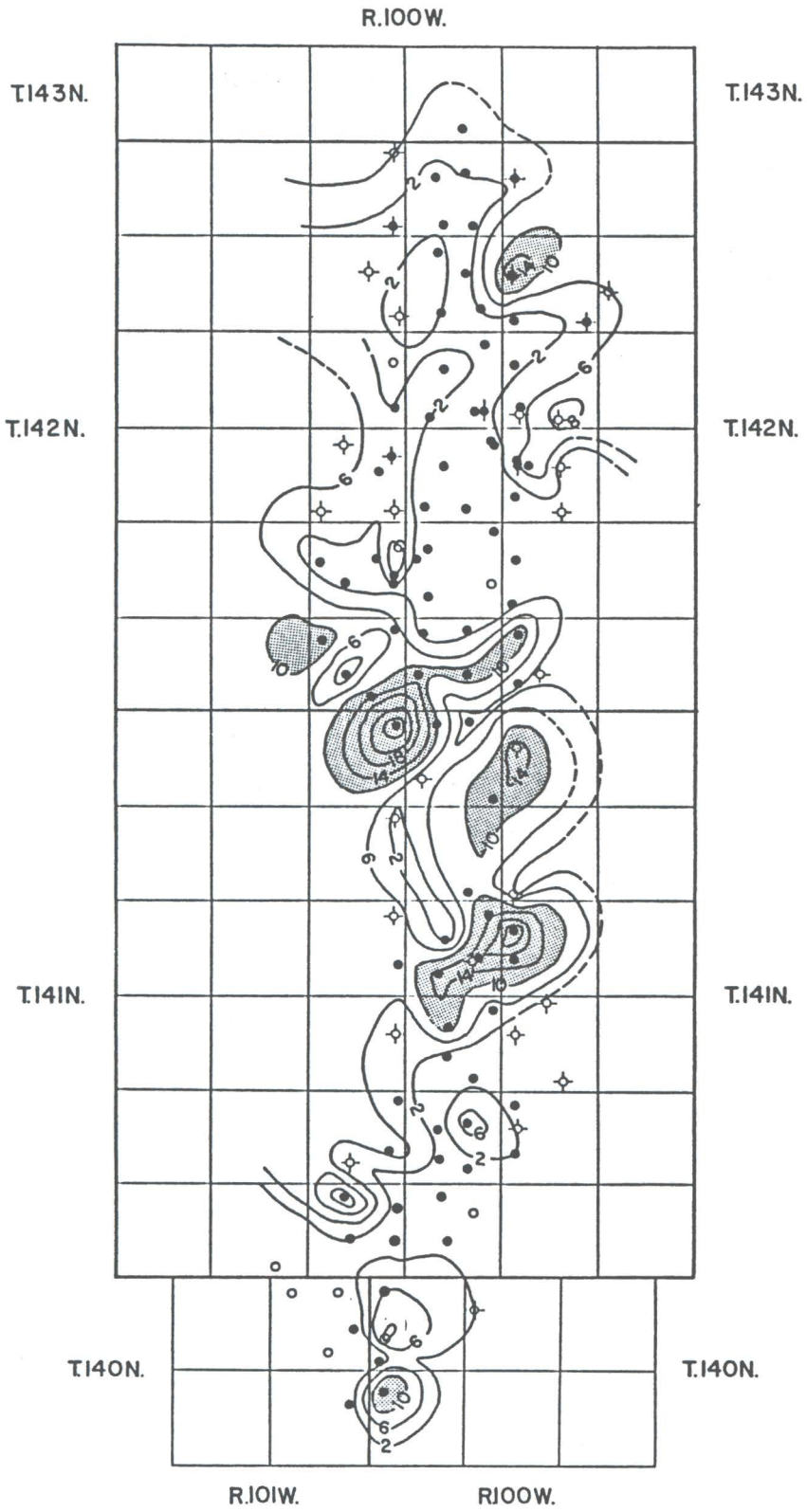


Figure 85 Porosity isopach map of the upper porosity zone showing the aggregate footage of porous rock with greater than 8 percent critical porosity. Contour interval is four feet.

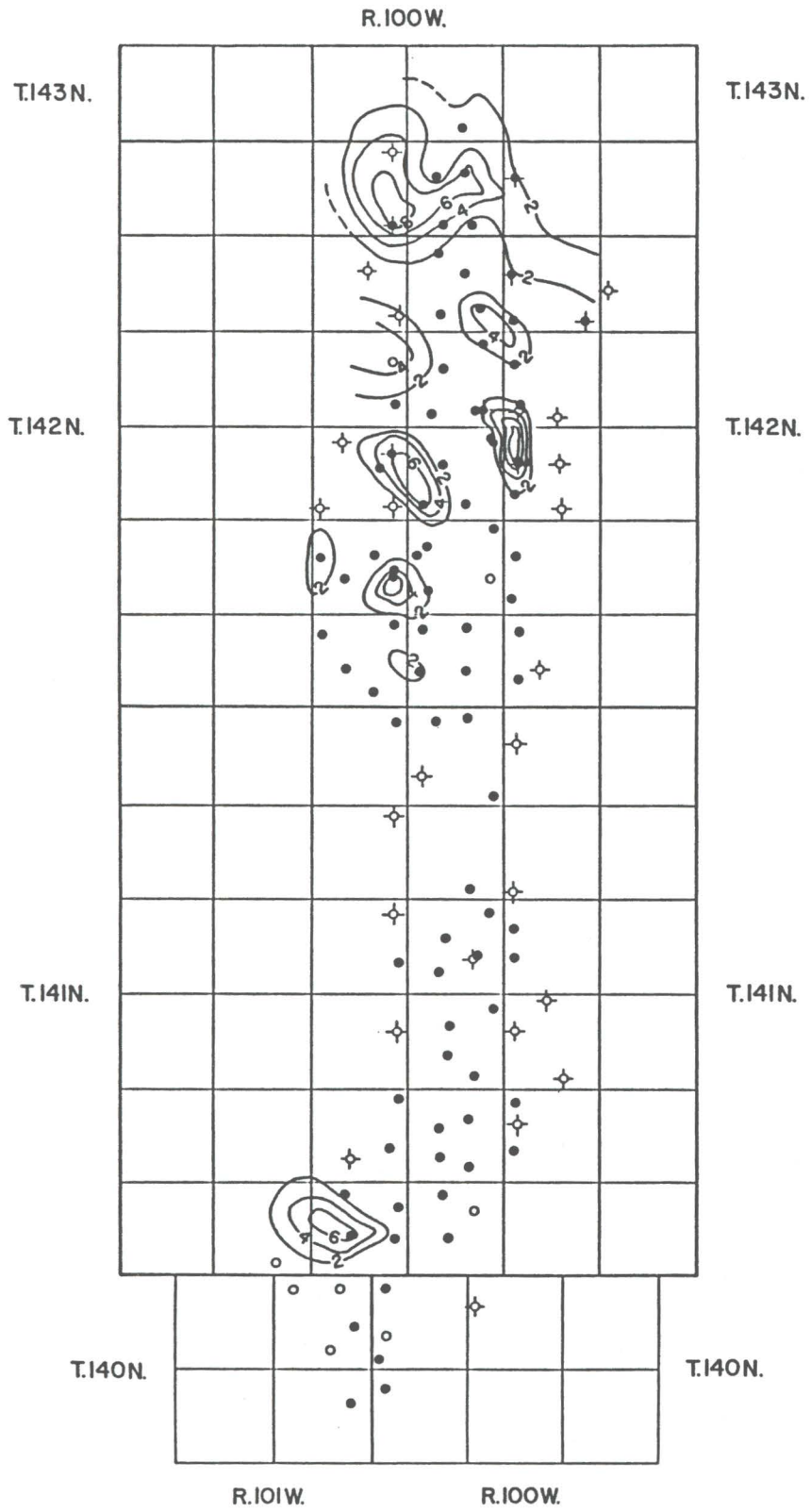
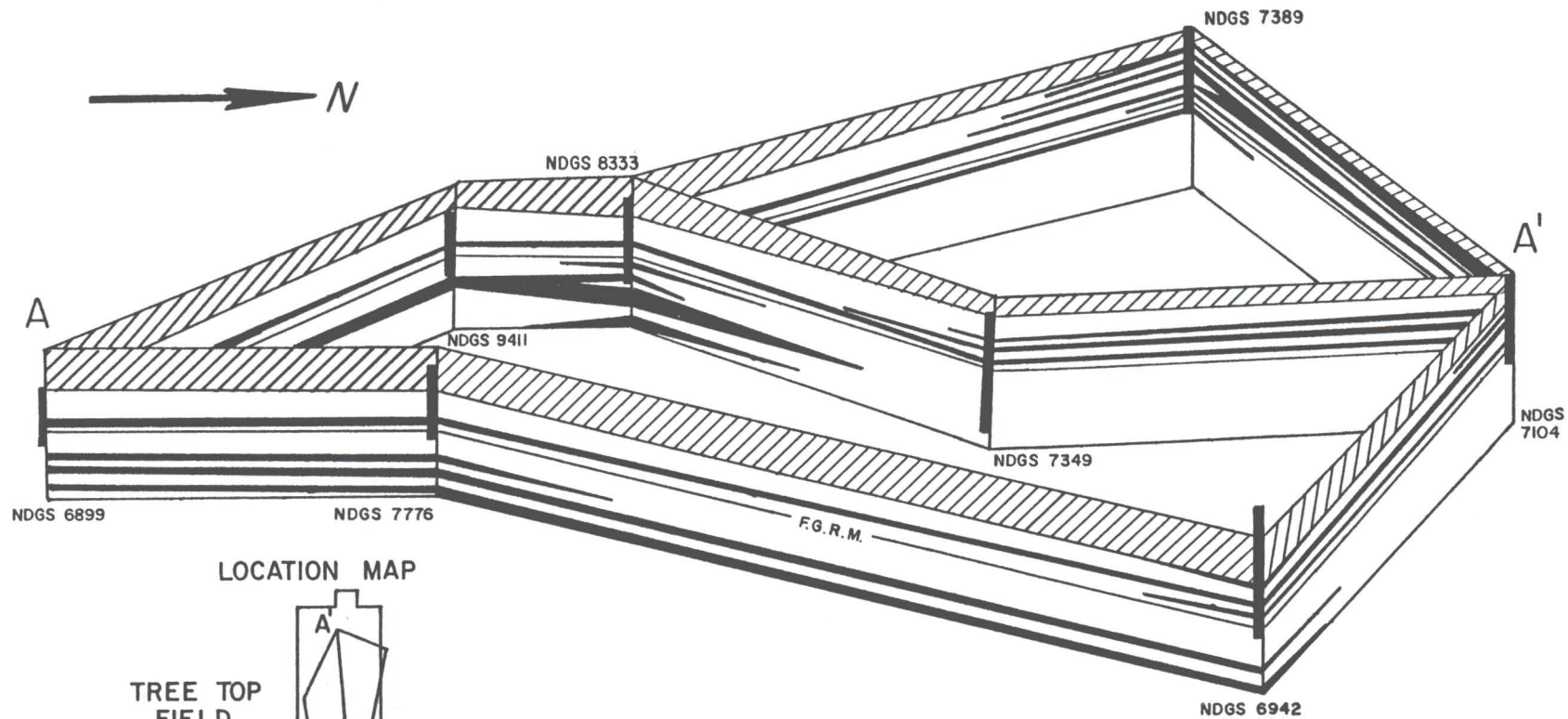
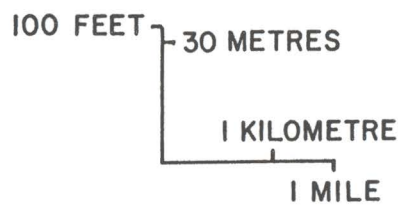
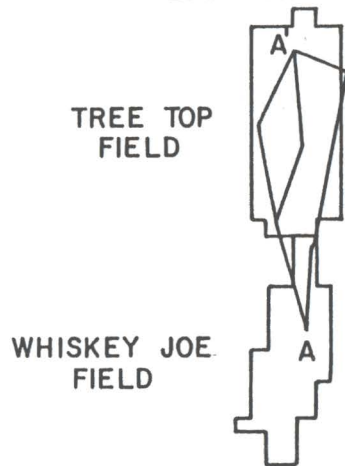





Figure 86 Fence diagram illustrating the distribution of porous zones within the upper Mission Canyon Formation in the study area (critical porosity is 8 percent) and their relation to the overlying anhydrite. F. R. G. M. represents the Fryburg gamma-ray marker



LOCATION MAP



-  ANHYDRITE
-  POROUS ZONES
-  CORE
- DATUM: STATE A

progradation continued over this area, reflux dolomitization of the sediments created intercrystalline porosity. With time and continued dolomitization, mud-rich, sublittoral sediments were progressively dolomitized downward until the magnesium ions were eventually exhausted or mixed with fresher waters. The decreased percentage of dolomite within the echinoderm wackestone lithotype, the lowermost lithotype, reflects this decrease in magnesium-rich fluids available for dolomitization.

Dolomitizing fluids were generally restricted to the less-cemented, mud-rich sediments. Early calcite cementation of allochem-rich sediments (intraclast bioclast wackestone packstone and laminated mudstone lithotypes) effectively inhibited dolomitization of these sediments.

The lesser amounts of dolomite within the neomorphic wackestone lithotype may be due to the combined processes of neomorphism and dedolomitization. Dolomite that may have been present in this lithotype at one time may have been dedolomitized during neomorphism. This same process of dedolomitization along with fracturing may have created both a source and a conduit for continued dolomitization in the relatively uncemented, mud-rich sediments below (dolomudstone lithotype).

## DIAGENETIC HISTORY

### Introduction

The diagenetic history of rocks of the upper Mission Canyon and lower Charles Formations in Treetop and Whiskey Joe fields represents a complex system of post-depositional diagenetic processes. In order to determine the relative timing of diagenetic events, eogenetic and mesogenetic diagenetic features were examined microscopically using a light microscope and a scanning electron microscope. Many of the diagenetic features were not visible in core samples and only became evident when examined this way. The relative distribution and timing of eogenetic and mesogenetic processes in the study area are illustrated in Table 2.

### Eogenetic Diagenesis

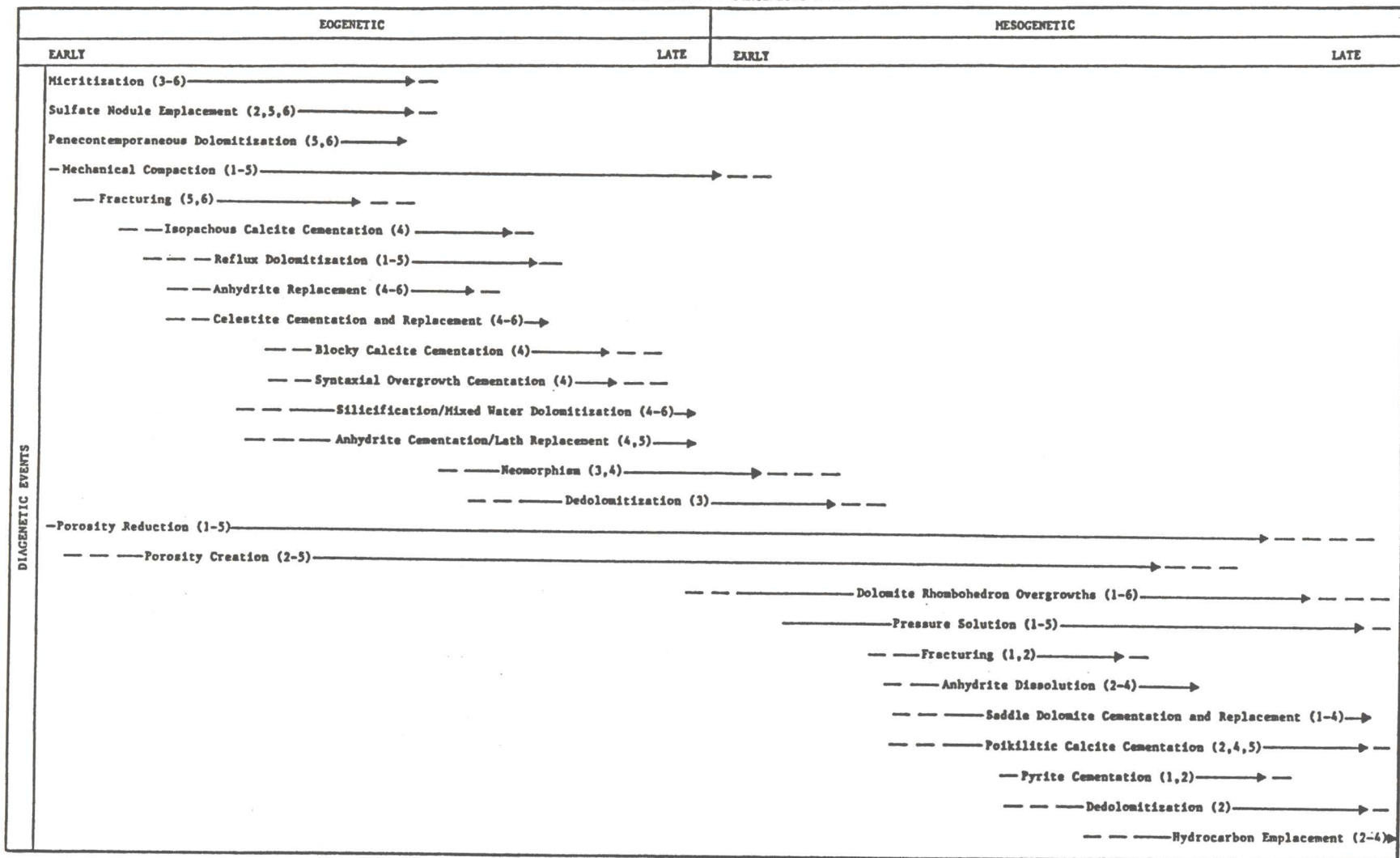
Major eogenetic diagenetic events in the study area include micritization, sulfate nodule emplacement, compaction, dolomitization, calcite cementation (isopachous, blocky, and syntaxial), neomorphism, dedolomitization, silica cementation and replacement, secondary porosity formation, and primary and secondary porosity reduction. Other eogenetic events include fracturing and anhydrite and celestite cementation and replacement.

Most pore fluids present during eogenetic diagenesis reflect near-surface water conditions and include

Table 2 Relative timing (eogenetic, mesogenetic) of diagenetic events and their relation to the distribution of lithotypes. Numbers located under each diagenetic event correspond to lithotypes in the following manner: 1) echinoderm wackestone lithotype, 2) dolomudstone lithotype, 3) neomorphic wackestone lithotype, 4) intraclast bioclast wackestone packstone lithotype, 5) laminated mudstone lithotype, and 6) anhydrite lithotype.



RELATIVE TIMING OF DIAGENETIC EVENTS



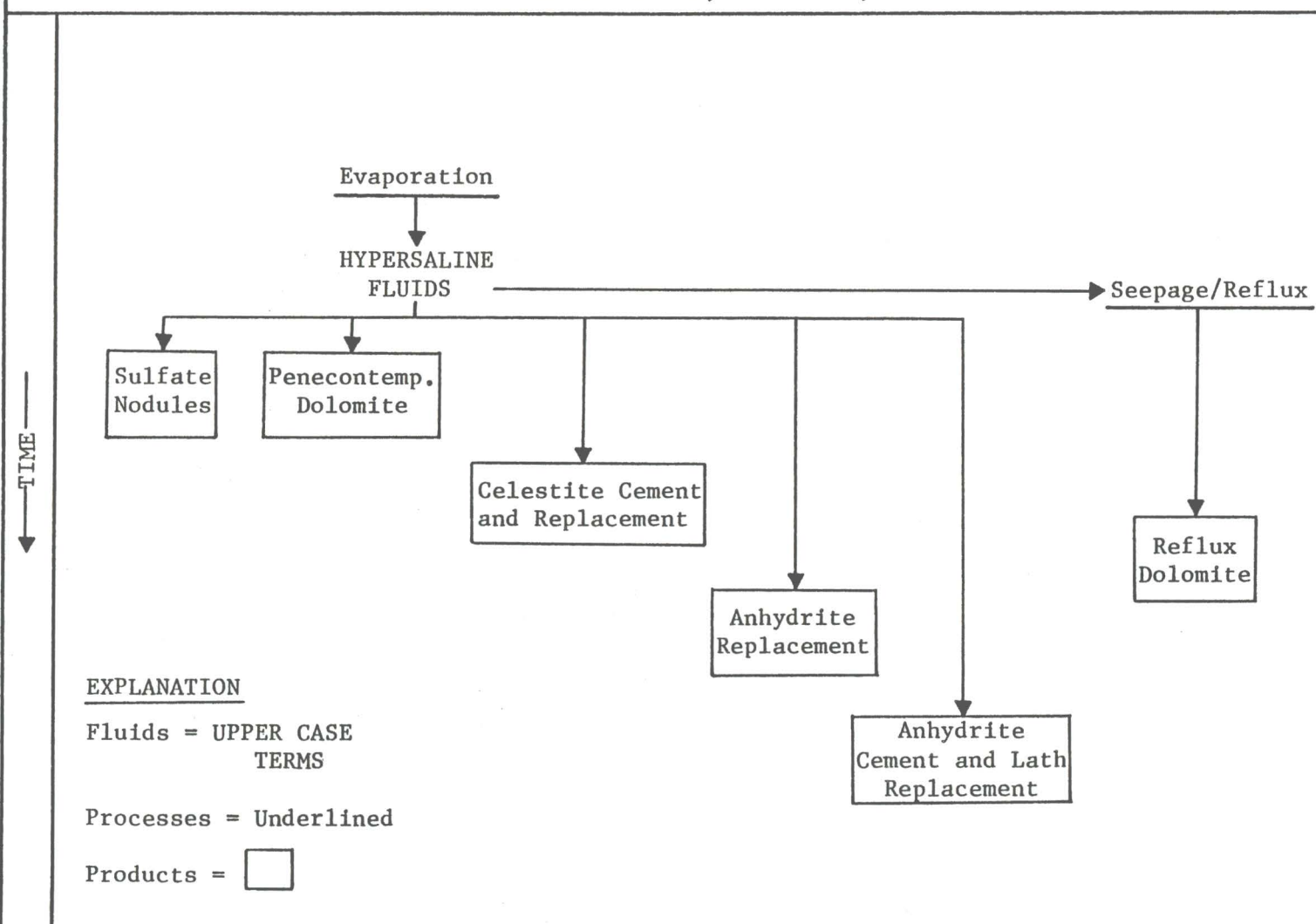
hypersaline, normal marine, and rainstorm-generated meteoric water. The majority of early diagenetic events and features were a result of the chemical interaction between these surface-related waters and the sediments (Fig. 87).

One of the earliest diagenetic events to occur in the study area took place in the littoral areas. Evaporation and refluxing of hypersaline fluids in supralittoral areas resulted in the formation of hypersaline vadose and phreatic zones. Hypersaline vadose conditions in littoral and supralittoral sediments are suggested by the early emplacement of displacive sulfate nodules and the penecontemporaneous replacement of those sediments by fine-grained dolomite. Penecontemporaneous dolomitization and sulfate precipitation were results of the surface evaporation of hypersaline brines and the subsequent increase in the Mg/Ca ratio (Illing and others, 1965; McKenzie and others, 1980).

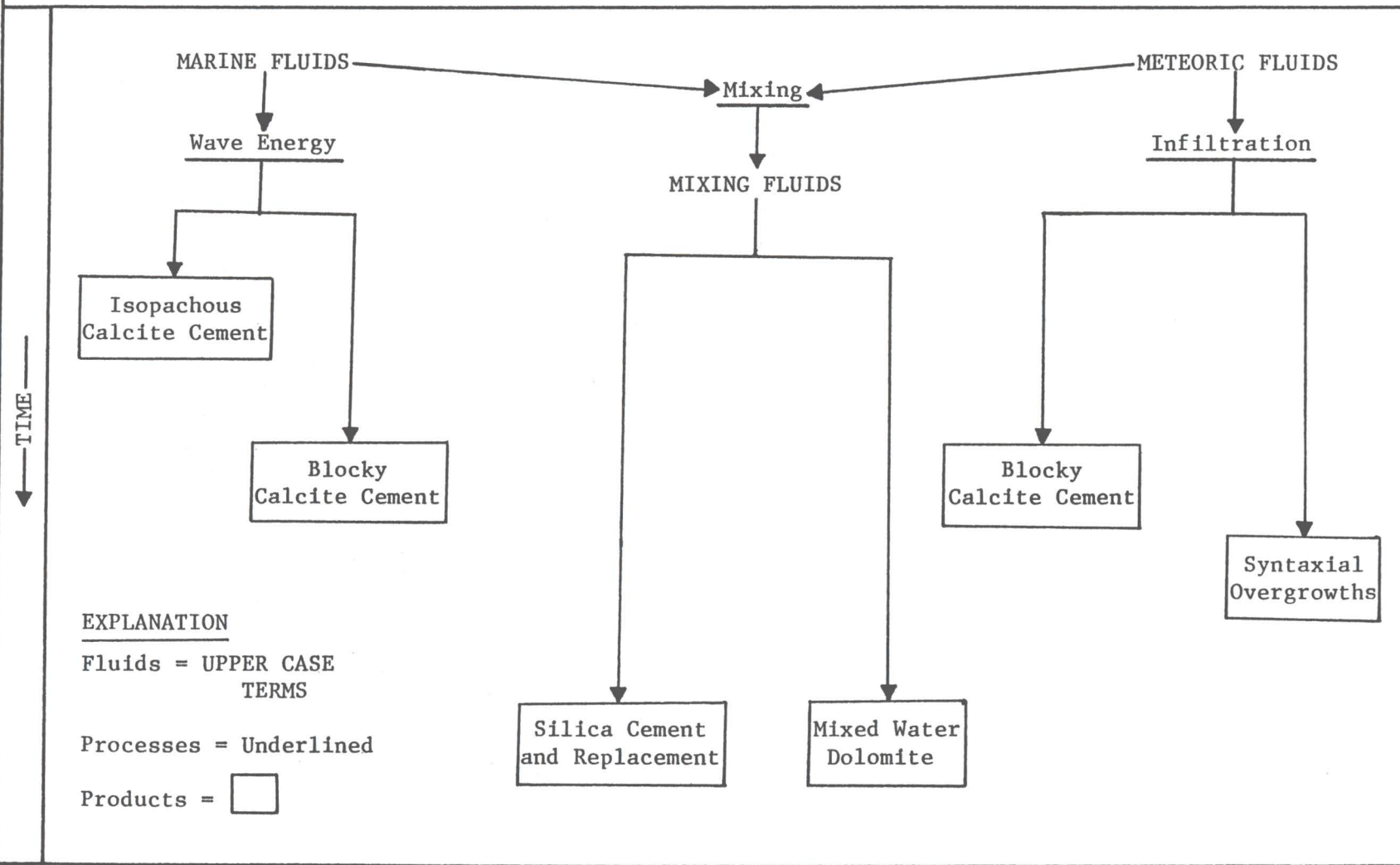
Refluxing and seepage of the hypersaline brines into the subsurface produced reflux dolomitization early in the diagenetic history of the study area. Reflux dolomitization was a continual process active during most of eogenetic diagenesis. As the magnesium-enriched, hypersaline fluids continued to migrate downward, reflux dolomitization of sublittoral sediments took place. The creation of secondary intercrystalline porosity, prominent in the dolomudstone lithotype, was a result of this dolomitization process.

Figure 87 Schematic diagram illustrating the relation between time and eogenetic fluids, processes, and products.

EOGENETIC FLUIDS, PROCESSES, AND PRODUCTS



EOGENETIC FLUIDS, PROCESSES, AND PRODUCTS  
(continued)



Although mud-rich sublittoral sediments were most often replaced by reflux dolomite, a few of the sublittoral grainstones were also dolomitized. Ward and Halley (1985) suggest that it may be difficult for dolomite to nucleate on calcite cement-rimmed (isopachous) grainstone substrates. The grainstones, existing in areas with less water circulation, were not subjected to early isopachous calcite cementation and thus were more susceptible to dolomitization.

Sediments deposited in the sublittoral environment contain pores which are saturated with marine water (Longman, 1980). Two near-surface diagenetic zones recognized in the sublittoral environment and containing diagenetic features related to the marine pore waters are: 1) a stagnant phreatic zone in which water movement through the sediment is slow or nonexistent, and 2) an agitated phreatic zone in which water is forced through the pores (Longman, 1980). In the study area, most of the upper Mission Canyon sublittoral lithotypes were initially subjected to diagenetic processes operating in these two marine phreatic diagenetic zones.

The echinoderm wackestone, dolomudstone, neomorphic wackestone, and intraclast bioclast wackestone packstone lithotypes were influenced by diagenetic processes in the stagnant marine phreatic zone. The absence of large quantities of early cement, as in these sublittoral lithotypes, is suggestive of a stagnant

diagenetic marine environment where water movement through the pores is limited (Longman, 1980).

Along the uppermost surface of the stagnant marine zone, the lack of both water movement and early cementation may have created an environment conducive to micritization by boring algae (Longman, 1980). Micritization of allochems in the study area probably occurred in the stagnant marine zone and is generally limited to allochems in the intraclast bioclast wackestone packstone and, rarely, the laminated mudstone lithotypes.

The lack of early cementation in the mud-rich, sublittoral sediments may also have rendered the sediments more susceptible to mechanical compaction and, in fact, mechanical compaction features are prevalent in the mud-rich lithologies in the study area. The early compaction of sublittoral sediments may have resulted in the loss of much of the primary porosity in the study area. Some of the ions present in the fluids expelled during compaction may have contributed to the processes of dolomitization and cementation.

In an agitated zone, marine water is able to flow easily through the sediment and this continuous migration of fluids commonly results in the precipitation of isopachous, grain-coating cement (Longman, 1980). In the study area, wave-generated marine waters may have been forced through sublittoral shoals creating the needed agitated conditions. Grainstones of the intraclast

bioclast wackestone packstone lithotype were most affected by the agitated conditions and many of the allochems in these rocks are surrounded by isopachous, grain-coating cement.

Meteoric and mixed water diagenetic features of the upper Mission Canyon rocks in the study area are generally restricted to the first 7 to 15 metres (23 to 49 feet) beneath the surface and occur in thin, 1 to 5 centimetre (0.4 to 2 inches) lenses or in patches. Blocky calcite, syntaxial overgrowths, mixed water dolomite, silica, and early porosity changes in the study area were most likely the result of meteoric and mixed water conditions in the phreatic diagenetic zone.

In the study area, meteoric waters, introduced during periodic rainstorms occasionally infiltrated the sublittoral sediments. Meteoric water initially entered supralittoral and littoral sediments through interparticle, intercrystalline and fracture pores. The meteoric waters migrated into the phreatic zone and began precipitating calcite cement. The intraclast bioclast wackestone packstone lithotype was most affected by the meteoric-derived pore waters and contains examples of both blocky calcite and syntaxial overgrowth cement.

According to Longman (1980), blocky calcite and syntaxial overgrowth cement tend to precipitate in the phreatic zone. Longman states that calcium-poor meteoric waters will initially dissolve calcite as the waters



migrate through the sediment into the phreatic zone and eventually become calcite-saturated. Blocky calcite and syntaxial overgrowth cement may then begin to precipitate from these waters (Longman, 1980).

Blocky calcite cement may also have precipitated in the stagnant marine environment. Given and Wilkinson (1985) suggest that equant calcite cement may form in diagenetic environments with different fluid chemistries, including marine and meteoric. A reduction of interparticle porosity following isopachous calcite cementation may have reduced agitation and allowed blocky calcite to slowly fill the remaining pores.

During meteoric diagenesis, porosity may be reduced or created (Longman, 1980). Reduction of both primary and secondary porosity in the study area occurred when blocky calcite and silica cements were precipitated from meteoric and mixed pore waters. Dissolution of allochems in the meteoric diagenetic zone created the moldic pores and vuggy pores of the intraclast bioclast wackestone packstone and laminated mudstone lithotypes.

Eogenetic diagenesis in the mixed water phreatic zone may have begun with the introduction and mixing of silica-rich, meteoric fluids with marine waters. Once the fluids are in the phreatic zone, movement of the mixed subsurface water will generally take place by convection (Hanshaw and others, 1971).

Mixing of pore waters in the study area produced

isolated areas containing both silicification and mixed water dolomitization. Knauth (1979) suggests that the mixing of meteoric and marine waters in nearshore environments may result in silicification, and it appears that silica-enriched, mixing fluids may have been responsible for silica cementation and replacement in the littoral and upper sublittoral sediments in the study area.

Mixed water dolomite can occur, not because of an increase in the Mg/Ca ratio of the pore waters but because of a reduction in other pollutant ions (such as silicon) (Folk and Land, 1975). The small, isolated patches of mixed water dolomite present in the study area may have formed following silicification. The removal of pollutant ions (such as silicon) in the mixing fluids following silicification may have allowed mixed water dolomitization to occur.

The same mixed water influence may have been responsible for local neomorphism and dedolomitization in the study area. Following mixed water dolomitization, pore fluids may have become slightly more enriched in calcium, allowing further calcite cementation to occur. Within rocks of the neomorphic wackestone lithotype, calcite cementation may have continued until the only remaining porosity existed within solution films between crystal boundaries. The migration of these solution films may have then led to neomorphism. In the study area, neomorphism may have been a slow process which continued through much

of eogenetic time. Dedolomitization, commonly associated with neomorphism in rocks of the neomorphic wackestone lithotype, may have occurred when migrating solution films encountered scattered dolomite rhombohedra.

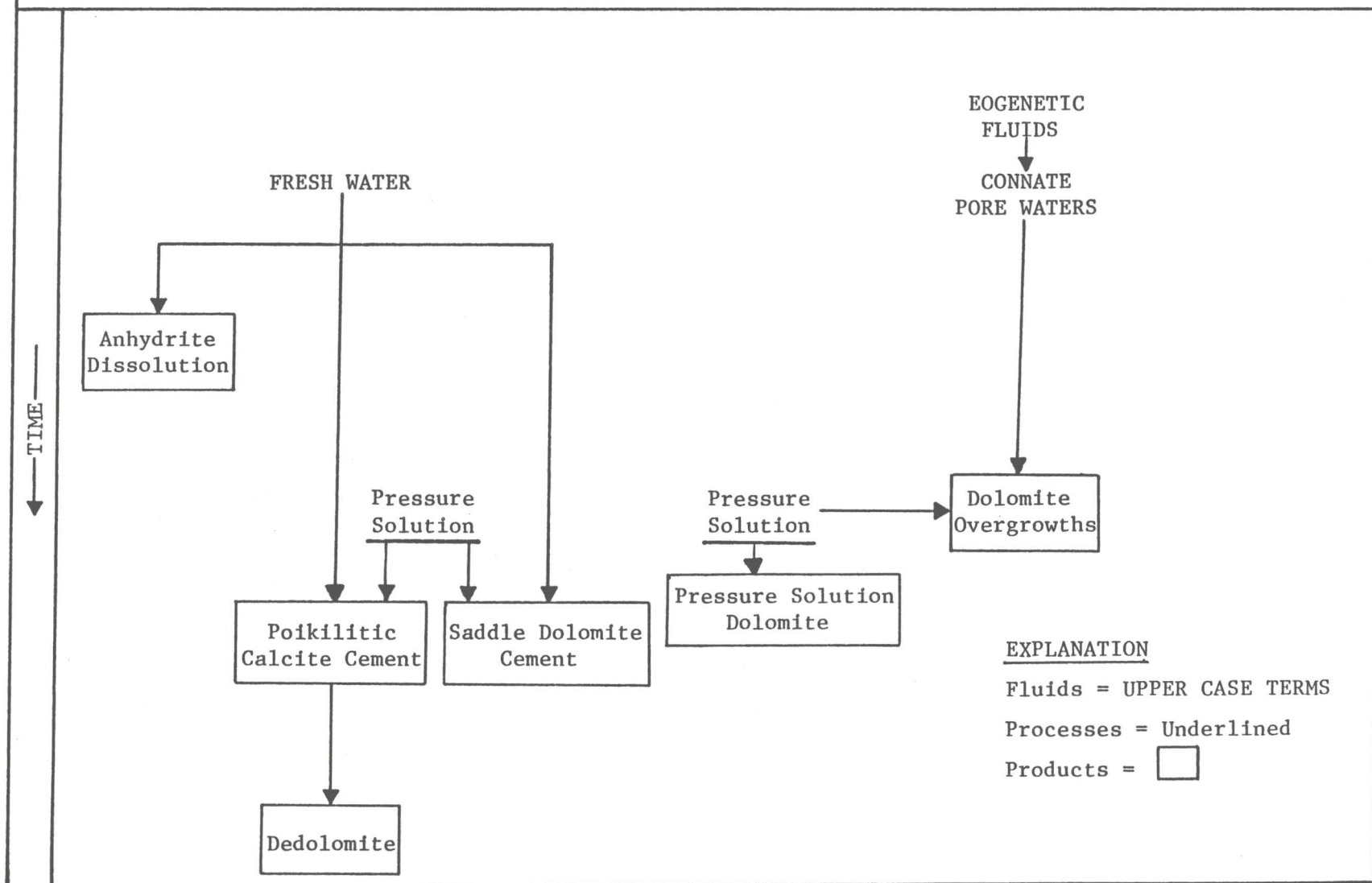
#### Mesogenetic Diagenesis

Mesogenetic diagenetic events in upper Mission Canyon rocks of Treetop and Whiskey Joe fields include porosity reduction, poikilitic calcite cementation, anhydrite dissolution, dedolomitization, saddle dolomite cementation and replacement, pressure solution, fracturing, pyrite cementation and replacement, and hydrocarbon emplacement. The products of mesogenetic diagenesis occur sporadically in the study area, making the relative distribution of the features and timing of diagenetic events difficult to determine (Table 2).

Blatt and others (1980) suggest that the state of carbonate diagenesis is dependent on the chemistry and distribution of the pore fluids and their rate of movement through the deposits. In the study area, local rather than regional changes in pore water chemistry became important during mesogenetic diagenesis (Fig. 88). Mesogenetic fluid migration through pores was complicated by various factors such as local changes in permeability, fracturing, and eogenetic cementation. The distribution of secondary porosity, created during eogenetic diagenesis, also exerted control over the movement and direction of pore waters. Connate pore waters originally derived from the surface

Figure 88 Schematic diagram illustrating the relation between time and mesogenetic fluids, processes, and products.

MESOGENETIC FLUIDS, PROCESSES, AND PRODUCTS



were mixed with fresher waters moving updip through the basin. Mixing of the chemically differing pore waters created a complex diagenetic environment.

The concept of late mesogenetic freshwater diagenesis has been proposed for the Billings anticline area (Stephens, 1986) and the Little Knife Field to the east (Lindsay and Roth, 1982). According to Berg and Mitsdarffer (1986), a relatively fresh water lens is currently present in the Billings Anticline area. Downy (1984) suggests that groundwater, migrating eastward through the Madison aquifer in the Williston Basin, is now discharging along the eastern edge of the basin. A continuous recharge of fresh water into the Madison aquifer in the west has led to a relatively fresh water influx in the study area.

The vertical distribution of the fresh water lens in the study area is unclear but diagenetic features related to the lens indicate that it lies mainly within the dolomudstone and possibly the neomorphic wackestone lithotypes. A migration of relatively fresh water into the study area may have contributed to anhydrite dissolution, poikilitic calcite cementation, saddle dolomite cementation and replacement, dedolomitization, pyrite cementation and replacement, and hydrocarbon emplacement.

Lindsay and Roth (1982) suggested anhydrite dissolution in the Little Knife Field, similar to the anhydrite dissolution in the study area, was a mesogenetic

event resulting from the fresh water influx. The fresh water is migrating along the regional dip through porous zones interconnected by fracture systems (Downy, 1984). The relatively fresh water, depleted in sulfate ions, may have led to the dissolution of anhydrite in the study area (mainly the nodules in the dolomudstone lithotype) and resulted in the release of calcium ions into the pore water system. The calcium-enriched fluids induced local precipitation of poikilitic calcite and pyrite cement into the pores left by dissolution, as evidenced by the calcite and anhydrite nodules of the dolomudstone lithotype. The large percentage of intercrystalline porosity in the dolomudstone lithotype may also have created conditions suitable for local poikilitic calcite cementation. Continued growth of the poikilitic calcite cement into the surrounding dolomite matrix could have resulted in the formation of small, patchy areas of dedolomitization.

The same late stage fresh water influx may have been responsible for the precipitation of saddle dolomite in the study area. Beales and Hardy (1980) suggest that migrating, basin-derived, sulfate-depleted solutions could effectively remove anhydrite and later precipitate saddle dolomite. Saddle dolomite is commonly associated with anhydrite dissolution and poikilitic calcite cementation in the dolomudstone lithotype, suggesting that a similar mechanism of dissolution and precipitation occurred in the study area.

Pressure solution may also have contributed to mesogenetic poikilitic calcite and saddle dolomite cementation in the study area. Fractures associated with stylolites in the echinoderm wackestone and dolomudstone lithotypes are generally calcite-filled, suggesting that fluids released during stylolitization may have been a source of calcium and magnesium ions needed for poikilitic calcite and saddle dolomite cementation.

Porosity in Treetop and Whiskey Joe fields was greatly affected by mesogenetic diagenesis. Some of the porosity created during eogenetic diagenesis was occluded during mesogenetic diagenesis, mainly by poikilitic calcite and saddle dolomite cementation.



## CONCLUSIONS

- 1) Rocks of the upper Mission Canyon and lower Charles Formations in Treetop and Whiskey Joe fields can be separated into six lithotypes based on the similarity and abundance of distinct features common to a group of rocks. Both depositional and diagenetic features were used to distinguish each lithotype. Lithotypes are: 1) echinoderm wackestone, 2) dolomudstone, 3) neomorphic wackestone, 4) intraclast bioclast wackestone packstone, 5) laminated mudstone, and 6) anhydrite.
- 2) The upper Mission Canyon and lower Charles Formations represent carbonate and evaporite deposition in a shallow epeiric sea. The upper Mission Canyon and lower Charles Formations in the study area were separated into sublittoral (echinoderm wackestone, dolomudstone, neomorphic wackestone, and intraclast bioclast wackestone packstone lithotypes), littoral (laminated mudstone lithotype), and supralittoral (anhydrite lithotype) depositional environments.
- 3) Rocks of the upper Mission Canyon and lower Charles Formations in Treetop and Whiskey Joe fields underwent numerous surface-related and deep-burial processes which include micritization, mechanical compaction, dolomitization, cementation, replacement, fracturing, porosity reduction and creation, neomorphism, and pressure solution.

- 4) Pore types within rocks of the upper Mission Canyon Formation in Treetop and Whiskey Joe fields include two primary pore types: interparticle and intraparticle; and four secondary pore types: intercrystalline, moldic, vuggy, and fracture.
- 5) Intercrystalline pores are the most abundant pore type in the study area.
- 6) Intercrystalline pores were divided into three pore shapes: 1) polyhedral, 2) tetrahedral, and 3) interboundary-sheet. Polyhedral pores are the most common pore shape in the study area while interboundary-sheet pores are the predominant type of pore throat.
- 7) Porous rocks in the upper Mission Canyon of Treetop and Whiskey Joe fields can be grouped into three porosity zones. The delineation of porosity zones was based on correlatable wire-line log characteristics within the study area.
- 8) Isopach maps of the aggregate thicknesses of porous rocks with greater than 8 percent critical porosity in the three porosity zones reflect trends in the distribution of porosity in the study area which are: 1) north-northwestward across the study area, porosity zones tend to parallel the overlying anhydrite and 2) toward the north-northwest, the thickest accumulations of porous rock occur progressively higher stratigraphically within each porosity zone. Progradation of

littoral and supralittoral environments north-northwestward over sublittoral environments and early dolomitization may have been a controlling factor in the aerial distribution of porosity in the study area.

- 9) Six inter-pore minerals were identified in the study area and include calcite, anhydrite, dolomite, silica, pyrite, and celestite.
- 10) Eogenetic diagenetic processes include micritization, mechanical compaction, dolomitization, cementation, replacement, secondary porosity creation, primary and secondary porosity reduction, fracturing, and neomorphism.
- 11) Pore fluids present during eogenetic diagenesis reflect near-surface water conditions and include hypersaline, marine, and rainstorm-generated meteoric waters.
- 12) Shallow, subsurface diagenetic zones include hypersaline vadose and phreatic, sublittoral stagnant and agitated phreatic, and meteoric and mixing phreatic.
- 13) Mesogenetic diagenetic processes include cementation, replacement, porosity reduction, dedolomitization, pressure solution, fracturing, and hydrocarbon emplacement.
- 14) Pore fluids present during mesogenetic diagenesis include connate pore water, fresh water, and fluids released during pressure solution.

APPENDICES

APPENDIX A

Legal descriptions and Locations of Described Cores

The legal descriptions and locations of cores used in this study are listed in order according to Township, Range, and section location. The cored interval described are given in feet according to the core depth followed by the wire-line log depth.

<u>CORE</u>	<u>LOCATION</u>	<u>INTERVAL</u>
NDGS #7104 W. H. Hunt Trust Estate Rodakowski #1	SE/SW, Sec. 3, T142N, R100W	9700-9760 (core) 9710-9770 (log)
NDGS #7283 W. H. Hunt Trust Estate Rodakowski U. S. A. #1	SE/SW, Sec. 10, T142N, R100W	9645-9703 (core) 9652-9710 (log)
NDGS # 6942 W. H. Hunt Trust Estate Johnson #1-12	NW/SW, Sec. 12, T142N, R100W	9670-9782 (core) 9666-9778 (log)
NDGS #7097 W. H. Hunt Trust Estate Dorothy Osadchuk #1	SE/SE, Sec. 15, T142N, R100W	9630-9689 (core) 9640-9699 (log)
NDGS #7389 W. H. Hunt Trust Estate No. 3 Egly	NE/NW, Sec. 21, T142N, R100W	9533-9592 (core) 9513-9572 (log)
NDGS #7351 W. H. Hunt Trust Estate Egly #2	SE/NE, Sec. 21, T142N, R100W	9622-9717 (core) 9634-9729 (log)
NDGS #6914 W. H. Hunt Trust Estate Fritz #1	NE/NE, Sec. 22, T142N, R100W	9616-9660 (core) 9618-9662 (log)
NDGS #7352 W. H. Hunt Trust Estate Fritz A-1	SE/NW, Sec. 22, T142N, R100W	9604-9660 (core) 9612-9668 (log)
NDGS #7349 W. H. Hunt Trust Estate Fritz #2	SW/SE, Sec. 22, T142N, R100W	9560-9655 (core) 9674-9669 (log)
NDGS #7776 Al-Aquitaine Exploration LTD, 3-141-100 BN #2-3	SE/SE, Sec. 3, T141N, R100W	9440-9490 (core) 9450-9500 (log)

NDGS #8333 Shell Oil Company U. S. A. #41-4	NE/NE, Sec. 4, T141N, R100W	9355-9432 (core) 9360-9437 (log)
NDGS #9411 Al-Aquitaine Exploration LTD, BN #1-9	NE/NE, Sec. 9, T141N, R100W	9452-9494 (core) 9469-9511 (log)
NDGS #6899 Al-Aquitaine Exploration LTD, U. S. #1-22	NE/NE, Sec. 22, T141N, R100W	9460-9506 (core) 9456-9502 (log)

## APPENDIX B

### Core and Thin Section Descriptions

The following core and thin section descriptions are from core located in the Wilson-M. Laird Core and Sample Library, Grand Forks, North Dakota. The descriptions are listed according to location. Depths given are both those footages marked on cores and the corresponding wire-line log depths. Thin section descriptions are indented and are preceded by TS.

NDGS #7104

W.H. Hunt Trust Estate Rodakowski #1  
SE/SW, Sec. 3, T142N, R100W

Cored Interval (9700-9760) Log Interval (9710-9770)

9700-9705 (core) Wackestone to Packstone

Dolostone, light to medium brown; containing replaced allochems (bioclasts?). Slightly laminated, interbedded with nodular-mosaic anhydrite. Black, wispy stringers and microstylolites common. Intercrystalline and moldic porosity estimated at less than 5%.

TS 9702 Dolomitized, anhydritic, bioclastic wackestone-packstone; 45-50% dolomite (matrix replacement, allochem replacement), 40-45% anhydrite (allochem replacement, felted-nodular matrix), 1-5% calcite (allochem); no visible porosity.

9705-9717 (core) Wackestone to Packstone

Dolomitic limestone, light to dark brown; containing peloids, ostracodes and unknown bioclasts (?). Allochems appear in layers and decrease in abundance upward. Laminated to slightly bedded with minor zones of bioturbation. Black, wispy stringers and microstylolites common. Nodular anhydrite increasing in abundance upward. Estimated intercrystalline and small vuggy porosity 5-10% and decreasing to less than 5% in the upper 3 feet.

TS 9707 Anhydritic, peloid, calcisphere dolowackestone-packstone; 70-75% dolomite (matrix replacement, allochem replacement, saddle dolomite cement), 20-25% anhydrite (matrix and allochem replacement), trace calcite (matrix); slightly laminated to microstylolitic; no visible porosity.

9717-9721.5 (core) Wackestone

Dolomitic limestone, dark brown; containing ostracodes, intraclasts and brachiopod fragments (?). Wispy laminations and microstylolites common, rare

suture seam stylolite present near 9717-9718.  
Estimated intercrystalline and small vuggy porosity less than 10%.

TS 9718 Bioclast, algal, echinoderm, intraclast wackestone; 90-95% calcite (matrix, neomorphic spar, allochem), 1-5% dolomite (matrix replacement, associated with microstylolites); micritized allochems, calcite-filled fracture, microstylolites; no visible porosity.

TS 9720 Dolomitic, ostracode, algal (?) mudstone; 35-40% dolomite (matrix replacement, saddle dolomite cement), 35-40% calcite (matrix, allochem, cement), trace anhydrite (cement); laminated to microstylolitic; 15-20% intercrystalline and vuggy porosity.

9721.5-9751.5 (core) Mudstone and Wackestone  
Dolomitic limestone, medium brown; containing anhydrite-replaced bioclasts (?) and ostracodes. Intensely bioturbated with occasional preserved burrow and black, wispy stringers. Stylolites and microstylolites are common; scattered vugs (1 mm to 1 cm) filled with calcite/anhydrite are associated with minor amounts of authigenic pyrite. Estimated intercrystalline and minor moldic porosity 5-15%.

TS 9725.5 Dolomitized mudstone; 65-70% dolomite (matrix replacement), 5-10% calcite (cement); microstylolites; 15-20% intercrystalline and vuggy porosity.

TS 9744 Dolomudstone; 90-95% dolomite (matrix replacement); 1-5% calcite (cement), trace pyrite, trace quartz silt; laminated; trace intercrystalline porosity.

TS 9749 Dolomitized mudstone; 65-70% dolomite (matrix replacement, saddle dolomite cement), 10-15% calcite (cement), trace anhydrite (cement), trace quartz silt; dedolomitization (?); 10-15% intercrystalline porosity.

9751.5-9752 (core) Mudstone  
Dolostone, quartz silt, dark gray to black. Intensely microstylolitic with associated pyrite. No visible porosity.

9752-9760 (core) Mudstone  
Same as 9721.5-9751.5 (core). Estimated intercrystalline and small vuggy porosity 10-15%.

TS 9752.5 Dolomitized, bioclast mudstone; 65-70%



dolomite (matrix replacement, saddle dolomite cement), 15-20% quartz silt (angular to subrounded), 5-10% pyrite (vug-lining cement, matrix), 1-2% calcite (allochem), trace anhydrite (allochem replacement ?); trace vuggy porosity.

## NDGS #7283

W. H. Hunt Trust Estate Rodakowski USA #1  
SE/SW, Sec. 10, T142N, R100W  
Cored Interval (9645-9703) Log Interval (9652-9712)

## 9645-9653 (core) Mudstone

Anhydrite and dolomitic anhydrite, light to medium olive gray. Small intraclasts are scattered within mosaic and nodular-mosaic anhydrite. Black, wispy laminations and microstylolites common. No visible porosity.

TS 9652.5 Anhydrite; 90-95% anhydrite (felted matrix, contorted), 1-5% dolomite (matrix in thin stringers); rare peloids (dolomitized); no visible porosity.

## 9653-9659.5 (core) Mudstone

Dolostone, medium brown; containing anhydrite-replaced bioclasts, anhydrite-replaced ostracodes and rare gastropod. Slightly laminated with anhydrite nodules randomly dispersed throughout. Black, wispy stringers and microstylolites present. Estimated inter-crystalline porosity less than 5%.

TS 9654.5 Dolomitized mudstone; 60-65% dolomite (matrix replacement), 10-15% calcite (matrix, cement ?), 10-15% anhydrite (matrix replacement); 1-5% vuggy porosity (mainly in lower half of slide away from anhydrite).

TS 9657 Dolomitized, ostracode, bioclast, algal, gastropod mudstone; 45-50% dolomite (matrix replacement), 30-35% calcite (matrix, allochem, cement), 10-15% anhydrite (matrix replacement, laths up to 2 mm long, 0.5 mm wide); no visible porosity.

## 9659.5-9666 (core) Mudstone

Anhydrite (nodular-mosaic), dolomitic anhydrite and dolostone, light to medium gray. Black, wispy laminations are present but rare. Estimated inter-crystalline porosity less than 10%.

TS 9659.5 Anhydrite; 90-95% anhydrite (felted matrix, contorted), 1-5% dolomite (matrix

replacement); rare peloids (dolomitized); no visible porosity.

9666-9677 (core) Wackestone to Packstone

Dolomitic limestone, medium brown; containing intraclasts, ostracodes, anhydrite-replaced bioclasts, brachiopod fragments, calcispheres (?), and rare rugose horn coral. Laminated, microstylolites common. Minor amounts of authigenic pyrite associated with allochems. Estimated intercrystalline, small vuggy, moldic and fracture porosity 5%.

TS 9666.5 Dolomitized, peloid, algal, bioclast, calcisphere, foram (?) wackestone-packstone; 65-70% dolomite (matrix replacement, allochem replacement, cement), 1-5% anhydrite (allochem replacement, cement); many allochems were micritized prior to dolomitization; 20-25% moldic, vuggy and intercrystalline porosity.

TS 9667 Dolomitized, peloid, intraclast, calcisphere, bioclast, wackestone-packstone; 60-65% dolomite (matrix replacement, allochem replacement) 10-15% silica (matrix replacement, pore lining cement, fracture-fill cement); 1-5% anhydrite (allochem replacement, matrix replacement); worm tubes present; rare suture seam stylolite; 10-15% vuggy and moldic porosity.

TS 9673 Dolomitized, peloid, calcisphere, foram, algal, ostracode, bioclast packstone; 45-50% dolomite (matrix replacement, associated with stylolites), 35-40% calcite (matrix, allochem, fracture-fill); compaction, microstylolites; 5-10% moldic (below microstylolites), fracture (above microstylolites) porosity.

9677-9702.5 (core) Mudstone to Wackestone

Dolomitic limestone, medium to dark brown; containing ostracodes, echinoderm fragments and rare coral fragments, all of which appear clustered within 5-10 cm zones. Commonly bioturbated with black, wispy stringers and occasional preserved burrows, microstylolites and stylolites. Calcite/anhydrite-filled vugs and vertical, calcite-filled fractures are present but rare. Estimated intercrystalline and small vuggy porosity 10-20%.

TS 9678.5 Dolomitic, echinoderm, bioclast mudstone; 70-75% calcite (matrix, allochem), 20-25% dolomite (matrix replacement, associated with microstylolites); compaction, microstylolites common, rare suture seam stylolite; trace vuggy porosity.

TS 9688 Dolomitized mudstone; 60-65% dolomite (matrix replacement), 5-10% anhydrite (cement, allochem replacement), 1-5% calcite (matrix); 15-20% intercrystalline and vuggy porosity.

TS 9695 Dolomudstone; 75-80% dolomite (matrix replacement, saddle dolomite (?) cement), anhydrite (allochem replacement (?), cement); allochem ghosts may be present; 1-5% intercrystalline porosity.

9702.5-9703 (core) Mudstone  
Dolostone, quartz silt, black. Intensely microstylolitic to laminated with associated pyrite. Grades downward into medium brown, dolomitic mudstone similar to 9677-9702.5. Estimated intercrystalline porosity less than 5%.

NDGS #6942

W.H. Hunt Trust Estate Johnson #1-12  
NW/SW, Sec. 12, T142N, R100W

Cored Interval (9670-9782) Log Interval (9666-9778)

9670-9742 (core) Mudstone  
Anhydrite, dolomitic anhydrite, dolostone, dolomitic limestone, light olive gray to medium brown; containing rare, anhydrite-replaced unknown allochems and ostracodes. Laminated to crenulated (algal) laminated grading into, and interbedded with, massive, massive-bedded, mosaic, bedded-mosaic, nodular, bedded nodular, and distorted, elongated, nodular anhydrite. Black, wispy laminations with small, anhydrite-filled fractures common. Stylolites present but rare. No visible porosity.

TS 9680 Ostracode dolomudstone; 75-80% dolomite (matrix, allochem replacement), 5-10% silica (chert: allochem replacement), 5-10% anhydrite (allochem replacement); horizontally orientated, wispy laminations to contorted, wispy laminations; no visible porosity.

TS 9683 Anhydritic, dolomitized mudstone; 45-50% anhydrite (felted matrix, allochem replacement), 40-45% dolomite (matrix replacement), 1-2% pyrite (contorted wisps), trace quartz silt; anhydrite replaced peloids (?); no visible porosity.

TS 9685.5 Anhydritic dolomudstone; 75-80% anhydrite (detrital, felted matrix), 10-15% dolomite (contorted, wispy laminations), 1-5% silica (authigenic quartz), trace celestite; detrital anhydrite appears in layers (approximately 1 mm wide) between dolomite

laminations; no visible porosity.

TS 9686 Dolomitic, anhydritic, peloid mudstone; 35-40% anhydrite (matrix, lath replacement), 35-40% dolomite (matrix replacement), 10-15% quartz silt (angular); laminated with thin (approximately 1 mm) interbedded layers of quartz and anhydrite; no visible porosity.

TS 9687 Dolomitic, peloid mudstone; 30-35% calcite (allochem, matrix) 35-40% dolomite (matrix replacement), 20-25% anhydrite (bedded matrix); interbedded anhydrite and dolomitic mudstone; no visible porosity.

TS 9713 Peloid, algal, calcisphere, ostracode dolomudstone; 70-75% dolomite (matrix replacement, allochem replacement), 5-10% anhydrite (matrix, allochem replacement, fracture-fill cement), 1-5% calcite (allochem), trace celestite (fracture-fill); rare microstylolites, cryptalgal laminated to laminated; no visible porosity.

TS 9715 Dolomitized, algal, peloid, calcisphere, ostracode, bioclast mudstone; 40-45% dolomite (matrix replacement, allochem replacement, cement), 35-40% calcite (matrix, allochem, fracture-fill cement), 10-15% anhydrite (matrix replacement, allochem replacement, fracture-fill cement), trace celestite (allochem replacement, fracture-fill); no visible porosity.

TS 9723 Dolomitized, anhydritic mudstone; 55-60% dolomite (matrix replacement), 35-40% anhydrite (matrix); very fine grained; no visible porosity.

TS 9725 Dolomitic, anhydritic, partially silicified mudstone; 50-55% anhydrite (matrix, nodules), 25-30% silica (authigenic quartz: pore lining), 10-15% dolomite (matrix replacement), trace celestite; no visible porosity.

TS 9733 Dolomitic, peloid, algal, calcisphere, ostracode mudstone to packstone; 30-35% calcite (allochem), 25-30% dolomite (matrix replacement, allochem replacement), 15-20% anhydrite (allochem replacement, nodules, matrix), 5-10% silica (chert: cement); stylolites, anhydrite-filled vertical fractures, graded bedding (?); 1-5% vuggy, intercrystalline porosity.

9742-9752 (core) Mudstone to Wackestone  
Limestone, calcareous dolostone, dolostone, dark brown; containing ostracodes, small brachiopod fragments and

unknown bioclasts, all of which decrease in abundance upward. Laminated with occasional scour surfaces (?). Slightly bioturbated in areas with black, wispy stringers, microstylolites and rare, anhydrite-filled vertical fractures present. Estimated intercrystalline, moldic and vuggy porosity 15-20%.

TS 9745 Dolomudstone; 70-75% dolomite (matrix replacement, saddle dolomite cement), 1-5% anhydrite (fracture-fill, allochem replacement ?); 15-20% intercrystalline, fracture porosity.

TS 9750.5 Dolomitized, peloid, algal, calcisphere, mudstone; 50-55% dolomite (matrix replacement, cement), 35-40% calcite (matrix, allochem); 1-5% intercrystalline porosity.

9752-9753 (core) Grainstone

Limestone, medium brown; containing (micrite coated) intraclasts, unknown bioclasts. Graded bedded with occasional microstylolites, rare, large amplitude (15 cm) suture seam stylolite and subhorizontal calcite-filled fracture. No visible porosity.

TS 9752 Peloid, intraclast, algal, foram, ostracode, bioclast packstone-grainstone; 90-95% calcite (allochem, cement, matrix), 1-5% dolomite (allochem replacement, matrix replacement, associated with stylolites); stylolites, slightly bedded; no visible porosity.

9753-9755 (core) Mudstone and Wackestone

Limestone, dark brown; containing echinoderm fragments and calcispheres. Microstylolites and calcite-filled vertical fractures common. No visible porosity.

9755-9778 (core) Mudstone

Dolomitic limestone and calcareous dolostone, light to dark brown; containing ostracodes, peloids, unknown bioclasts and rugose horn corals (near 9765). Commonly bioturbated with black, wispy stringers and laminations, occasional preserved burrows, abundant microstylolites and rare, large amplitude suture seam stylolite (15 cm). Anhydrite-filled, vertical fractures and vugs, some with associated authigenic pyrite and minor open fractures, are present. Estimated intercrystalline, small vuggy and rare moldic porosity 10-20%.

9778-9779 (core) Mudstone

Dolostone, quartz silt, black. Intensely microstylolitic to laminated with associated pyrite. No visible porosity.

TS 9779 Quartz silt mudstone; 30-35% quartz silt (angular to subangular, concentrated in microstylolites), 1-5% dolomite (matrix replacement), 60-65% insoluble material (in microstylolites); abundant microstylolites, no visible porosity.

9779-9782 (core) Mudstone  
Same as 9755-9778. Occasional calcite-filled vugs. Estimated intercrystalline and small vuggy porosity 10%.

TS 9780 Dolomitized mudstone; 60-65% dolomite (matrix replacement, allochem replacement), 5-10% calcite (cement), 1-5% anhydrite (cement), 1-5% pyrite (lining vugs), 10-15% quartz silt (subangular); microstylolites; trace intercrystalline porosity.

NDGS #7097

W. H. Hunt Trust Estate Dorothy Osadchuck #1  
SE/SE, Sec. 15, T142N, R100W

Cored Interval (9630-9689) Log Interval (9640-9699)

9630-9634 (core) Mudstone to Wackestone  
Limestone, light to medium brown. Laminated with occasional bedded-nodular anhydrite and rare stylolites. Dark brown anhydrite laths superimposed on laminated mudstone. Estimated small vuggy porosity less than 5%.

TS-9631.8 Dolomitized, peloid, ostracode wackestone-packstone; 40-45% dolomite (matrix replacement, saddle dolomite cement), 30-35% anhydrite (felted matrix, lath replacement), 15-20% calcite (matrix, cement, allochem); stylolite; no visible porosity.

9634-9637 (core missing)

9637-9641 (core) Wackestone  
Dolostone, medium tan to medium brown; containing intraclasts and rare, replaced bioclasts. Laminated with occasional anhydrite nodules. Microstylolites are common. Large, suture seam stylolite at 9641 separates this lithology from underlying lithology (9641-9651). Estimated intercrystalline, small vuggy and moldic porosity 10%.

TS-9637 Calcisphere (?), ostracode (?), peloid dolowackestone; 70-75% dolomite (matrix replacement, saddle dolomite cement), 5-10% anhydrite (felted, in nodules), trace pyrite; 10-15% vuggy porosity.

- 9641-9651 (core) Mudstone to Wackestone  
Dolomitic limestone, dark brown; containing replaced bioclasts. Laminated to slightly bioturbated. Microstylolites and vertical fractures common. Estimated vuggy, intercrystalline and fracture porosity 10%.
- TS-9645 Algal, ostracode mudstone; 85-90% calcite (matrix, allochem), 5-10% dolomite (matrix replacement); compaction; no visible porosity.
- 9651-9658 (core) Wackestone to Packstone  
Limestone, dark brown to dark gray; containing ostracodes, intraclasts, brachiopod and echinoderm fragments. Small burrows, microstylolites and stylolites common. Estimated vuggy porosity 10%.
- TS-9652.5 Dolomitic, echinoderm, coral, bioclast mudstone; 70-75% calcite (matrix, allochem), 20-25% dolomite (allochem replacement, matrix replacement); microstylolites; 1-2% intercrystalline porosity.
- 9658-9661 (core missing)
- 9661-9676.5 (core) Mudstone to Wackestone  
Dolomitic limestone, dark brown; containing ostracodes, echinoderm fragments, unknown bioclasts and rare, rugose horn corals. Commonly bioturbated with numerous black, wispy stringers. Occasional calcite/anhydrite-filled vugs, stylolites and small vertical fractures. Estimated intercrystalline and moldic porosity 10-15%.
- TS-9661.5 Dolomudstone; 70-75% dolomite (matrix replacement), 10-15% calcite (cement, matrix ?); 5-10% intercrystalline porosity.
- TS-9668.7 Dolomudstone; 75-80% dolomite (matrix replacement), 5-8% anhydrite (felted matrix, nodules, fracture-fill cement), 1-2% calcite (cement), trace quartz silt; 5-10% intercrystalline, vuggy and fracture porosity.
- TS-9675.7 Dolomitized mudstone; 65-70% dolomite (matrix replacement), 5-10% calcite (cement, fracture-fill cement), 1-5% anhydrite (nodules), trace quartz silt; 10-15% vuggy, intercrystalline and fracture porosity.
- 9676.5-9676.8 (core) Mudstone  
Dolostone, quartz silt, black. Moderately laminated with abundant microstylolites. Estimated porosity less than 5%.

TS-9676.5 Quartz silt, dolomitic mudstone; 25-30% dolomite (matrix replacement), 20-25% quartz silt (subangular), 40-45% insoluble material (microstylolites); abundant microstylolites; no visible porosity.

9676.8-9688.6 (core) Mudstone to Wackestone  
Calcareous dolostone, dark brown; containing possible echinoderm fragments and unknown allochems. Commonly bioturbated with large (up to 2 cm) calcite/anhydrite-filled vugs generally surrounded by authigenic pyrite. Dense, black microstylolites and stylolites common. Estimated intercrystalline and small vuggy porosity 5-15%.

TS-9683.2 Dolomudstone; 85-90% dolomite (matrix replacement, saddle dolomite cement); 5-10% intercrystalline porosity.

9688.6-9689 (core) Mudstone  
Dolostone, quartz silt, black. Intensely microstylolitic to slightly laminated and associated with authigenic pyrite. No visible porosity.

NDGS #7389

W. H. Hunt Trust Estate No. 3 Egly  
NE/NW, Sec. 21, T142N, R100W

Cored Interval (9533-9592) Log Interval (9513-9572)

9533-9542 (core) Mudstone  
Dolostone and anhydrite, light olive gray to light brown; containing ostracodes, calcispheres (?) and peloids. Laminated to cryptalgal laminated with interbedded-nodular and bedded-mosaic anhydrite minor soft sediment deformation. Estimated vuggy porosity less than 5%.

TS 9535 Dolomitized, anhydritic, ostracode, peloid calcisphere (?) mudstone to wackestone; 50-55% dolomite (matrix replacement, allochem replacement), 40-45% anhydrite (bedded matrix); bedded to laminated; micritization of allochems (dolomitized); no visible porosity.

TS 9538 Dolomitized, peloid, ostracode, calcisphere wackestone-packstone; 50-55% dolomite (matrix replacement, allochem replacement by saddle dolomite) 20-25% calcite (allochem, cement, matrix), 5-10% anhydrite (matrix, allochem replacement, cement?); bedded; 5-10% vuggy, intercrystalline, moldic and intraparticle porosity.



- 9542-9546 (core) Wackestone to Packstone  
Dolostone and anhydrite, tan to light brown; containing intraclasts, ostracodes and calcispheres. Dolostones commonly interbedded with bedded-nodular and nodular, intraclastic anhydrite. Black, wispy stringers, microstylolites, stylolites, calcite/anhydrite-filled vugs and calcite-filled fractures common. Estimated intercrystalline, small vuggy and moldic porosity 5%.
- 9546-9570 (core) Mudstone  
Limestone and dolomitic limestone, medium to dark brown; containing anhydrite-replaced allochems. Bioturbated with rare preserved burrows, black, wispy laminations, abundant microstylolites, stylolites and small, vertical, calcite-filled and open fractures. Estimated vuggy, minor moldic and fracture porosity 10-15%.
- TS 9546 Dolomitic, peloid, intraclast, bioclast, foram, calcisphere, algal packstone; 75-80% calcite (allochem, cement, matrix), 15-20% dolomite (matrix replacement, minor allochem replacement); stylolite (?), micritization of some allochems; no visible porosity.
- TS 9554 Dolomitic, siliceous, bioclast, foram, brachiopod (?), ostracode (?) wackestone; 55-60% calcite (allochem, matrix, fracture-fill cement), 20-25% silica (chert: matrix replacement, allochem replacement, mainly in upper half of slide), 10-15% dolomite (matrix replacement, fracture-fill cement, decreases away from chert); microstylolites, vertical fracture filled with calcite and dolomite; trace intraparticle and vuggy porosity.
- TS 9557 Dolomitized mudstone; 45-50% dolomite (matrix replacement, saddle dolomite cement), 25-30% calcite (cement, allochem ?), 1-5% anhydrite (cement); 10-15% intercrystalline and vuggy porosity.
- TS 9567 Dolomitized mudstone; 45-50% dolomite (matrix replacement, saddle dolomite cement), 35-40% calcite (allochem ?), matrix; small, vertical fractures; 5-10% intercrystalline, vuggy and fracture porosity.
- 9570-9576 (core) Wackestone  
Limestone, dark brown; containing rugose horn corals, coral fragments, echinoderm fragments and rare Syringopora coral. Slightly laminated with black, wispy stringers, microstylolites, occasional stylolites and open fractures. Estimated small vuggy, moldic (?) and fracture porosity 10%.

## 9576-9584 (core) Mudstone

Dolostone, dark to medium brown; containing anhydrite-replaced allochems. Commonly bioturbated with occasional preserved burrows, black, wispy stringers, large (1-2 cm) anhydrite-filled vugs and rare anhydrite-filled fractures. Estimated intercrystalline and small vuggy porosity 10-15%.

TS 9577 Dolomudstone; 85-90% dolomite (matrix replacement, saddle dolomite cement), 1-5% calcite (cement?), 1-5% anhydrite (cement), trace quartz silt; microstylolites; no visible porosity

TS 9582 Dolomitized, bioclast, echinoderm, coral wackestone; 55-60% calcite (allochem, matrix), 35-40% dolomite (matrix replacement); compaction; no visible porosity.

## 9584-9585 (core) Mudstone

Dolostone, quartz silt, dark gray to black. Alternating between densely microstylolitic zones with associated pyrite and less microstylolitic, bioturbated zones. No visible porosity.

## 9585-9592 (core) Wackestone

Dolomitic limestone, dark gray; containing echinoderm fragments, unknown bioclasts and brachiopod fragments (?). Commonly microstylolitic and stylolitic with small calcite/anhydrite nodules and both calcite-filled and open fractures. Estimated intercrystalline and fracture porosity less than 5%.

NDGS #7351

W.H. Hunt Trust Estate Egly #2  
SE/NE, Sec. 21, T142N, R100W

Cored Interval (9622-9717) Log Interval (9634-9729)

## 9622-9629 (core) Mudstone and Wackestone

Dolostone and anhydrite, light gray to medium brown; containing intraclasts (mainly in anhydrite), ostracodes and calcispheres (?). Laminated to cryptalgal laminated, interbedded with nodular, mosaic and massive anhydrite. Black, wispy laminations and microstylolites, stylolites and rare calcite-filled fracture present. No visible porosity.

TS 9623.5 Dolomitized, anhydritic, peloid, ostracode mudstone; 60-65% dolomite (matrix replacement, allochem replacement), 30-35% anhydrite (allochem replacement, felted matrix); micritized (dolomitized) allochems; no visible porosity.

TS 9624.5 Dolomitized, anhydritic, peloid, ostracode mudstone; 55-60% dolomite (matrix replacement, allochem replacement), 35-40% anhydrite (felted matrix, allochem replacement (or detrital ?), trace calcite (within dolomite rhombs); micrite-rimmed allochems (dolomitized); trace intercrystalline porosity.

TS 9625.5 Dolomudstone; 75-80% dolomite (matrix replacement, saddle dolomite replacement of allochem or cement), 10-15% calcite (cement, allochem), 1-5% anhydrite (cement); micrite-rimmed (dolomitized) allochems; trace intercrystalline porosity.

TS 9626.5 Dolomitic, foram, echinoderm (?), brachiopod wackestone; 65-70% calcite (matrix, allochem, neomorphic spar), 25-30% dolomite (associated with stylolite); large stylolite, compaction, micritized allochems; trace interparticle porosity.

9629-9634 (core) Mudstone and Wackestone  
Limestone, medium brown; containing intraclasts, unknown bioclasts, ostracodes and rugose horn corals. Slightly bioturbated with occasional preserved burrows, black, wispy stringers and microstylolite swarms. Estimated small vuggy and moldic porosity 5-10%.

TS 9633 Dolomitic, siliceous, foram mudstone; 25-30% dolomite (large, matrix replacement rhombs), 25-30% silica (chert: matrix replacement), 20-25% calcite (neomorphic spar, matrix); 10-15% vuggy porosity (greater in cherty areas).

9634-9652 (core) Mudstone  
Dolomitic limestone, dark brown; containing ostracodes, occasional rugose horn corals and rare bryozoan, generally appearing in subhorizontal beds. Commonly bioturbated with occasional, small, preserved burrows, black, wispy stringers and calcite/anhydrite-filled vugs. Estimated small vuggy and intercrystalline porosity 10-15%.

TS 9642 Dolomitized mudstone; 45-50% calcite (neomorphic spar, matrix, allochem), 40-45% dolomite (matrix replacement, allochem replacement); 1-5% vuggy and intercrystalline porosity.

9652-9657 (core missing)

9657-9659 (core) Mudstone  
Calcareous dolostone, medium brown; containing

echinoderm fragments (?). Commonly bioturbated with black, wispy stringers and large (up to 2 cm) calcite-filled vugs. Estimated intercrystalline porosity 10%.

9659-9660 (core) Mudstone

Dolostone, quartz silt, dark gray to black. Alternating between intensely microstylolitic zones and less microstylolitic, bioturbated zones with abundant black, wispy material. Authigenic pyrite is closely associated with microstylolites. No visible porosity.

TS 9659.5 Dolomitized, quartz silt mudstone; 55-60% dolomite (matrix replacement), 15-20% quartz silt (angular), 15-20% insoluble material (microstylolites); abundant microstylolites; no visible porosity.

9660-9669 (core) Mudstone

Calcareous dolostone, dark brown; containing unknown bioclasts and echinoderm fragments (?). Commonly bioturbated with occasional preserved burrows, black, wispy stringers and rare stylolite. Large calcite/anhydrite-filled vugs and fractures are associated with minor amounts of authigenic pyrite. Estimated intercrystalline porosity 5-10%.

9669-9683 (core) Mudstone and Wackestone

Dolomitic limestone, dark brown to dark gray; containing echinoderm fragments (increasing in abundance downward), intraclasts (?) and occasional rugose horn corals. Commonly bioturbated with black, wispy stringers, small, stylolites and small, calcite-filled fractures. Estimated intercrystalline porosity less than 5%.

TS 9669.5 Dolomitized, foram, ostracode mudstone; 65-70% dolomite (matrix replacement), 25-30% calcite (neomorphic spar, cement and fracture-fill cement), trace anhydrite, trace quartz silt; microstylolites, dedolomitization (?); no visible porosity.

TS 9674 Dolomudstone 70-75% dolomite (matrix replacement, allochem replacement, saddle dolomite cement), 20-25% calcite (cement), trace anhydrite; dedolomitization (?); no visible porosity.

TS 9680.5 Echinoderm, brachiopod, bryozoan wackestone-packstone; 80-85% calcite (matrix, allochem, fracture-fill cement), 5-10% dolomite (matrix replacement, fracture-fill cement), 1-5% anhydrite (allochem replacement), trace quartz silt; stylolite, compaction; no visible porosity.

## 9683-9717 (core) Wackestone and Packstone

Dolomitic limestone, medium brown; containing echinoderm fragments, rugose horn corals, unknown bioclasts, occasional brachiopod fragment and rare Syringopora coral. Abundant microstylolites, occasional stylolites, fractures and rare, small, calcite-filled vugs. Estimated intercrystalline, small vuggy and rare intraparticle porosity 5-10%.

TS 9686 Dolomitic, echinoderm, brachiopod, bioclast wackestone-packstone; 55-60% calcite (allochem, matrix), 35-40% dolomite (matrix replacement, allochem replacement, associated with microstylolites), 1-2% anhydrite (matrix replacement); microstylolites, minor compaction; trace intraparticle porosity.

TS 9690.5 Dolomitic, echinoderm, brachiopod wackestone-packstone; 60-65% calcite (allochem, matrix), 25-30% dolomite (matrix replacement, allochem replacement), 1-5% silica (chert: nodule replacement of matrix and rare allochem); minor compaction; no visible porosity.

TS 9694 Dolomitized, echinoderm, brachiopod (?) wackestone; 50-55% dolomite (matrix replacement, allochem replacement), 35-40% calcite (matrix, allochem), trace pyrite; compaction, 1-5% intercrystalline and intraparticle porosity.

TS 9700 Echinoderm, brachiopod, bryozoan, ostracode, wackestone-packstone; 85-90% calcite (allochem, matrix, rare cement), trace anhydrite (cement), trace pyrite; compaction; 5-10% intraparticle and interparticle porosity.

TS 9705 Echinoderm, brachiopod, bioclast wackestone; 85-90% calcite (matrix, allochem), 1-5% dolomite (matrix replacement), trace anhydrite (cement); compaction; 1-5% intraparticle and interparticle porosity.

TS 9714 Dolomitized, echinoderm, brachiopod mudstone-wackestone; 60-65% dolomite (matrix replacement, minor allochem replacement), 30-35% calcite (allochem), trace anhydrite (allochem replacement); no visible porosity.

NDGS #6914

W.H. Hunt Trust Estate Fritz #1  
NE/NE, Sec. 22, T142N, R100W

Cored Interval (9616-9660) Log Interval (9618-9662)

## 9616-9619.7 (core) Mudstone

Limestone, medium brown. Black, wispy stringers and laminations common. Small (1 mm), dark brown anhydrite laths scattered throughout. Estimated small vuggy porosity less than 5%.

## 9619.7-9623.5 (core) Mudstone

Dolostone, anhydritic dolostone and anhydrite, light to medium brown. cryptalgal laminated to thinly laminated, interbedded with mosaic, massive-bedded and nodular anhydrite. No visible porosity.

TS 9621.6 Dolomitized, peloid mudstone; 65-70% dolomite (matrix replacement, allochem replacement), 20-25% calcite (matrix, allochem), trace anhydrite (matrix, allochem); no visible porosity.

## 9623.5-9625 (core) Packstone

Limestone, medium brown; containing (micrite-coated) intraclasts and unknown bioclasts. Slightly laminated. Estimated vuggy and interparticle porosity 5%.

TS 9623.5 Dolomitized, algal, peloid, calcisphere wackestone-packstone; 50-55% dolomite (matrix replacement, allochem replacement), 20-25% calcite (allochem, cement), trace anhydrite (cement); cryptalgal laminated; 15-20% moldic and intercrystalline porosity.

TS 9624.5 Dolomitized, calcisphere, foram, ostracode wackestone-packstone; 55-60% dolomite (matrix replacement, allochem replacement), 30-35% calcite (allochem, rare cement), 1-2% anhydrite (allochem); compaction; 1-2% moldic, intercrystalline and intraparticle porosity.

## 9625-9634 (core) Wackestone to Packstone

Limestone, dolomitic limestone, medium brown; containing intraclasts, coral and brachiopod fragments, ostracodes and unknown bioclasts. Commonly laminated with black, wispy stringers, microstylolites and occasional calcite-filled vugs. Suture seam stylolite near 9634 separates this lithology from underlying lithology. Estimated vuggy, moldic and intercrystalline (?) porosity 10% near the bottom, decreasing upward to less than 5%.

TS 9627 Calcisphere, algal, brachiopod, echinoderm

wackestone; 90-95% calcite (allochem, matrix), 1-5% dolomite (matrix replacement); compaction, stylolite; no visible porosity.

TS 9634 Dolomitized, brachiopod, bioclast, echinoderm wackestone-packstone; 50-55% dolomite (matrix replacement, allochem replacement), 40-45% calcite (allochem); compaction, possible microstylolites; trace fracture porosity.

9634-9636 (core) Wackestone

Limestone, dark brown to black; containing echinoderm fragments and rugose horn corals. Abundant microstylolites and stylolites. No visible porosity.

9636-9648 (core) Wackestone

Limestone, medium brown; containing intraclasts, echinoderm fragments, rugose horn corals, ostracodes and rare Syringopora coral and fenestrate bryozoan. Many allochems appear in 4-6 cm thick layers. Slightly bioturbated with black, wispy stringers, microstylolites and stylolites. Estimated small vuggy and minor intraparticle porosity 5-15%.

TS 9640 Dolomitized, coral, echinoderm wackestone-packstone; 50-55% dolomite (matrix replacement, allochem replacement), 35-40% calcite (allochem, matrix, cement (in coral)), 1-2% anhydrite (cement in coral); 1-2% intraparticle (coral) porosity.

TS 9644.5 Dolomitized, echinoderm, coral wackestone-packstone; 45-50% dolomite (matrix replacement, allochem replacement, minor cement), 40-45% calcite (allochem, neomorphic spar, cement); compaction, microstylolites; 1-5% intercrystalline and intraparticle (coral) porosity.

9648-9657.8 (core) Mudstone to Wackestone

Dolomitic limestone, dark brown; containing echinoderm fragments and rugose horn corals. Decreasingly bioturbated (upward) with occasional preserved burrows, abundant microstylolites, stylolites and rare calcite-filled vugs and fractures. Estimated intercrystalline and small vuggy porosity 10-20%.

TS 9652 Dolomudstone; 75-80% dolomite (matrix replacement, allochem replacement ?), 5-10% calcite (fracture-fill, nodule), 5-10% anhydrite (nodule); fractures, mostly calcite-filled, stylolites, microstylolites; trace fracture porosity.

9657.8-9658 (core) Mudstone

Dolostone, quartz silt, dark gray to black. Intensely microstylolitic with associated

authigenic pyrite. Estimated intercrystalline porosity less than 5%.

TS 9657.8 Dolomitic, quartz silt, mudstone; 35-40% dolomite (matrix replacement), 35-40% quartz silt (angular to subangular), 15-20% insoluble material (microstylolites), 1-2% pyrite; abundant microstylolites; no visible porosity.

9658-9660 (core) Mudstone

Dolostone, dark gray to black; containing rare echinoderm fragments and unknown allochems. Commonly bioturbated with black, wispy stringers, microstylolites, stylolites and occasional calcite-filled vugs with associated authigenic pyrite. Estimated intercrystalline and vuggy porosity less than 10%.

TS 9658.6 Quartz silt, dolomudstone; 70-75% dolomite (matrix replacement), 5-10% quartz silt (angular to subangular), 10-15% insoluble material (microstylolites), 1-2% pyrite (pore-lining cement); stylolite and abundant microstylolites; no visible porosity.

NDGS #7352

W.H. Hunt Trust Estate Fritz A-1  
SE/NW, Sec. 22, T142N, R100W

Cored Interval (9604-9660) Log Interval (9612-9668)

9604-9625 (core) Mudstone to Wackestone

Dolostone, anhydrite, dolomitic limestone, light olive gray to tan; containing intraclasts and unknown bioclasts. Laminated to cryptalgal laminated grading into and interbedded with massive-bedded, nodular-mosaic and nodular anhydrite. Occasional microstylolites, stylolites and small vertical fractures. Dark brown anhydrite laths (1 mm) scattered throughout dolomite and dolomitic limestones. Estimated intercrystalline and small vuggy porosity less than 5%.

TS 9606 Dolomitized, anhydritic, intraclast, peloid packstone; 40-45% dolomite (matrix replacement, allochem replacement), 40-45% anhydrite (allochem replacement, cement), 5-10% silica (chert: cement, minor allochem replacement); many allochems have a micrite rim (dolomitized); trace intraparticle porosity.

TS 9609.5 Dolomitized, anhydritic, intraclast, peloid, calcisphere, ostracode, bioclast, wackestone; 50-55% dolomite (matrix replacement, allochem replacement), 40-45% anhydrite (allochem replacement,



cement), trace calcite (cement); many allochems have micrite rims (dolomitized); trace moldic porosity.

TS 9612.5 Dolomitic, mudstone; 60-65% calcite (matrix), 20-25% dolomite (matrix replacement, larger rhombs associated with anhydrite, smaller rhombs associated with calcite), 5-10% anhydrite (matrix, matrix replacement as laths); bedded anhydrite and calcite; no visible porosity.

TS 9615 Dolomitic, bioclast (ghosts) mudstone; 40-45% calcite (matrix), 30-35% dolomite (matrix replacement), 15-20% anhydrite (matrix replacement, matrix); bedded calcite and anhydrite; no visible porosity.

9625-9634.5 (core) Wackestone  
Limestone, dark brown; containing rugose horn corals, ostracodes and unknown bioclasts. Slightly bioturbated near 9631 feet. Commonly microstylolitic and stylolitic with occasional small, vertical fractures. Estimated small vuggy porosity 5%.

TS 9629.5 Dolomitic, echinoderm, brachiopod, algal (?), ostracode (?), mudstone to wackestone; 80-85% calcite (matrix, neomorphic replacement), 10-15% dolomite (matrix replacement, large rhombs); microstylolite, compaction; trace intraparticle porosity.

9634.5-9637 (core) Grainstone  
Limestone, medium brown; containing (micrite-coated) intraclasts, ostracodes, brachiopods and coral fragments. Stylolites, one of which separates this lithology from underlying lithology. Estimated vuggy to interparticle (?) porosity 10%.

TS 9635 Intraclast, peloid, brachiopod, foram, bryozoan, ostracode (?) grainstone; 90-95% calcite (allochems, cement (including syntaxial overgrowths), 1-5% dolomite (allochem replacement), trace anhydrite (cement); minor compaction in areas, some micritization of allochems; trace vuggy and interparticle porosity.

9637-9652 (core) Wackestone to Packstone  
Dolomitic limestone, medium brown; containing (micrite-coated) intraclasts, ostracodes, rugose horn corals and brachiopod fragments. Commonly bioturbated with preserved burrows, abundant black, wispy stringers, stylolites and microstylolites. Estimated small vuggy and intercrystalline porosity 10-15%.

TS 9648 Dolomitic, echinoderm, coral, bioclast

wackestone-packstone; 60-65% calcite (matrix, allochem), 30-35% dolomite (matrix replacement, allochem replacement, dirty appearance); no visible porosity.

TS 9651 Dolomitized, echinoderm, coral wackestone; 50-55% dolomite (matrix, dirty appearance), 35-40% calcite (allochem, matrix, neomorphic spar); 1-5% intercrystalline porosity.

9652-9659.5 (core) Mudstone to Wackestone  
Dolostone, dark brown; containing peloids (?), ostracodes, echinoderm fragments and calcite-replaced allochems. Commonly bioturbated with black, wispy stringers and laminations, thick (up to 1.5 cm) stylolites and occasional calcite-filled vugs. Estimated intercrystalline and small vuggy porosity 10%.

TS 9654 Dolomudstone, 75-80% dolomite (matrix replacement, saddle dolomite cement); black, insoluble material present; 15-20% intercrystalline and vuggy porosity.

9659.5-9660 (core) Mudstone  
Dolostone, quartz silt, dark gray to black. Alternating between densely microstylolitic zones and less microstylolitic, slightly bioturbated zones with associated pyrite. Estimated intercrystalline porosity less than 5%.

TS 9660.3 Quartz silt, dolomudstone; 70-75% dolomite (matrix replacement), 15-20% quartz silt (angular to subangular), 1-5% pyrite; no visible porosity.

NDGS # 7349

W.H. Hunt Trust Estate Fritz #2

SW/SE, Sec. 22, T142N, R100W

Cored Interval (9560-9655) Log Interval (9574-9669)

9560-9572 (core) Mudstone  
Dolostone, anhydrite, calcareous dolostone, light gray to light brown; containing intraclasts, mainly between 9570-9572 feet. Thinly laminated to bedded, grading into, and interbedded with, massive-bedded, bedded-mosaic and nodular anhydrite. Rare microstylolites and stylolites. Estimated intercrystalline porosity 5%.

TS 9564 Dolomitic, peloid (?) mudstone; 35-40% calcite (matrix, allochem), 20-25% dolomite (matrix replacement), 10-15% anhydrite (matrix); bedded

calcite and anhydrite; no visible porosity.

9572-9586 (core) Mudstone to Wackestone

Dolomitic limestone, medium brown to black; containing intraclasts, ostracodes, echinoderm fragments, anhydrite replaced allochems and rare rugose horn coral. Commonly bioturbated with occasional preserved burrow, black, wispy stringers, abundant microstylolites and stylolites. Estimated vuggy and intercrystalline porosity less than 10%.

TS 9572 Dolomitic, peloid, bioclast, intraclast, calcisphere (?), ostracode wackestone-packstone 60-65% calcite (matrix, cement (neomorphic ?), allochem), 25-30% dolomite (matrix replacement, saddle dolomite cement), trace anhydrite (cement); micritized allochems, stylolite; 1-5% interparticle porosity.

TS 9583.2 Cherty, dolomitic mudstone; 40-45% calcite (matrix), 25-30% silica (chert: cement, matrix and allochem (?) replacement), 20-25% dolomite (cement, matrix replacement); bedded; 1-2% intraparticle and vuggy porosity.

9586-9595 (core missing)

9595-9605 (core) Mudstone

Dolomitic limestone, medium brown; containing echinoderm fragments and ostracodes. Commonly bioturbated with occasional preserved burrows, black, wispy stringers, microstylolites, stylolites, and rare, calcite/anhydrite-filled vugs. Estimated vuggy and intercrystalline porosity 10-15%.

TS 9604 Dolomudstone; 70-75% dolomite (matrix replacement, saddle dolomite cement), 1-5% calcite (cement), trace quartz silt; 15-20% intercrystalline porosity.

9605-9625 (core) Mudstone

Calcareous dolostone, medium brown to black; containing echinoderm fragments, unknown bioclasts, rip-up clasts (near 9611 feet) and rare rugose horn coral. Commonly bioturbated with occasional preserved burrow. Black, wispy stringers, stylolites and dense microstylolite swarms common. Occasional calcite-filled vugs and fractures generally surrounded by authigenic pyrite. Estimated intercrystalline and minor vuggy porosity 5%.

TS 9607 Dolomitic, quartz silt mudstone; 60-65% insoluble material (stylolites), 15-20% dolomite (matrix replacement), 10-15% quartz silt (angular to subangular), trace pyrite; abundant microstylolites;

no visible porosity.

TS 9611 Dolomitized, cherty, echinoderm mudstone; 50-55% dolomite (matrix replacement), 35-40% silica (chert: nodular, replacement and fracture-fill cement), 1-5% calcite (matrix); no visible porosity.

TS 9617.5 Dolomitized bioclast, echinoderm, foram wackestone; 60-65% dolomite (matrix replacement), 15-20% calcite (allochem, vug and fracture-fill cement), 10-15% anhydrite (radiate, vug-filling cement), trace pyrite (0.5-1 mm cubes); microstylolites; no visible porosity.

9625-9628.5 (core) Wackestone  
Dolomitic limestone, dark gray to black; containing abundant echinoderm fragments, and rare rugose coral and *Syringopora* coral. Abundant microstylolites, stylolites and small calcite-filled vertical fractures. No visible porosity.

TS 9627 Dolomitized, bioclast, echinoderm, coral wackestone; 50-55% dolomite (matrix replacement, saddle dolomite cement), 30-35% calcite (cement, allochem); stylolite; 5-10% vuggy and intercrystalline porosity.

9628.5-9635 (core) Mudstone to Wackestone  
Calcareous dolostone, medium brown; containing echinoderm fragments and rugose horn corals. Commonly bioturbated with rare preserved burrow, occasional microstylolites and calcite-filled vugs and fractures. Estimated intercrystalline and small vuggy porosity 10%.

TS 9633 Echinoderm, bioclast, coral, brachiopod wackestone-packstone; 85-90% calcite (matrix, allochem), 5-10% dolomite (mainly associated with stylolites), trace pyrite; stylolites, compaction; no visible porosity.

9635-9655 (core) Wackestone to Packstone  
Dolomitic limestone and calcareous dolostone, light to dark gray; containing echinoderm fragments, unknown bioclasts and rugose horn corals. Bioturbation occurs in areas containing little or no microstylolites. Rare, calcite-filled vertical fractures present. Estimated intercrystalline and vuggy porosity 10%.

TS 9637 Bioclast, echinoderm, brachiopod packstone; 85-90% calcite (allochem, matrix), 5-10% dolomite (matrix replacement); stylolites, compaction; no visible porosity.

TS 9652 Dolomitic, bioclast, echinoderm, brachiopod wackestone-packstone; 80-85% calcite (matrix, allochem, cement), 10-15% dolomite (associated with stylolites); stylolites (two separate events), compaction; no visible porosity.

## NDGS #7776

Al-Aquitaine Exploration Ltd. 3-141-100 BN #2-3  
SE/SE, Sec. 3, T141N, R100W

Cored Interval (9440-9490) Log Interval (9450-9500)

9440-9454.5 (core) Mudstone to Packstone  
Dolostone and anhydritic dolostone, light olive gray to tan; intraclastic. Thinly laminated with occasional soft sediment deformation, bedded-nodular and nodular anhydrite (increasing upward). Estimated vuggy porosity 5%.

TS 9451.5 Dolomitized, anhydritic, peloid, intraclast packstone to grainstone; 55-60% dolomite (cement, allochem replacement), 30-35% anhydrite (allochem replacement, matrix, nodules); micritization of allochems (dolomitized); possible graded bedding; 1-5% moldic and vuggy porosity.

9454.5-9460 (core) Wackestone  
Dolomitic limestone, dark brown to black; containing ostracodes, intraclasts and unknown bioclasts. Commonly bioturbated with abundant stylolites and microstylolites. No visible porosity.

TS 9456 Foram, bioclast, intraclast, calcisphere, algal wackestone-packstone; 90-95% calcite (matrix, allochem, neomorphic spar), 1-5% dolomite (associated with stylolites); compaction, micritization of allochems, microstylolites; no visible porosity.

9460-9462.5 (core) Grainstone  
Limestone, medium brown; containing intraclasts, peloids (micrite-coated), small rugose horn corals, and small brachiopods. Occasional, small, anhydrite-filled vugs. No visible porosity.

TS 9460 Peloid, ostracode, foram, algal, intraclast grainstone; 95-98% calcite (allochem, cement), 1-2% anhydrite (allochem replacement), trace dolomite (allochem and cement replacement); micritization of allochems; no visible porosity.

9462.5-9477.5 (core) Wackestone to Packstone  
Limestone, dark brown to black; containing echinoderm fragments, intraclasts, large rugose

horn corals, ostracodes (?) and rare fenestrate bryozoan. Commonly bioturbated with abundant microstylolites, occasional stylolites and rare chert nodule. Estimated vuggy and moldic porosity 5-10% (decreasing upward).

TS 9468 Bioclast, coral, brachiopod packstone; 90-95% calcite (matrix, allochem, neomorphic spar), 1-5% dolomite (matrix replacement, allochem replacement); microstylolites (?), compaction; trace intraparticle porosity.

TS 9470 Bryozoan, peloid, foram, intraclast, coral, ostracode, echinoderm, brachiopod packstone to grainstone; 80-85% calcite (matrix, allochem, cement), 5-10% dolomite (saddle dolomite cement, allochem replacement); stylolite, micritization of some allochems; 1-5% interparticle porosity.

TS 9476 Bioclast, echinoderm, coral, brachiopod wackestone; 85-90% calcite (allochem, matrix), 5-10% dolomite (matrix replacement, allochem replacement, associated with stylolites), trace pyrite; stylolites, compaction; no visible porosity.

9477.5-9484.5 (core) Mudstone

Dolostone, medium brown; containing small, replaced bioclasts. Commonly bioturbated with occasional preserved burrows and microstylolites. Large (1-2 cm) vugs filled with calcite/anhydrite. Small, vertical fractures are calcite-filled. Estimated intercrystalline porosity 15%.

9484.4-9487 (core) Mudstone

Dolostone, quartz silt, dark gray to black. Alternating between densely microstylolitic zones and less microstylolitic, bioturbated (?) zones. No visible porosity.

TS 9485 Dolomitized, quartz silt mudstone; 60-65% dolomite (matrix replacement), 20-25% insoluble material (microstylolites), 5-10% quartz silt (angular to subangular), trace pyrite; microstylolites common; no visible porosity.

9487-9490 (core) Mudstone

Dolostone, dark gray to medium brown. Commonly bioturbated with calcite/anhydrite-filled vugs. Estimated intercrystalline and small vuggy porosity 5-10%.

TS 9490 Dolomudstone; 70-75% dolomite (matrix replacement, cement), 15-20% calcite (cement), trace anhydrite (cement); 1-5% intercrystalline porosity.

NDGS #8333

Shell Oil Company U. S. A. #41-4

NE/NE, Sec. 4, T141N, R100W

Cored Interval (9355-9432) Log Interval (9360-9437)

## 9355-9363 (core) Mudstone

Dolostone, dolomitic anhydrite and anhydrite, light olive gray to tan; containing peloids. Laminated, commonly grading into, and interbedded with, nodular to massive-bedded anhydrite. stylolites and micro-stylolites common. Small, vertical fractures, some anhydrite-filled, occur rarely. No visible porosity.

TS 9355 Dolomitic, anhydritic, peloid, algal, calcisphere mudstone; 35-40% dolomite (matrix replacement, allochem replacement), 25-30% anhydrite (felted nodular matrix, matrix replacement as laths), 20-25% calcite (matrix, allochem), 1-5% quartz silt (angular); stylolites and microstylolites, compaction, micritization of some allochems; no visible porosity.

TS 9359.5 Peloidal anhydrite; 90-95% anhydrite (felted matrix, allochem replacement), 1-5% dolomite (matrix), trace silica (authigenic quartz); microstylolites; no visible porosity.

## 9363-9387.5 (core) Mudstone to Packstone

Dolomitic limestone and dolostone, dark gray to brown; containing (in non-laminated zones) echinoderm fragments, rugose horn corals, rare *Syringopora* coral, rare bryozoan, and unknown bioclasts. Cryptalgal laminated to laminated (increasing upward). Commonly microstylolitic and stylolitic with rare, subvertical fractures. Estimated vuggy and intercrystalline porosity 5-10%.

TS 9377 Dolomitic, bioclast, echinoderm, brachiopod, peloid packstone; 65-70% calcite (matrix, allochem, allochem replacement), 20-25% dolomite (matrix replacement, allochem replacement); minor compaction, micritization of some allochems; 1-5% vuggy and interparticle porosity.

TS 9381.5 Dolomitic, brachiopod, echinoderm wackestone-packstone; 70-75% calcite (allochem, matrix, cement), 20-25% dolomite (matrix replacement, allochem replacement), 1-2% silica (chert: matrix and allochem replacement in a small area); compaction, minor micritization of allochems; trace intraparticle porosity.

TS 9384 Coral, echinoderm, foram, brachiopod packstone; 60-65% calcite (allochem, cement, matrix),

5-10% dolomite (saddle dolomite cement, associated with stylolite), 1-5% anhydrite (cement); stylolite, compaction; 15-20% intraparticle (coral), vuggy, moldic and intercrystalline porosity.

9387.5-9396 (core) Mudstone

Dolostone, olive brown to dark brown. Commonly bioturbated with black, wispy stringers and laminations, large (1-2 cm) calcite/anhydrite-filled vugs and rare, vertical fractures. Estimated intercrystalline, vuggy and fracture porosity 10-15%.

TS 9389 Dolomudstone; 75-80% dolomite (matrix replacement, cement), 1-5% anhydrite (allochem replacement, cement); 10-15% intercrystalline porosity.

TS 9395 Dolomudstone; 85-90% dolomite (matrix replacement), 1-5% quartz silt, 1-2% calcite (fracture-fill and pore-filling cement), 1-2% insoluble material; no visible porosity.

9396-9397 (core) Mudstone

Dolostone, quartz silt, dark gray to black. Intensely microstylolitic with associated authigenic pyrite. No visible porosity.

TS 9396.2 Dolomitized, quartz silt mudstone; 55-60% dolomite (matrix replacement), 20-25% quartz silt (angular), 5-10% insoluble material (microstylolites), 1-2% pyrite; abundant microstylolites; no visible porosity.

9397-9403 (core) Mudstone to Wackestone

Dolomitic limestone, dark gray to dark gray-brown; containing calcite-replaced bioclasts and ostracodes. Commonly bioturbated with rare, preserved burrow and occasional vertical fracture. Estimated intercrystalline, small vuggy and fracture porosity 5-10%.

9403-9417 (core) Mudstone

Dolostone, dark brown; containing unknown bioclasts. Commonly bioturbated with rare, preserved burrow, anhydrite-filled vugs, microstylolites and stylolites. Microstylolites increase in abundance upward. Estimated intercrystalline porosity 5-10%.

TS 9408.3 Dolomudstone; 80-85% dolomite (matrix replacement, allochem replacement by saddle dolomite) 5-10% quartz silt (angular, associated with microstylolites), 1-2% calcite (fracture-fill cement, allochem), trace anhydrite (allochem replacement), trace pyrite (associated with microstylolites), trace



quartz silt; microstylolites common; 1-2% intercrystalline porosity.

TS 9416.5 Dolomitized mudstone; 60-65% dolomite (matrix replacement, allochem replacement), 25-30% calcite (neomorphic replacement of matrix), 1-2% anhydrite (matrix replacement); no visible porosity.

9417-9419 (core) Wackestone  
Limestone, dark gray; containing echinoderm fragments and rugose horn corals. Abundant microstylolites and small, calcite-filled fractures. No visible porosity.

9419-9426 (core) Mudstone to Wackestone  
Calcareous dolostone, medium to dark brown; containing ostracodes, unknown bioclasts and rare Syringopora coral. Bioturbation, stylolites, anhydrite-filled vugs common. Authigenic pyrite associated with Syringopora coral. Estimated intercrystalline and small vuggy porosity 10%.

TS 9420 Dolomitized, coral, brachiopod (?) wackestone-packstone; 45-50% dolomite (matrix replacement, allochem replacement), 20-25% calcite (neomorphic spar, allochem), 15-20% anhydrite (allochem replacement), 1-5% pyrite (cement); no visible porosity.

TS 9424 Dolomitized, bioclast, calcisphere, echinoderm mudstone; 40-45% dolomite (matrix replacement, allochem replacement), 25-30% calcite (neomorphic replacement of matrix and allochem), trace anhydrite (allochem replacement); 20-25% intercrystalline and vuggy porosity.

9426-9432 (core) Mudstone to Wackestone  
Dolomitic limestone and dolostone, light gray to dark brown; containing rugose horn corals, Syringopora coral and coral fragments, echinoderm fragments, ostracodes, brachiopod fragments (?) and unknown bioclasts. Commonly bioturbated with black, wispy stringers, microstylolites, stylolites, and occasional calcite-filled vugs. Estimated intercrystalline, vuggy and rare intraparticle porosity 10-20%.

TS 9428 Dolomitic, echinoderm, brachiopod wackestone-packstone; 70-75% calcite (allochem, matrix), 20-25% dolomite (matrix replacement), trace pyrite; trace intercrystalline and intraparticle porosity.

TS 9432 Dolomitized, echinoderm, bioclast mudstone; 60-65% dolomite (matrix replacement, allochem

replacement), 5-10% calcite (allochem, cement); 20-25% intercrystalline, vuggy and moldic porosity.

## NDGS #9411

Al-Aquitaine Exploration LTD. BN. #1-9

NE/NE, Sec. 9, T141N, R100W

Cored Interval (9452-9494) Log Interval (9469-9511)

## 9452-9453 (core) Grainstone

Limestone, medium brown; containing partially micritized intraclasts and bioclasts. Calcite-filled vertical fracture. Estimated small vuggy and rare interparticle porosity 1-5%.

TS 9452 Bioclast, peloid, foram, intraclast grainstone; 85-90% calcite (allochem, cement), trace dolomite (allochem replacement), trace anhydrite (allochem replacement, cement replacement); micritization of allochems; 5-10% interparticle and intraparticle porosity.

## 9453-9469.5 (core) Wackestone

Dolomitic limestone, medium brown to black; containing (micrite-coated) intraclasts and bioclasts, echinoderm fragments, rugose horn corals, and rare Syringopora coral and fenestrate bryozoa. Minor soft sediment deformation near 9464 feet. Bioturbated in areas with black, wispy stringers and abundant microstylolites and stylolites. Silicified zones present. Vertical fractures associated with stylolites. Estimated intercrystalline and small vuggy porosity 1-5%.

TS 9458 Dolomitic, bioclast, echinoderm, coral, brachiopod wackestone; 65-70% calcite (matrix, allochem, neomorphic spar), 10-15% dolomite (matrix replacement, cement), 1-2% anhydrite (matrix replacement, allochem replacement); 5-10% vuggy, interparticle and intercrystalline porosity.

## 9469.5-9477 (core) Mudstone

Dolostone, medium brown; containing anhydrite-replaced allochems and echinoderm fragments (?). Commonly bioturbated with occasional preserved burrows, black, wispy stringers and anhydrite-filled vugs. Estimated intercrystalline and small vuggy porosity 5-10%.

TS 9469.5 Dolomudstone; 80-85% dolomite (matrix replacement, saddle dolomite cement), trace quartz silt, trace pyrite; 10-15% intercrystalline porosity.

## 9477-9479 (core) Mudstone

Dolostone, quartz silt, dark gray to black. Alternating between intensely microstylolitic zones and less microstylolitic, bioturbated zones; both zones containing associated authigenic pyrite. No visible porosity.

TS 9477 Dolomudstone; 80-85% dolomite (matrix replacement, saddle dolomite cement), 5-7% calcite (cement), 1-2% anhydrite (allochem replacement?), trace pyrite, trace quartz silt; 1-5% intercrystalline porosity.

## 9479-9490 (core) Mudstone and Wackestone

Calcareous dolostone and dolostone, dark brown; containing echinoderm fragments, unknown bioclasts and occasional calcite-replaced allochems. Intensely bioturbated with rare preserved burrows. Black, wispy stringers, anhydrite/calcite-filled vugs and fractures with associated authigenic pyrite, and open vertical fractures. Estimated intercrystalline and fracture porosity less than 10%.

TS 9481 Dolomudstone; 75-80% dolomite (matrix replacement, allochem replacement), 15-20% calcite (cement, dedolomitization), trace anhydrite (cement), trace quartz silt; trace intercrystalline porosity.

TS 9484 Dolomudstone; 70-75% dolomite (matrix replacement), 20-25% calcite (cement); microstylolites; no visible porosity.

## 9490-9494 (core) Wackestone

Limestone, dark gray to black; containing echinoderm fragments, rugose horn corals and unknown bioclasts. Occasionally bioturbated with abundant microstylolites. Estimated small vuggy porosity less than 5%.

TS 9494 Dolomitic, echinoderm, bioclast wackestone; 75-80% calcite (allochem, matrix, cement), 15-20% dolomite (matrix replacement, allochem replacement), trace anhydrite (allochem replacement); compaction; no visible porosity.

NDGS #6899

Al-Aquitaine Exploration Ltd. U.S. #1-22

NE/NE, Sec. 22, T142N, R100W

Cored Interval (9460-9506) Log Interval (9456-9502)

9460-9465 (core) Mudstone to Wackestone  
Dolostone and anhydritic dolostone, light gray to tan. Thinly laminated with interbedded nodular and massive anhydrite. Black, wispy stringers common. Estimated intercrystalline porosity less than 5%.

TS 9463 Peloid wackestone-packstone; 35-40% anhydrite (matrix), 25-30% silica (chert: matrix, replacement, allochem replacement), 20-25% dolomite (allochem replacement), 1-2% calcite (allochem); micritization of allochems (dolomitized); trace moldic porosity.

9465-9466 (core) Packstone to Grainstone  
Limestone, medium brown; containing micrite-coated peloids and bioclasts. Estimated interparticle porosity 10%.

TS 9465 Dolomitic, peloid, calcisphere, algal packstone; 55-60% silica (chert and authigenic quartz: matrix replacement, allochem replacement, cement), 20-25% dolomite (matrix replacement, allochem replacement), 1-5% anhydrite (cement), 1-5% pyrite (allochem), 1-2% calcite (allochem); rare worm tube present; 1-2% intraparticle porosity (peloids mainly).

9466-9469 (core) Wackestone  
Dolomitic limestone, dark brown; containing ostracodes, peloids and intraclasts (?). Bioturbated to slightly laminated with stylolites and occasional fractures present. No visible porosity.

9469-9470 (core) Grainstone  
Limestone, dark brown; containing micrite-coated intraclasts. No visible porosity.

TS 9469 Peloid, intraclast, foram, bioclast, calcisphere, ostracode, gastropod grainstone; 100% calcite (allochem, cement); many fossils are micritized or have micritic rims; trace intraparticle and interparticle porosity.

9470-9487.5 (core) Wackestone to Packstone  
Slightly dolomitic limestone, dark brown to black; containing echinoderm fragments, rugose horn corals and coral and brachiopod fragments. Occasionally bioturbated with microstylolites and stylolites common. Rare, vertical fractures present. Estimated

intercrystalline and fracture porosity less than 5%.

TS 9475.5 Pelioid, calcisphere, brachiopod, foram, echinoderm, wackestone-packstone; 90-95% calcite (matrix, allochem, cement), 1-5% dolomite (matrix replacement, allochem replacement), trace quartz silt; stylolites; trace fracture porosity.

TS 9481 Brachiopod, pelioid, echinoderm wackestone-packstone; 85-90% calcite (allochem, matrix), 5-10% dolomite (matrix replacement, allochem replacement, associated with stylolites), trace quartz silt; stylolites present; no visible porosity.

TS 9483 Dolomitic, bioclast, foram, ostracode (?), wackestone; 35-40% calcite (allochem, matrix), 35-40% dolomite (matrix replacement), 10-15% silica (chert: matrix replacement, allochem replacement), trace pyrite; microstylolites present; 1-5% vuggy and intraparticle porosity.

9487.5-9497 (core) Mudstone

Dolostone, light to medium brown. Intensely bioturbated with occasional preserved burrows. Black, wispy stringers, scattered calcite/anhydrite-filled vugs and small vertical fractures present. Estimated intercrystalline, small vuggy and minor fracture porosity 10-15%.

TS 9491.5 Dolomitized mudstone; 60-65% dolomite (matrix replacement, allochem replacement by saddle dolomite), 1-2% quartz silt (angular); 25-30% intercrystalline porosity.

9497-9497.5 (core) Mudstone

Dolostone, quartz silt, dark gray to black. Intensely microstylolitic with associated authigenic pyrite. No visible porosity.

9497.5-9506 (core) Mudstone to Wackestone

Dolostone, medium to dark brown; containing echinoderm fragments and unknown bioclasts. Commonly bioturbated with abundant black, wispy stringers, microstylolites and calcite/anhydrite-filled vugs surrounded by authigenic pyrite. Estimated intercrystalline porosity 5-10%.

## APPENDIX C

### Procedure for Making Pore Casts

Pore casts were made by impregnating rock chips with Araldite 6005, a low viscosity, low molecular weight epoxy. To use Araldite 6005, a four part mixing procedure was necessary. Araldite 6005 resin was first mixed in a one to one ratio with Dodecenyl Succinic Anhydride hardener. Dibutyl Phthalate, a plasticizer used to insure a good cutting consistency, was then added at 15 percent by weight. Just prior to usage, 2 percent by weight of the accelerator Benzyldimethylamine was added and the resulting mixture stirred for approximately 5 minutes until the epoxy achieved a clear yellow color. The Araldite 6005 epoxy was then poured into plastic cylindrical molds with removable bottoms approximately 2.5 centimetres (1 inch) in diameter and placed along with the sample rock chips in an oven to cure at 50 degrees Celsius for 30 minutes. Samples were then embedded in the epoxy, returned to the 50 degrees Celsius oven, and placed under vacuum for approximately 1 hour. The vacuum was then released and samples were allowed to remain in the oven at 50 degree Celsius to cure for 24 hours. After removing samples from the oven and allowing them to cool to room temperature, epoxy samples were removed from their plastic molds and polished with 600 grit to obtain a smooth, exposed surface for scanning electron microscopy. All samples were cut into squares (1

centimetre or less) and placed in 10 percent hydrochloric acid for 30 minutes up to 2 hours (depending on rock type) until an etched surface was obtained. Pore casts were then rinsed in distilled water. As a final step, pore casts were placed in an ultrasonic bath to remove any loose particles. Both sample chips and pore casts were mounted with either silver paint or colloidal graphite onto aluminum plugs and gold coated for scanning electron microscopy.

## REFERENCES CITED

- Adams, J. E., and Rhodes, M. L., 1960, Dolomitization by seepage refluxion: American Association of Petroleum Geologists Bulletin, v. 44, p. 1912-1920.
- Alexandersson, T. 1972, Micritization of carbonate particles: process of precipitation and dissolution in modern shallow-marine sediments: Bulletin of Geological Institutions of the University of Uppsala, New Series 3, No. 7, P. 210-236.
- Altschuld, N., and Kerr, S. D., Jr., 1982, Mission Canyon and Duperow reservoirs of the Billings Nose, Billings County, North Dakota, in Christopher, J. E., and Kaldi, J., eds., Fourth International Williston Basin Symposium: Saskatchewan Geological Society Special Publication No. 6, p. 103-112.
- Anderson, S. B., 1966, A look at the petroleum potential of southwestern North Dakota: North Dakota Geological Survey Report of Investigations No. 42, 3 p.
- Baker, P. A., and Kastner, M., 1981, Constraints on the formation of sedimentary dolomite: Science, v. 213, p. 214-216.
- Ballard, F. V., 1963, Structural and stratigraphic relations in the Paleozoic rocks of eastern North Dakota: North Dakota Geologic Survey Bulletin 40, 42 p.
- Bathurst, R. G. C., 1966, Boring algae, micrite envelopes and lithification of molluscan biosparites: Geology Journal, v. 5, p. 15-32.
- Bathurst, R. G. C., 1975, Carbonate sediments and their diagenesis, (second edition), developments in sedimentology, v. 12: New York, Elsevier, 658 p.
- Beach, D. K., and Schumacher, A. L., 1982, Stanley Field, North Dakota: economic and quantitative significance of mechanically compacted shallow-water limestone: American Association of Petroleum Geologists Bulletin, v. 66, p. 547.
- Beales, F. W., 1971, Cementation by white sparry dolomite, in Bricker, O. P., ed., Carbonate cements: Johns Hopkins University Studies, v. 19, p. 330-338.
- Beales, F. W., and Hardy, J. L., 1980, Criteria for the recognition of diverse dolomite types with an emphasis on studies on host rocks for Mississippi Valley-type ore deposits, in Zenger, D. H., Dunham, J. B., and



- Ethington, R. L., eds., Concepts and models of dolomitization: Society of Economic Paleontologists and Mineralogists Special Publication No. 28, p. 197-213.
- Berg, R. R., and Mitsdarffer, A. R., 1986, Effects of hydrodynamic flow on carbonate stratigraphic traps, Mission Canyon Formation, Billings Nose fields, North Dakota: American Association of Petroleum Geologists Bulletin, v. 75, p. 564.
- Blatt, H., Middleton, G., and Murray, R., 1980, Origin of sedimentary rocks (second edition): New Jersey, Prentice-Hall, 782 p.
- Bluemle, J. P., Anderson, S. B., and Carlson, C. G., 1980, Stratigraphic column of North Dakota: North Dakota Geological Survey, 1 p.
- Budai, J. M., Lohmann, K. C., and Owen, R. M., 1984, Burial dedolomite in the Mississippian Madison Limestone, Wyoming and Utah thrust belt: Journal of Sedimentary Petrology, v. 54, p. 276-288.
- Carlson, E. H., 1986, Orientated replacements of gypsum by celestite and their diagenetic significance: Geological Society of America Abstracts with Programs, v. 18, p. 557.
- Carlson, C. G., and Anderson, S. B., 1965, Sedimentary and tectonic history of North Dakota part of the Williston Basin: American Association of Petroleum Geologists Bulletin, v. 49, 1833-1846.
- Carlson C. G., and Anderson, S. B., 1966, A look at the lower and middle Madison of northwestern North Dakota: North Dakota Geological Survey Report of Investigations No. 43, 14 p.
- Choquette, P. W., and Pray, L. C., 1970, Geologic nomenclature and classification of porosity in sedimentary carbonates: American Association of Petroleum Geologists Bulletin, v. 54. p. 207-250.
- Collier, A. J., and Cathcart, S. H., 1922, Possibility of finding oil in laccolithic domes south of the Little Rocky Mountains, Montana: U. S. Geological Survey Bulletin 736, p. 171-178.
- Deffeyes, K. S., Lucia, F. J., and Weyl, P. K., 1965, Dolomitization of recent and Plio-Pleistocene sediments by marine evaporite waters on Bonaire, Netherlands Antilles, *in* Pray, L. C., and Murray, R. C., eds., Dolomitization and limestone diagenesis: a

symposium: Society of Economic Paleontologists and Mineralogists Special Publication No. 13, p. 71-88.

- Downy, J. S., 1984, Geohydrology of the Madison and associated aquifers in parts of Montana, North Dakota, South Dakota, and Wyoming: U. S. Geological Survey Professional Paper 1273-G, 47 p.
- Dunham, R. J., 1962, The classification of carbonate rocks according to depositional texture, *in* Ham, W. E., ed., Classification of carbonate rocks: American Association of Petroleum Geologists Memoir 1, p. 108-121.
- Dunnington, H. V., 1967, Aspects of diagenesis and shape change in stylolitic limestone reservoirs: Proceedings of the 7th World Petroleum Congress, Mexico, p. 339-352.
- Edie, R. W., 1958, Mississippian sedimentation and oil fields in southeastern Saskatchewan: American Association of Petroleum Geologists Bulletin, v. 42, p. 94-126.
- Elliott, T. L., 1982, Carbonate facies, depositional cycles and the development of secondary porosity during burial diagenesis, *in* Christopher, J. E., and Kaldi, J., eds., Fourth international Williston Basin symposium: Saskatchewan Geological Society Special Publication No. 6, p. 131-151.
- Fischer, H. J., Stephens, R. A., and Valvik, J. R., 1986, Topographically controlled carbonate facies in Mississippian epeiric sea deposits: Williston Basin, North Dakota: Geological Society of America Abstracts with Programs, v. 18, p. 602.
- Folk, R. L., 1959, Practical petrographic classification of limestones: American Association of Petroleum Geologists Bulletin, v. 43, p. 1-38.
- Folk, R. L., 1965, Some aspects of recrystallization in ancient limestones, *in* Pray, L. C., and Murray, R. C., eds., Dolomitization and limestone diagenesis: a symposium: Society of Economic Paleontologists and Mineralogists Special Publication No. 13, p. 14-48.
- Folk, R. L., 1974, The natural history of crystalline calcium carbonate: effect of magnesium content and salinity: Journal of Sedimentary Petrology, v. 44, p. 40-53.
- Folk, R. L., and Land, L. S., 1975, Mg/Ca ratio and salinity: two controls over crystallization of

- dolomite: American Association of Petroleum Geologists Bulletin, v. 59, p. 60-68.
- Folk, R. L., and Siedlecka, A., 1974, The "schizohaline" environment: its sedimentary and diagenetic fabrics as exemplified by Late Paleozoic rocks of Bear Island, Svalbard: Sedimentary Geology, v. 11, p. 1-15.
- Friedman, G. M., 1959, Identification of carbonate minerals by staining methods: Journal of Sedimentary Petrology, v. 29, p. 87-97.
- Fuller, J. G. C. M., 1956, Mississippian rocks and oilfields in southeastern Saskatchewan: Saskatchewan Department of Mineral Resources, Petroleum and Natural Gas Branch Report No. 19, 72 p.
- Gerhard, L. C., Anderson, S. B., LeFever, J. A., and Carlson, C. G., 1982, Geological development, origin, and energy mineral resources of Williston Basin, North Dakota: American Association of Petroleum Geologists Bulletin, V. 66, p. 989-1020.
- Given, R. K., and Wilkinson, B. H., 1985, Kinetic control of morphology, composition, and mineralogy of abiogenic sedimentary carbonates: Journal of Sedimentary Petrology, v. 55, p. 109-119.
- Gregg, J. M., and Sibley, D. F., 1984, Epigenetic dolomitization and the origin of xenotopic dolomite texture: Journal of Sedimentary Petrology, v. 54, p. 908-931.
- Hanshaw, B. B., Back, W., and Deike, R. G., 1971, A geochemical hypothesis for dolomitization by groundwater: Economic Geology, v. 66, p. 710-724.
- Harris, P. M., Kendall, C. G. St. C., and Lerche, I., 1985, Carbonate cementation—a brief review, in Schneidermann, N., and Harris, P. M., eds., Carbonate cements: Society of Economic Paleontologists and Mineralogists Special Publication No. 36, p. 79-95.
- Heckel, P. H., 1972, Recognition of ancient shallow marine environments, in Rigby, J. K., and Hamblin, W. K., eds., Recognition of ancient sedimentary environments: Society of Economic Paleontologists and Mineralogists Special Publication No. 16, p. 226-286.
- Hedgpeth, J. W., 1957, Classification of marine environments, in Hedgpeth, J. W., ed., Treatise on marine ecology and paleoecology: Geological Society of America Memoir 67, p. 17-27.

- Hsu, K. J., and Siegenthaler, C., 1969, Preliminary experiments and hydrodynamic movement induced by evaporation and their bearing on the dolomite problem: *Sedimentology*, v. 12, p. 11-25.
- Illing, L. V., Wells, A. G., and Taylor, J. C. M., 1965, Penecontemporary dolomite in the Persian Gulf, in Pray, L. C., and Murray, R. C., eds., *Dolomitization and limestone diagenesis: a symposium: Society of Economic Paleontologists and Mineralogists Special Publication No. 13*, p. 89-111.
- Irwin, M. L., 1965, General theory of epeiric clear water sedimentation: *American Association of Petroleum Geologists Bulletin*, v. 49, p. 445-459.
- Kobluk, D. R., and Risk, M. J., 1977, Micritization and carbonate grain binding by endolithic algae: *American Association of Petroleum Geologists Bulletin*, v. 61, p. 1069-1082.
- Knauth, L. P., 1979, A model for the origin of chert in limestone: *Geology*, v. 7, p. 274-277.
- Kupecz, J. A., 1984, Depositional environments, diagenetic history and petroleum entrapment in the Mississippian Mission Canyon Formation, Billings Anticline, North Dakota: Master's Thesis, Colorado School of Mines, 250 p.
- Laird, W. M., and Folsom, C. B. Jr., 1956, North Dakota's Nesson Anticline: North Dakota Geological Survey Report of Investigations 22, 12 p.
- Laporte, L. F., 1967, Carbonate deposition near mean sea level and resultant facies mosaic: Manilus Formation (Lower Devonian) of New York state: *American Association of Petroleum Geologists Bulletin*, v. 51, p. 73-101.
- Laporte, L. F., 1969, Recognition of a transgressive carbonate sequence within an epeiric sea, Helderberg Group (Lower Devonian) of New York state: *Society of Economic Paleontologists and Mineralogists Special Publication No. 14*, p. 98-119.
- Lindsay, R. F., and Roth, M. S., 1982, Carbonate and evaporite facies, dolomitization and reservoir distribution of the Mission Canyon Formation, Little Knife Field, North Dakota, in Christopher, J. E., and Kaldi, J., eds., *Fourth international Williston Basin symposium: Saskatchewan Geological Society Special Publication No. 6*, p. 153-179.

- Lippman, F., 1973, Sedimentary carbonate minerals: New York, Springer Verlag, 228 p.
- Longman, M. W., 1980, Carbonate diagenetic textures from nearsurface diagenetic environments: American Association of Petroleum Geologists Bulletin, v. 64, p. 461-487.
- Longman, M. W., 1981, Carbonate diagenesis as a control on stratigraphic traps: American Association of Petroleum Geologists, Education Short Course Note Series 21, 159 p.
- Maiklem, W. R., Bebout, D. G., and Glaister, R. P., 1969, Classification of anhydrite: a practical approach: Bulletin of Canadian Petroleum Geology, v. 17, p. 194-233.
- May, J. A., and Perkins, R. D., 1979, Endolithic infestation of carbonate substrates below the sediment-water interface: Journal of Sedimentary Petrology, v. 49, p. 357-377.
- McKenzie, J. A., Hsu, K. J., and Schneider, J. F., 1980, Movement of subsurface waters under the sabkha, Abu Dhabi, UAE, and its relation to evaporative dolomite genesis, in Zenger, D. H., Dunham, J. B., and Ethington, R. L., eds., Concepts and models of dolomitization: Society of Economic Paleontologists and Mineralogists Special Publication No. 28, p. 11-30.
- Moore, C. H., and Druckman, Y., 1981, Burial diagenesis and porosity evolution, Upper Jurassic Smackover Formation, Arkansas and Louisiana: American Association of Petroleum Geologists Bulletin, v. 65, p. 597-628.
- Murray, R. C., 1960, Origin of porosity in carbonate rocks: Journal of Sedimentary Petrology, v. 30, p. 59-84.
- Nelson, R. A., 1981, Significance of fracture sets associated with stylolite zones: American Association of Petroleum Geologists Bulletin, v. 65, p. 2417-2425.
- Peale, A. C., 1893, The Paleozoic section in the vicinity of Three Forks, Montana: U. S. Geological Survey Bulletin 110, 56 p.
- Petroleum Information Corporation, 1980, The Williston Basin: Petroleum Information Corporation, Denver, Colorado, 305 p.
- Porter, J. W., 1955, Madison complex in southeastern Saskatchewan and southwestern Manitoba: Alberta

- Society of Petroleum Geologists Journal, v. 3, p. 126-130.
- Radke, B. M., and Mathis, R. I., 1980, On the formation and occurrence of saddle dolomite: Journal of Sedimentary Petrology, v. 50, p. 1149-1168.
- Raiswell, R., 1982, Pyrite texture, isotopic composition and the availability of iron: American Journal of Science, v. 282, p. 1244-1263.
- Sandberg, C. A., 1962, Geology of the Williston Basin, North Dakota, Montana, and South Dakota with reference to subsurface disposal of radioactive waste: United States Department of the Interior, TEI-809, 148 p.
- Saskatchewan Geological Society, 1956, Report of the Mississippian names and correlations committee: Regina, Saskatchewan, 4 p.
- Schenk, C. J., and Richardson, R. W., 1985, Recognition of interstitial anhydrite dissolution: a cause of secondary porosity, San Andres Limestone, New Mexico, and upper Minnelusa Formation, Wyoming: American Association of Petroleum Geologists Bulletin, v. 69, p. 1064-1076.
- Seager, O. A., 1942, A test on the Cedar Creek Anticline, southeastern Montana: American Association of Petroleum Geologists Bulletin, v. 26, p. 861-864.
- Sears, S. O., and Lucia, F. J., 1980, Dolomitization of northern Michigan Niagara by brine refluxion and freshwater/seawater mixing, *in* Zenger, D. H., Dunham, J. B., and Ethington, R. L., eds., Concepts and models of dolomitization: Society of Paleontologists and Mineralogists Special Publication No. 28, p. 215-235.
- Shaw, A. B., 1964, Time in stratigraphy: New York, McGraw-Hill, 353 p.
- Shinn, E. A., Ginsburg, R. N., and Lloyd, R. M., 1965, Recent supratidal dolomite from Andros Island, Bahamas, *in* Pray, L. C., and Murray, R. C., eds., Dolomitization and limestone diagenesis: a symposium: Society of Economic Paleontologists and Mineralogists Special Publication No. 13, p. 112-123.
- Shinn, E. A., and Robbin, D. M., 1983, Mechanical and chemical compaction in fine-grained shallow water limestones: Journal of Sedimentary Petrology, v. 53, p. 595-618.
- Sibley, D. F., 1982, The origin of common dolomite fabrics-

- clues from the Pliocene: *Journal of Sedimentary Petrology*, v. 52, p. 1087-1100.
- Sloss, L. L., and Hamblin, R. H., 1942, Stratigraphy and insoluble residues of Madison Group (Mississippian) of Montana: *American Association of Petroleum Geologists*, v. 26, p. 305-335.
- Sloss, L. L., and Moritz, C. A., 1951, Paleozoic stratigraphy of southwestern Manitoba: *American Association of Petroleum Geologists Bulletin*, v. 35, p. 2135-2169.
- Smith, M. H., 1960, Revised nomenclature for the Williston Basin: *American Association of Petroleum Geologists Bulletin*, v. 44, p. 959-960.
- Stephens, R. A., 1986, Depositional history and diagenesis of the upper Mission Canyon Formation and lower Charles Formation (Mississippian), Billings County, North Dakota: Unpublished Master's Thesis, University of North Dakota, 236 p.
- Stephens, R. A., and Durall, R. L., 1985, Diagenesis of a portion of the upper Mississippian Mission Canyon Formation within the Williston Basin, North Dakota: *Society of Economic Paleontologists and Mineralogists Abstracts*, v. 2, p. 86.
- Thayer, P. A., 1983, Relationship of porosity and permeability to petrology of the Madison Limestone in rock cores from three test wells in Montana and Wyoming: *U. S. Geological Survey Professional Paper 1273-C*, 29 p.
- Thomas, G. E., 1954, The Mississippian of the northeastern Williston Basin: *Canadian Mining and Metallurgical Bulletin*, v. 503, p. 136-142.
- Wanless, H. R., 1979, Limestone response to stress: pressure solution and dolomitization: *Journal of Sedimentary Petrology*, v. 49, p. 437-462.
- Ward, W. C., and Halley, R. B., 1985, Dolomitization in a mixing zone of near-seawater composition, Late Pleistocene, northeastern Yucatan Peninsula: *Journal of Sedimentary Petrology*, v. 55, p. 0407-0420.
- Wardlaw, N. C., 1976, Pore geometry of carbonate rocks as revealed by pore casts and capillary pressure: *American Association of Petroleum Geologists Bulletin*, v. 60, p. 245-257.

Weaver, C. E., 1975, Construction of limpid dolomite:  
Geology, v. 3, p. 425-428.

Wilson, J. L., and Jordan, C., 1983, Middle shelf  
environment, in Scholle, P. A., Bebout, D. G., and  
Moore, C. H., eds., Carbonate depositional  
environments: American Association of Petroleum  
Geologists Memoir 33, p. 298-343.